Interaction between radiation and superconductors: Physics and Applications

Sergio Pagano

Dipartimento di Matematica e Informatica
Università di Salerno
Italy

Acknowledgements

Superconductive detectors group at University of Salerno

Orlando Quaranta, Stefania Marchetti, Nadia Martucciello

Superconductive detectors group at CNR Istituto di Cibernetica – Naples

Roberto Cristiano, Emanuela Esposito, Luigi Frunzio, Ciro Nappi, Mikkel Ejrnaes, Mikhail Lisitskyi, David Perez de Lara, Alessandro Casaburi

Superconductive detectors group at University of Naples "Federico II"

Antonio Barone, Giuseppe Peluso, Gianpiero Pepe, Loredana Parlato

Nanofabrication group at CNR Istituto di Fotonica e Nanotecnologie – Rome

Roberto Leoni, Gabriella Castellano, Alessandro Gaggero, Francesco Mattioli

The Sinphonia Project

Outline:

- A brief overview of superconductivity, superconductive materials and devices fabrication technologies

- Interaction with external perturbations:
  nonequilibrium superconductivity, energetic cascade

- Superconductive detectors:
  superheated granules, transition edge sensors, hot electron detectors, tunnel junctions, Josephson junctions

- A specific case: The Supeconducting Single Photon Detectors

- Applications:
  Dark Matter detection, X-ray to mm wave astronomy, Material analysys, Mass spectrometry, Telecommunications, …

- Concluding remarks

Superconductivity in one page

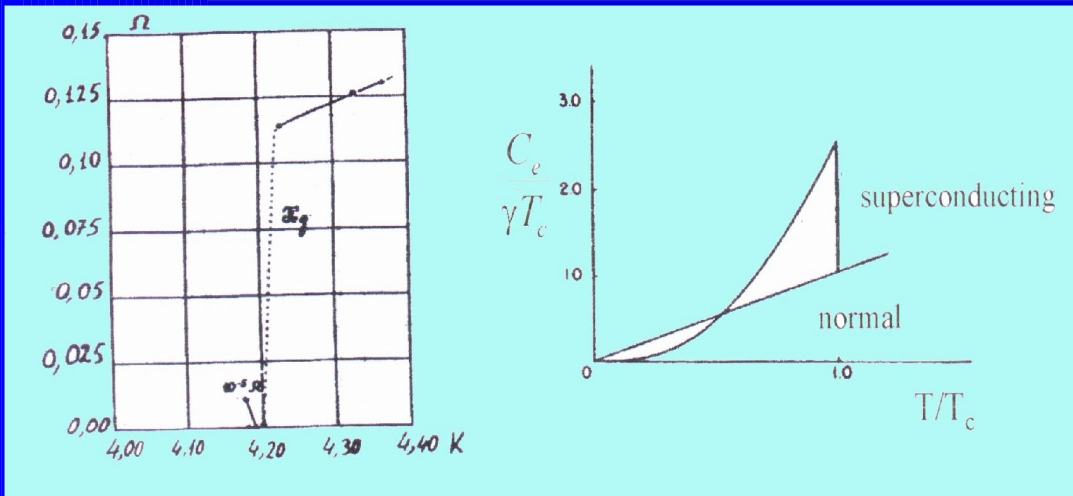

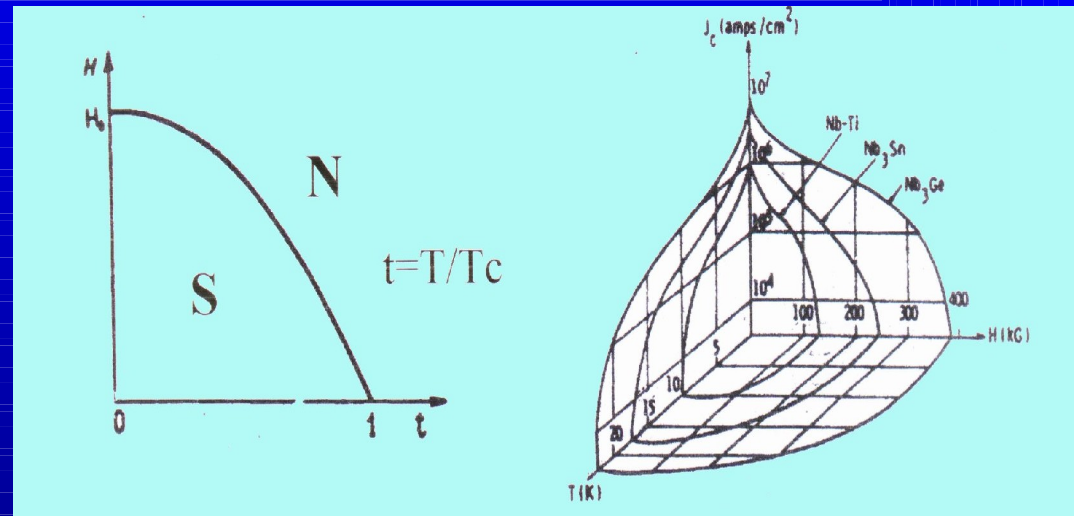

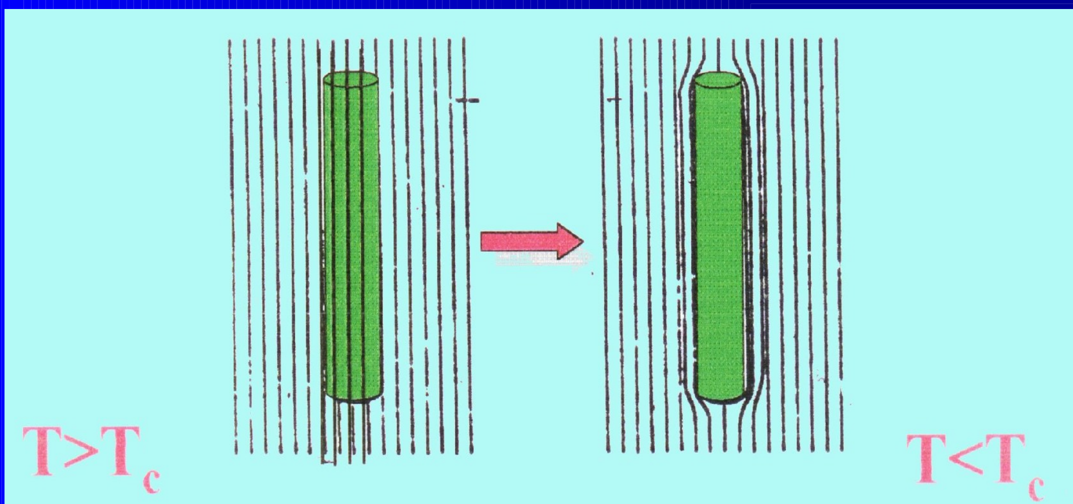

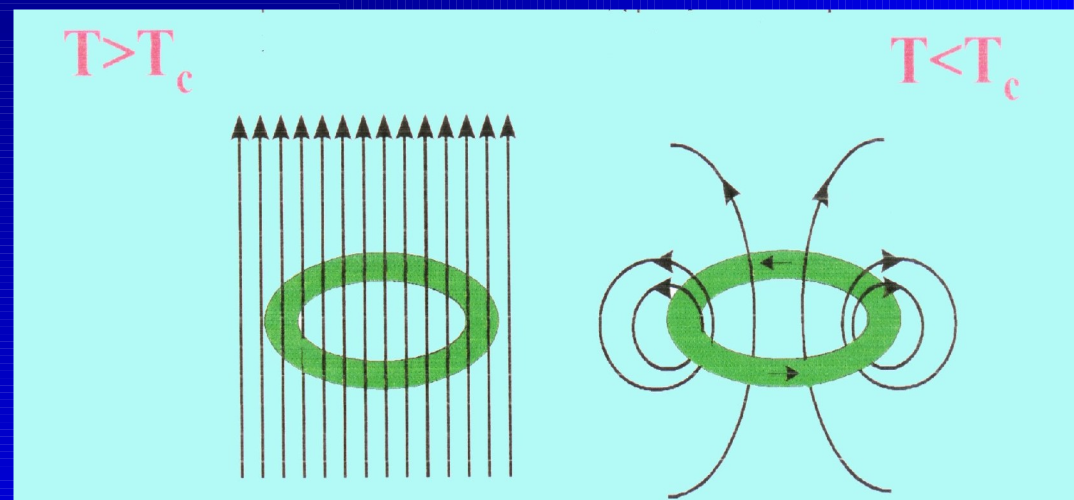

$Tc \propto m^{½}$

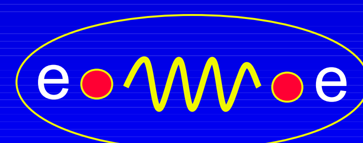

Cooper-Pair

Superconductive materials

Three interacting fluids

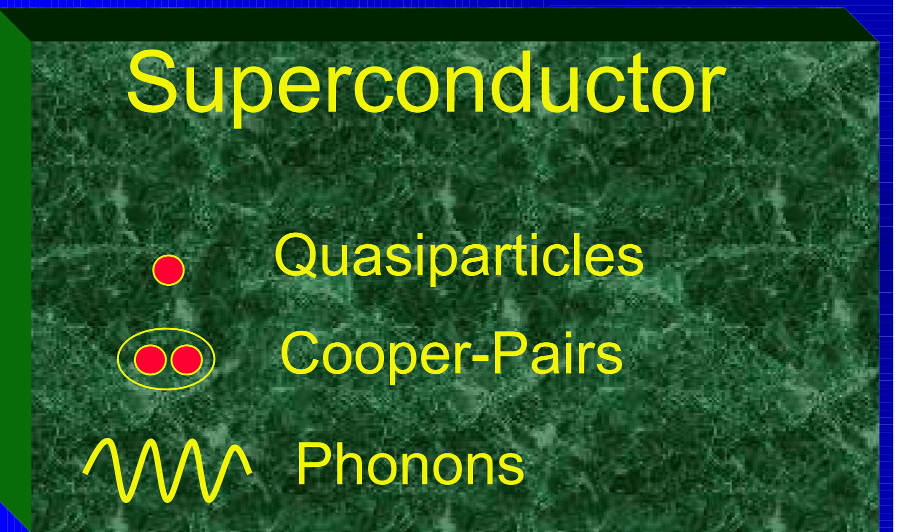

remarkable properties

Δ ~ 1 meV

$\hbar\omega_{Debye} > \Delta$

Superconductor	T_c (K)	Δ (meV)	$\hbar\omega_D$ (meV)
$Hg_{0.8}Tl_{0.2}Ba_2Ca_2Cu_3O_{8.3}$	150	22,48	?
$TlCa_2Ba_2Cu_3O_x$	133	?	?
$Bi_{1.8}Pb_{0.3}Sr_2Ca_2Cu_3O_{10+x}$	110	30	26
$YBa_2Cu_3O_{7-x}$	92.0	18	31
MgB_2	39.0	1.8, 6.8	77
NbN	16.0	2.50	35
Nb	9.26	1.52	24
Pb	7.19	1.33	10
V	5.30	0.81	33
Ta	4.48	0.66	22
Sn	3.75	0.59	17
Al	1.19	0.17	37
Ti	0.92	0.14	40
Mo	0.39	0.06	36

Evolution of thin film and device technology

1960-1980

devices based on combination of soft (Pb, In) and hard metals (Nb)
typical device scale: 10 μm   N. of junctions x chip ~ 100

1980-1990

fully refractory tunnel junction process Nb/AlOx/Nb technology
typical device scale: 3-10 μm N. of junctions x chip ~ 1000
first HTS Josephson junction devices (low reproducibility)

1990-2005

stable Nb/AlOx/Nb technology, also NbN/MgO/NbN (10K operation)
typical device scale 1-3 μm N. of junctions x chip ~ 10000
refined HTS junction tehnology N. of junctions x chip ~ 100

2005-?

submicron technology for LTS
large scale integration of HTS

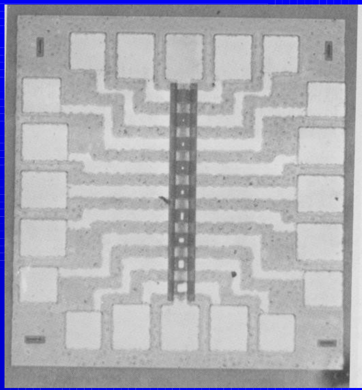

Madison 1974

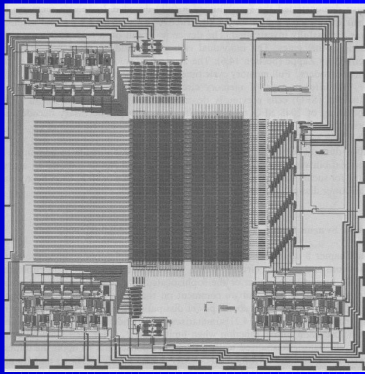

IBM-Zurich 1974

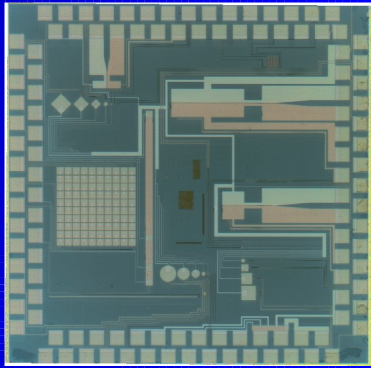

Napoli-Tsukuba 1992

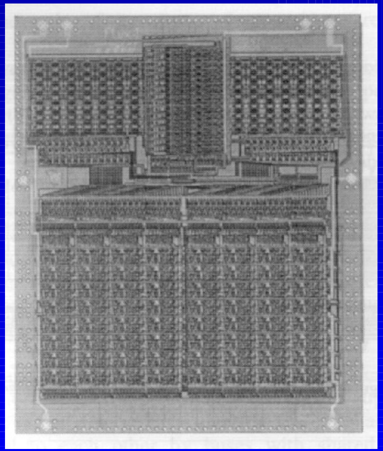

TRW-SUNY 2002

An ideal detector should satisfy the following conditions:

- Large enough signal-to-noise ratio.
- Creation and fast collection of free charge carriers (fast response).
- Large number of produced carriers for a given energy release of the impinging radiation (high energy resolution).
- Linear response to the deposited energy (proportionality).
- Fabrication process, geometrical definition, associated technologies.
- Material requirements to optimize radiation interaction (A,Z) and minimize radiation damage.
- Operational aspects and cost.

Advantages of superconductive detectors

- large number of quasiparticle creation by Cooper-pair breaking
- sharp normal - superconductor transition
- low heat capacitance
- kinetic inductance change
- wide choice of materials (A,Z,…..)

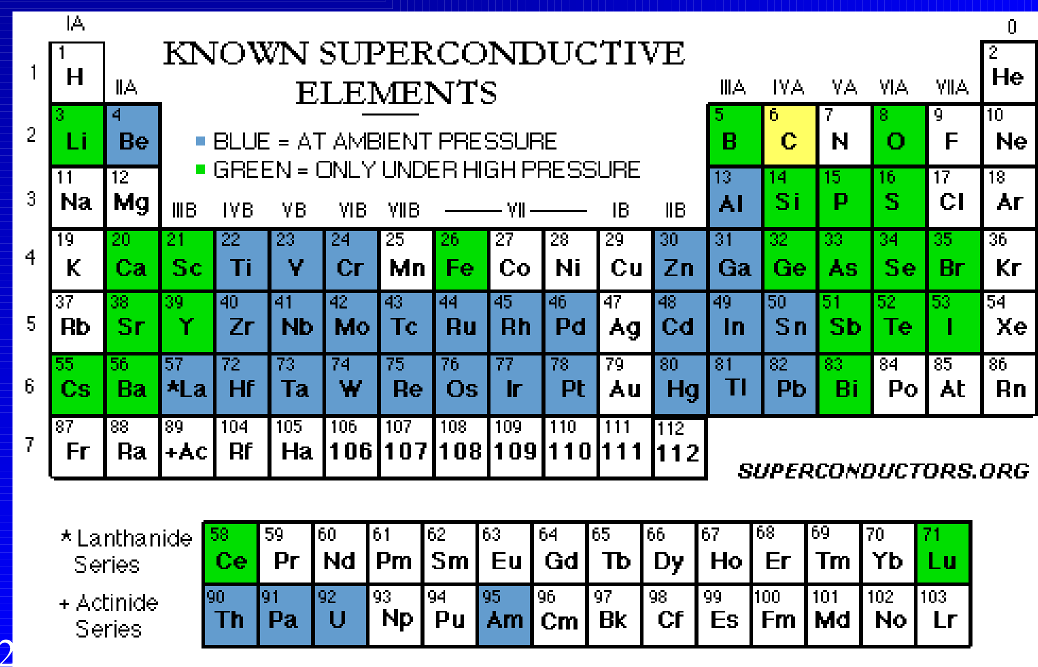

The energy cascade

The radiation interaction triggers a series of events where the released energy follows a "cascade" which involves several processes, ultimately affecting the superconductive state.

1st stage: energy absorption	
electron-electron scattering	0-10^{-15} s *
2nd stage: energy down conversion	
electron-phonon scattering	10^{-12} s
3rd stage: evolution of mixed distribution of qp-ph-pairs	
pair-breaking, recombination	10^{-9}-10^{-6} s
4th stage: thermalization	
thermal phonons	10^{-3} s

* direct pair breaking at t=0 ??

	non-equilibrium detector	*bolometers or thermal detector*
main actors:	hot electrons and quasiparticles	phonons
detection at:	2nd-3rd stage	4th stage

1^{st} stage: absorption of a photon

E

photon (of energy E)
photoelectric interaction

excited atom

primary photoelectron

Auger electron

secondary photon emission

multiple scattering
e-e

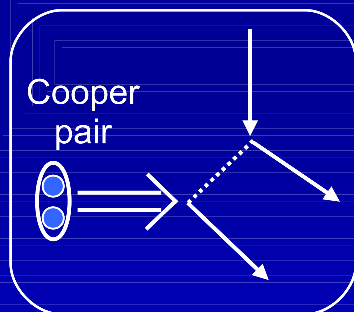

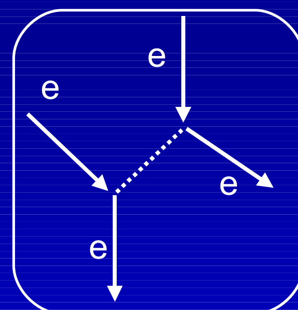

escape from the detector

continuous energy loss
from E to E_1~1 eV
Fermi level

escape peaks

E_1

time @ E_1 about 1 fs

1st stage: energy absorption from an energetic particle

other types of particles

Ionizing particles
(alpha, protons, charged ions, ecc)
neutral particles
(neutrons, neutrinos, WIMPs)

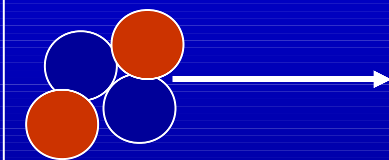

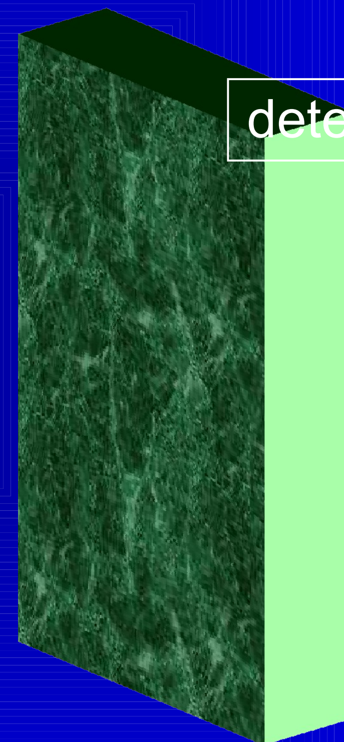

detector

DNA-fragments
300.000 a.m.u.

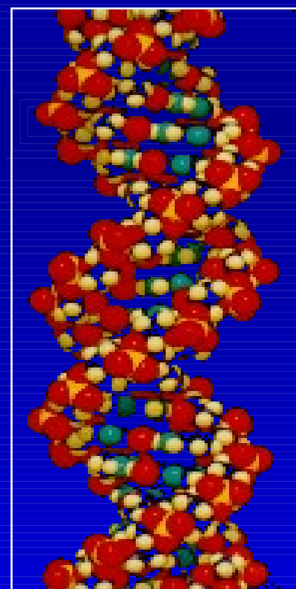

velocity → ionization or high energy phonons excitation

2nd stage: the decay processes

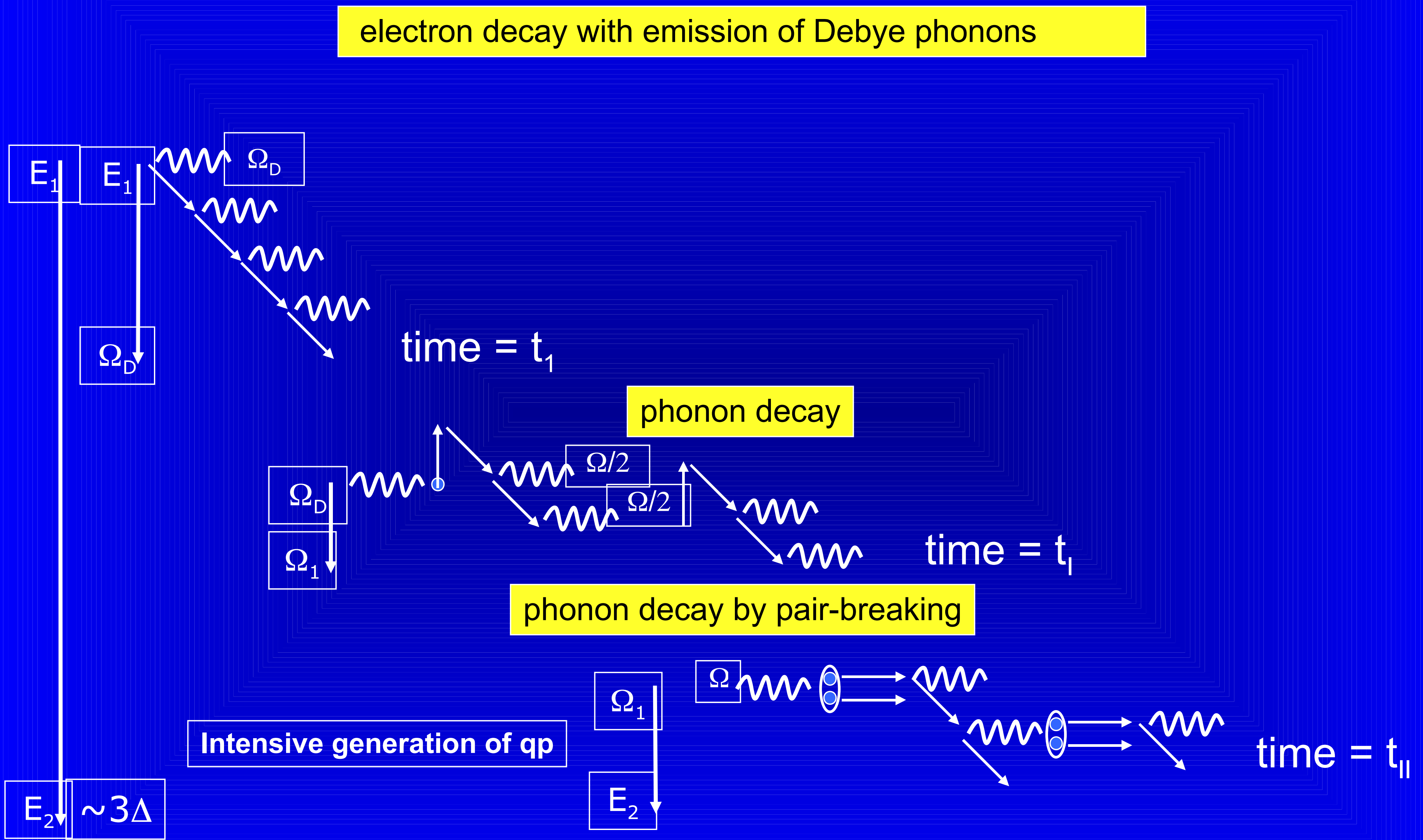

2^{nd} stage: material dependent relevant times

Metal	Tl	Hg	Sn	In	Pb	Nb	Ta	Al	Zn	Mo	Hf
t_1 ps	10.1	5.8	2.3	5.1	8.8	0.8	1.6	0.5	1.4	0.9	2.3
t_I ps	360	270	170	320	66	6.0	26	140	1.4 ns	100	400
t_{II} ps	14.6	0.3	21.8	7.4	1.0	1.15	15.5	1.3 ns	10 ns	16 ns	2.1 μs

$t = t_1$ Energy transfers from hot-electrons to phonons and forms the "phonon bubble"

$t = t_I$ Phonon down conversion where electrons act as mediating agents modifying the phonon spectral distribution and leaving the energy of the phonon system constant

$t = t_{II}$ long-lived electronic excitations while phonons act as mediators in quasiparticle downconversion (pair breaking is relevant)

the Hot Spot formation

During the 1st and 2nd stages a normal region is formed around the impact point. This is called the “hot spot”. In time, it expand , cool down and finally collapses when $T<T_c$

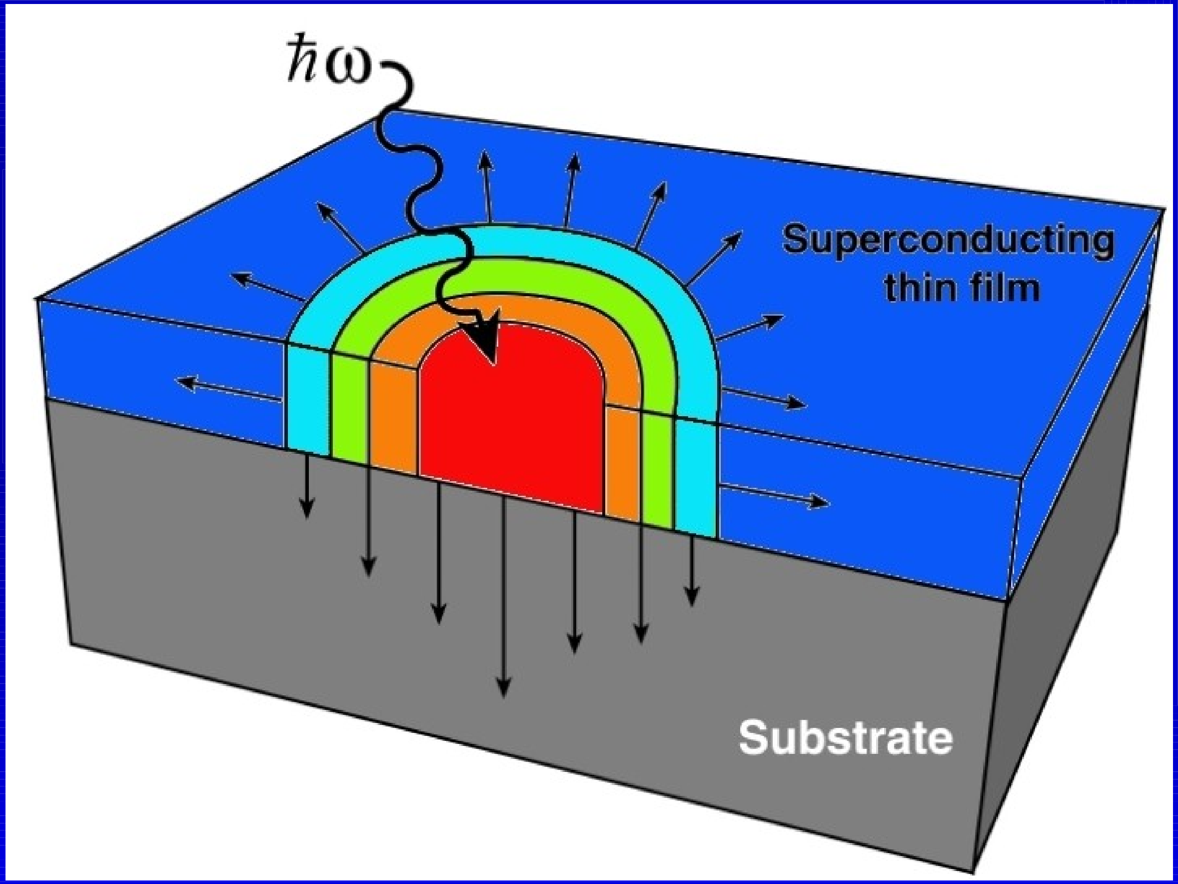

The hot spot size depends on:

Radiation energy, film properties and material parameters

3rd stage: pair breaking, qp and phonon interaction

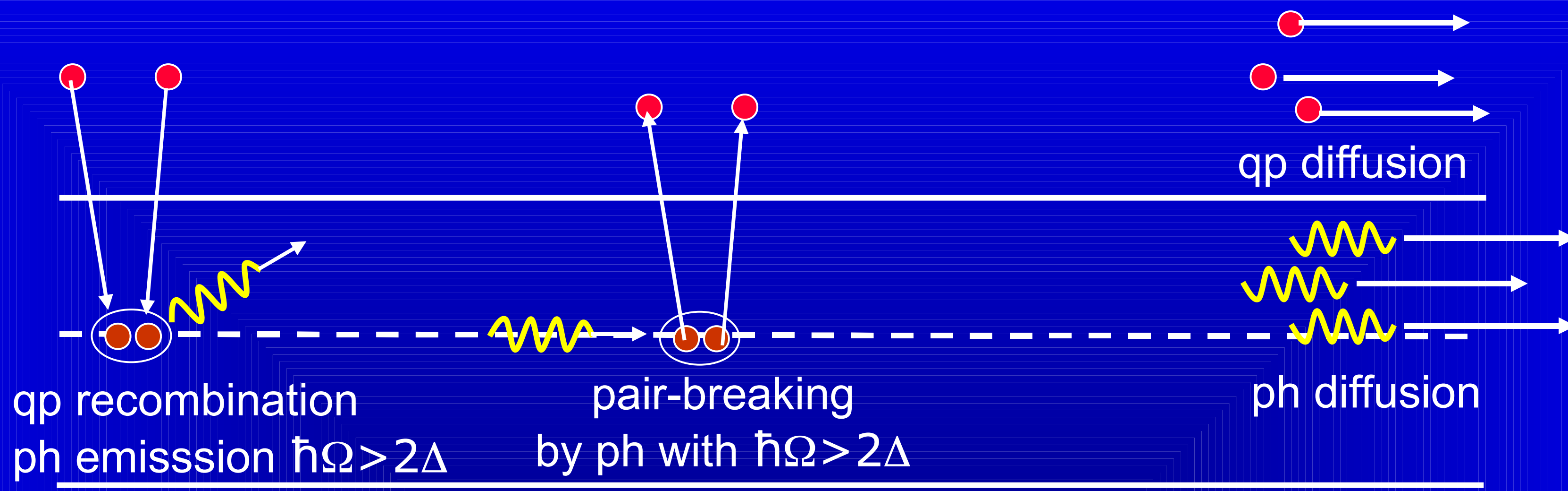

- Phonons and quasiparticles have low energy (few Δ) so they interact with each other and with Cooper pairs (at this stage the hot-spot is effectively relaxed).
- In each quasiparticle recombination process a phonon with energy $\hbar\Omega \geq 2\Delta$ is emitted. The phonons can break pairs or be scattered by other phonons or quasiparticles.
- When the phonon energy becomes $\hbar\Omega < 2\Delta$, they no longer contribute to pair-breaking.
- The excess phonons further relax down in energy and contribute to a general heating of the detector.
- At the same time quasiparticles and phonons can diffuse out from the superconductor.

3rd stage: the Rothwarf – Taylor Equations

$$\frac{\partial N_{qp}}{\partial t} = 2\tau_{pb}^{-1} N_{ph} - \tau_r^{-1} N_{qp}^2 - D\,\nabla^2 N_{qp} \qquad \frac{\partial N_{ph}}{\partial t} = \frac{\tau_r^{-1} N_{qp}^2}{2} - \tau_{pb}^{-1} N_{ph} - \tau_{es}^{-1} N_{ph}$$

N_{qp}, N_{ph} are the qp and ph numbers, D is the diffusion constant

qp recombination rate

$$\tau_r^{-1} = \frac{1}{2N_{qp,th}} \tau_0^{-1} \sqrt{\pi\left(\frac{2\Delta}{KT_c}\right)^5} \sqrt{\frac{T}{T_c}} \exp\left(-\frac{\Delta}{KT}\right)$$

pair breaking rate

$$\tau_{pb}^{-1}(2\Delta) = \tau_{0,ph}^{-1}\left[\Delta(T)/\Delta(0)\right]\left[1-2f(\Delta(T))\right]$$

ph escape rate

$$\tau_{es}^{-1} = \frac{\eta c_s}{4d}$$

	τ_0 (ns)	$\tau_{0,ph}$ (ps)
Nb	1.49	4
Pb	1.96	34
Ta	17.8	23
Sn	23.0	110
Al	4380	242

4^{rd} stage: thermalization of phonons

Radiation energy is completely converted by thermal phonons with $\Omega<2\Delta$ in heating of the superconductor to $T_0>T_{bath}$. Thus, due to the thermal contact with the environment, the equilibrium is restored.

time ~ 10^{-3} s

Energy cascade

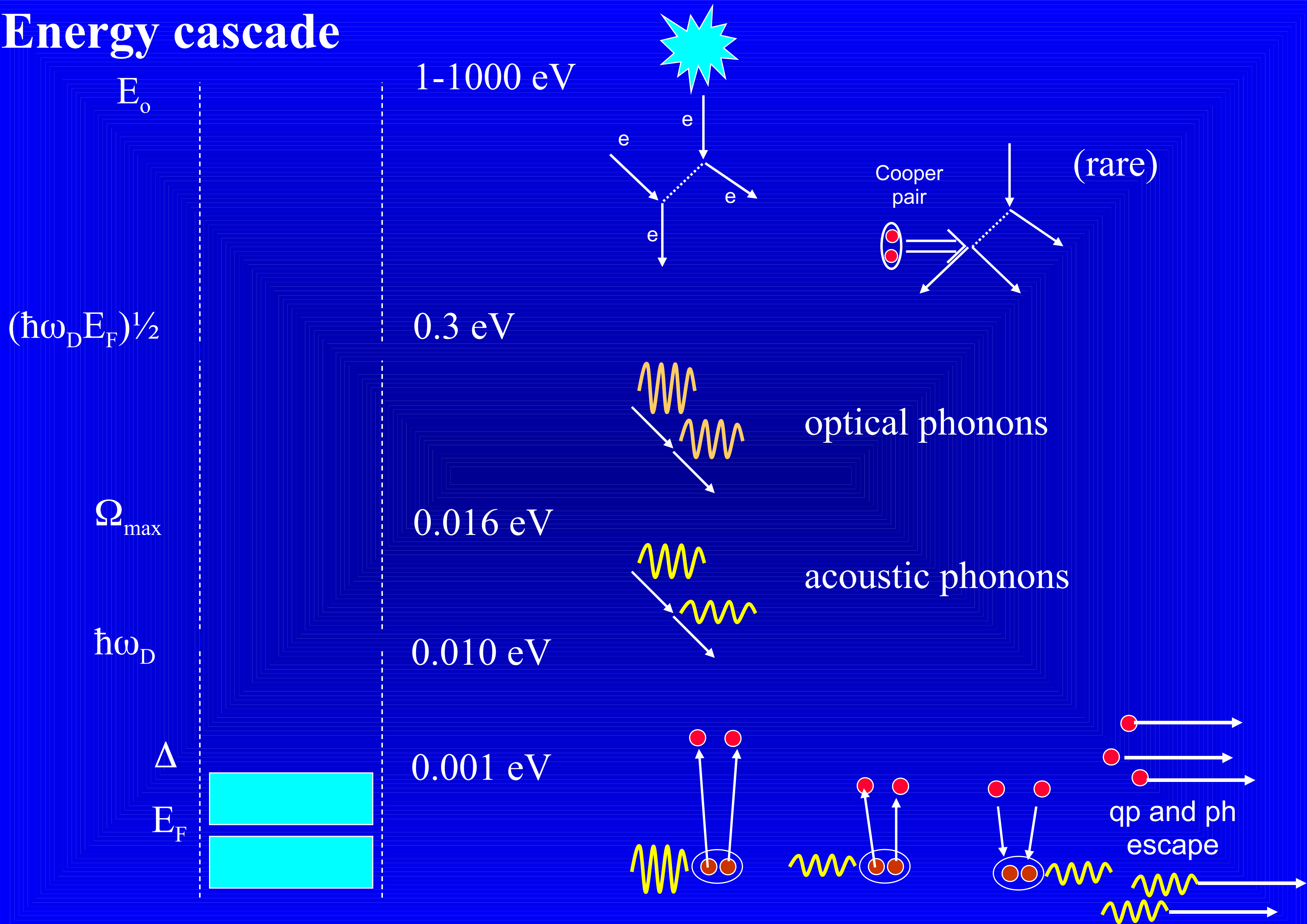

In summary:

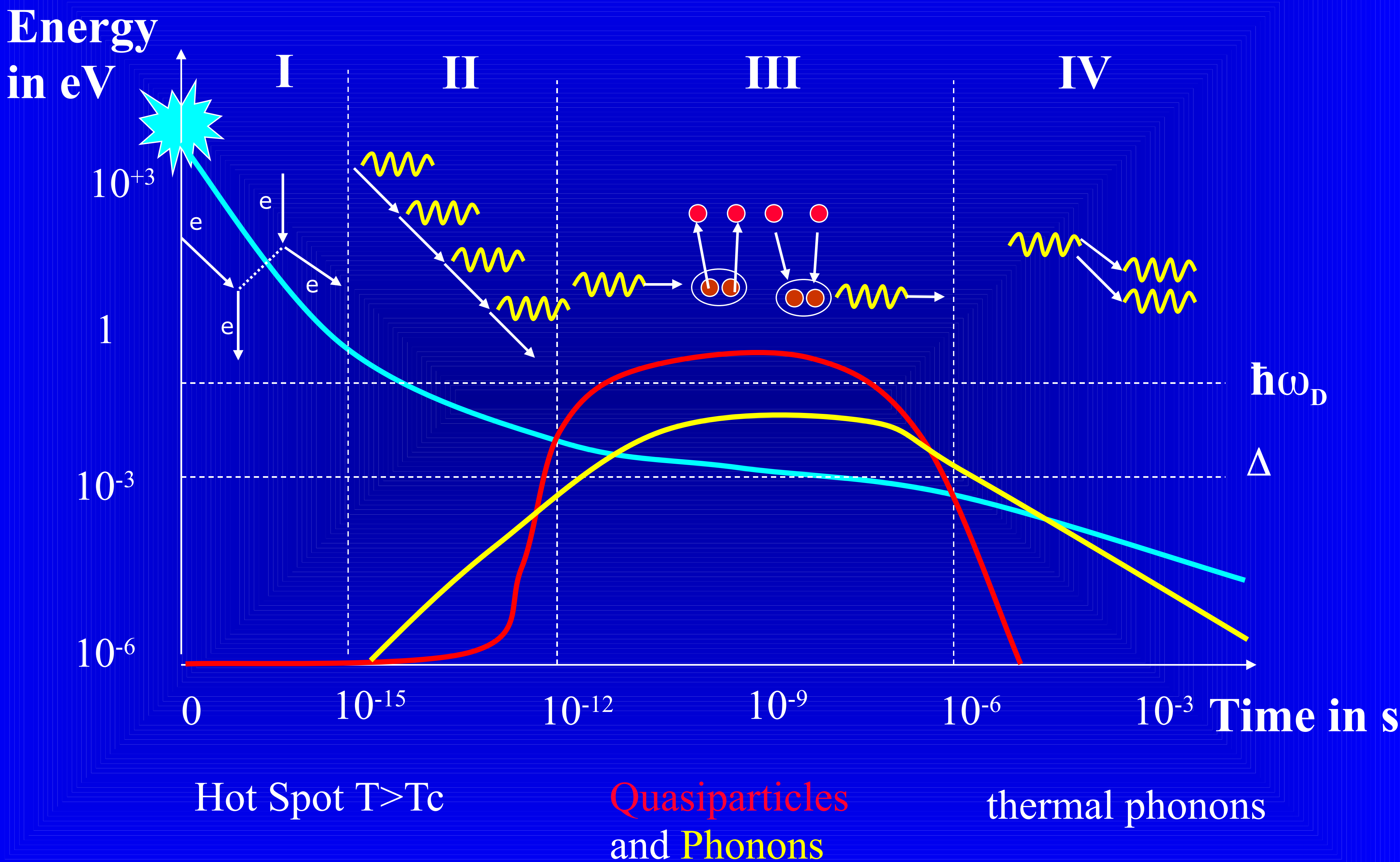
Energy in eV
I
II
III
IV
10^{+3}
1
10^{-3}
10^{-6}
e
e
e
e
$\hbar\omega_D$
Δ
0
10^{-15}
10^{-12}
10^{-9}
10^{-6}
10^{-3}
Time in s
Hot Spot T>Tc
Quasiparticles
and Phonons
thermal phonons

Superconducting Detectors

- Superheated Superconducting Granules: **SSG**
- Transition Edge Sensor: **TES**
  sharp normal-superconducting transition → resistance change
- Hot Electron Superconducting Photodetector: **HESP**
  Hot-spot creation → S/N transition or kinetic inductance change
- Superconducting Tunnel Junction: **STJ**
  Cooper-Pair breaking → creation of excess quasiparticles $N \sim E/\Delta$
  → increase of tunneling current
- Josephson Junctions: **JJ**
  Cooper-Pair breaking → decrease of Ic → fast change of voltage state

Supeheated Superconducting Granules: SSG

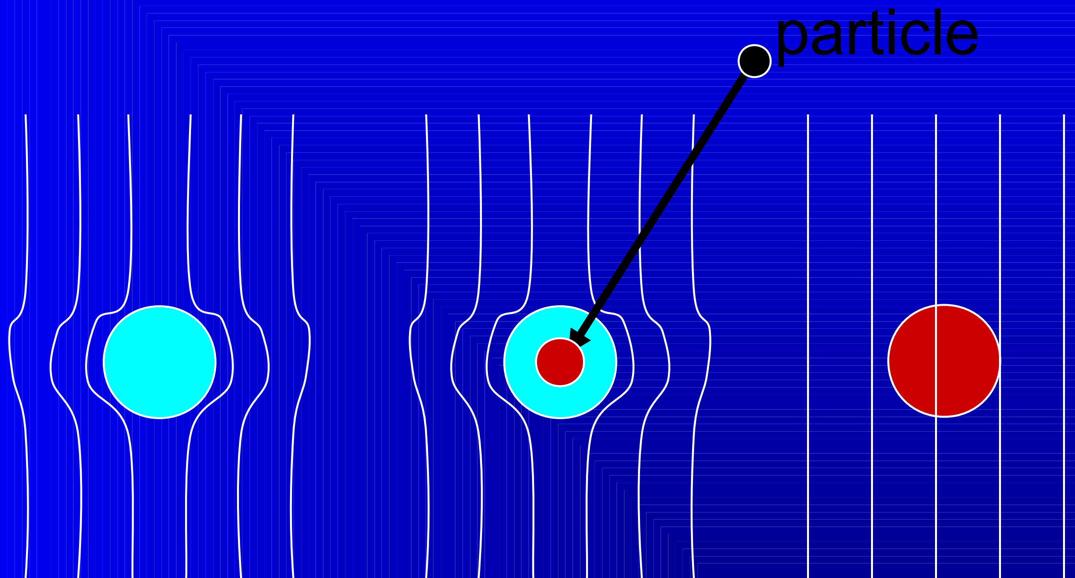

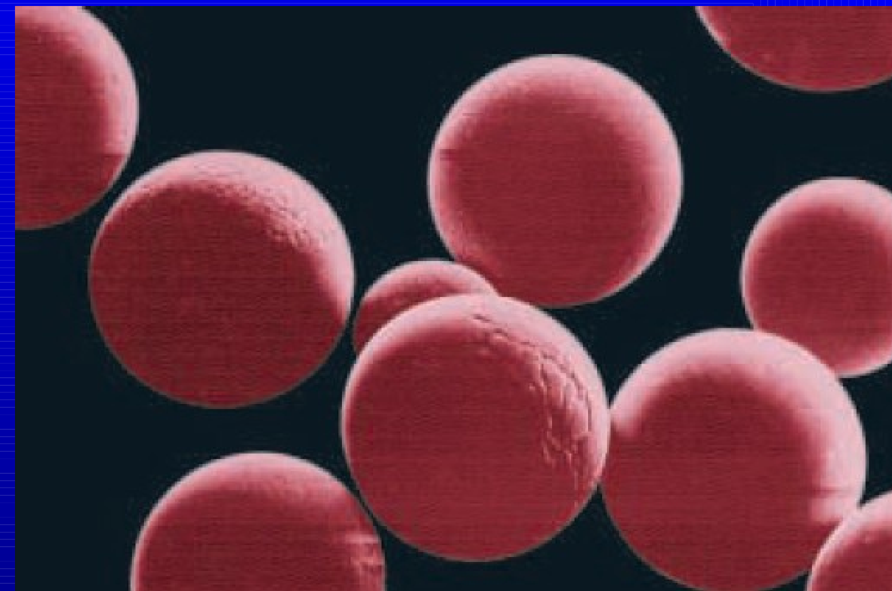

tin granules with a diameter of 30 μm

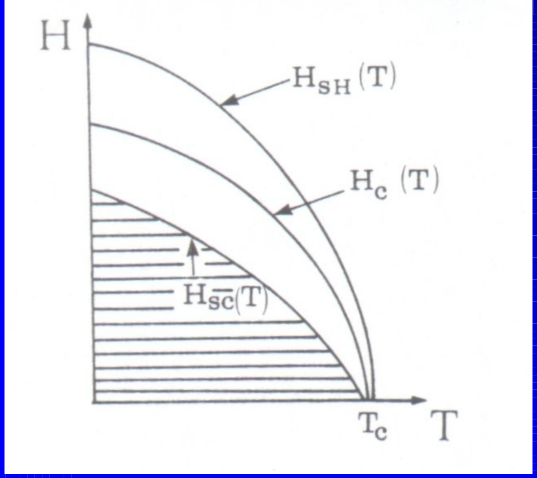

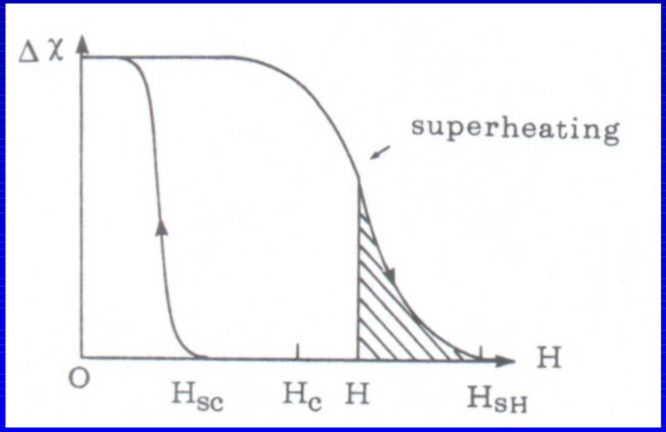

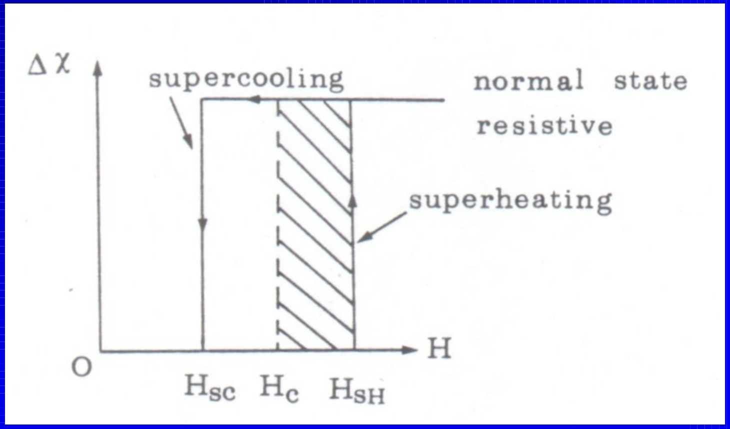

Planar Array of Superheated Superconductors: the PASS detector

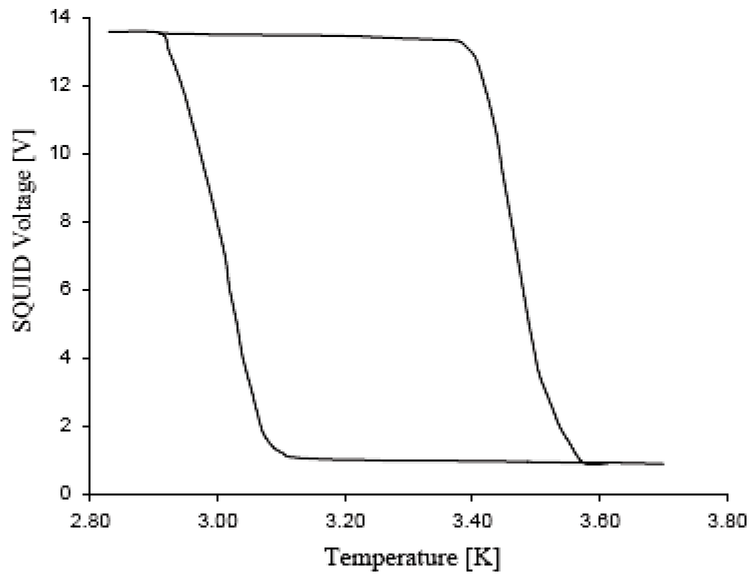

Fig. 3. Hysteresis curve showing superheating and supercooling of 3 M PASS sample.

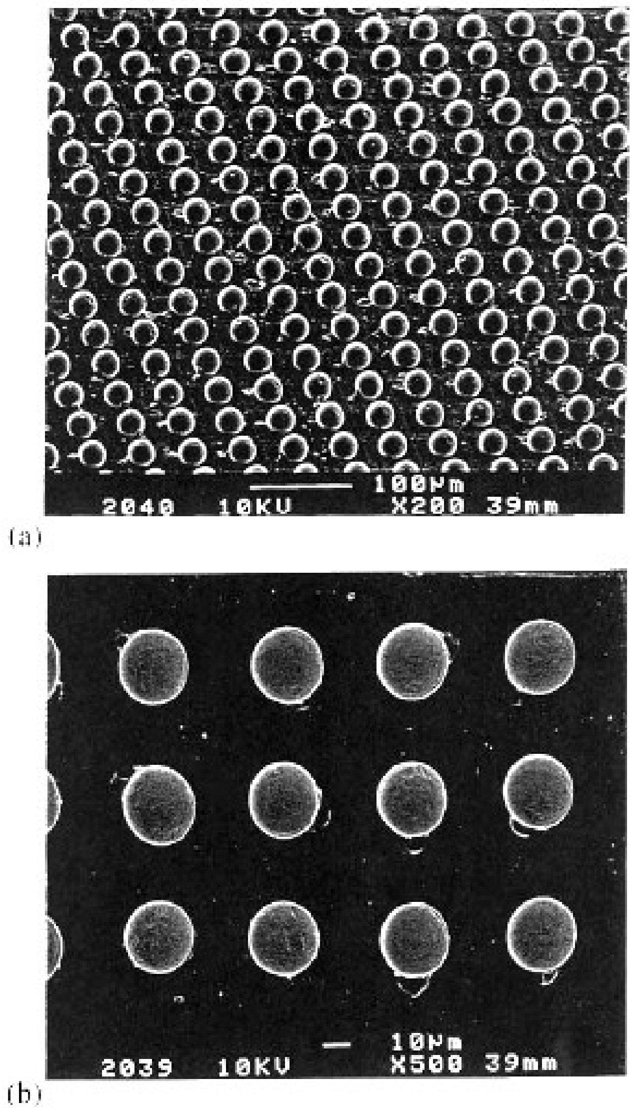

Fig. 2. 3 M sample after melting: (a) Scale 100 µm and (b) Scale 10 µm.

A. Kotlicki et al. / Nuclear Instruments and Methods in Physics Research A 520 (2004) 175–177

Transition Edge Sensor: TES

energy (after I, II, III and IV stage) → heat → themperature rise

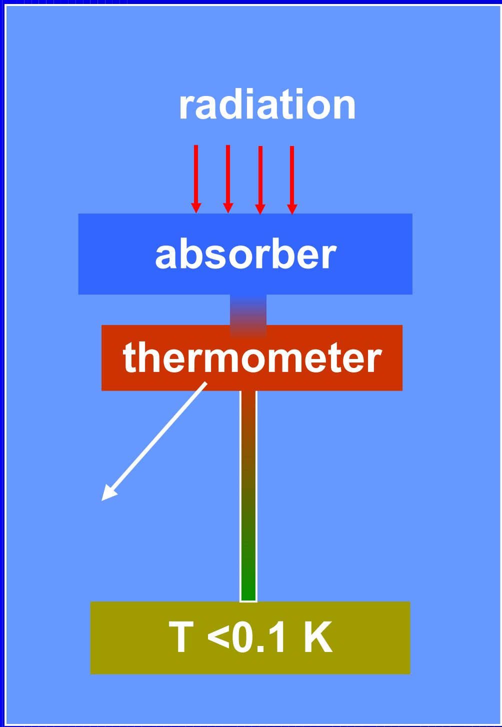

Needs:
a suitable material as absorber (mass vs speed)
a sensitive thermometer (super- vs semi-conductor)
low temperatures (heath capacity decreases with T)

Absorber + Thermometer

- **Insulator cristal + NTD Thermistor**
- **Superconductor + NTD Thermistor**
- **Insulating cristal + TES**
- **TES**

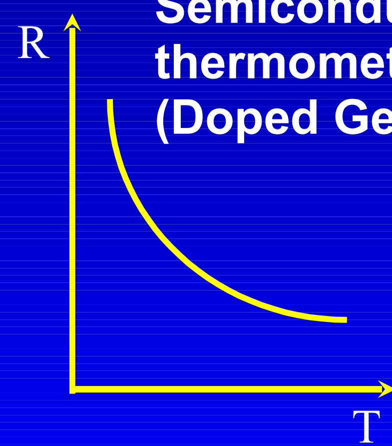

Semiconductor thermometer (Doped Ge or Si)

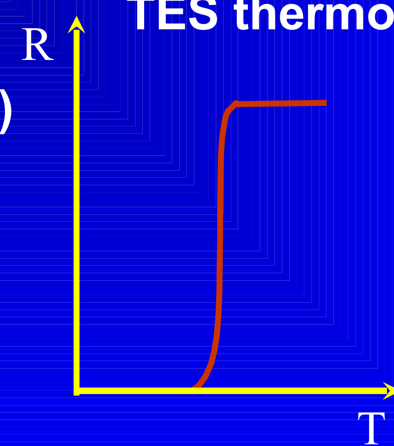

TES thermometer

Superconducting thin film at the S/N transition

Readout scheme

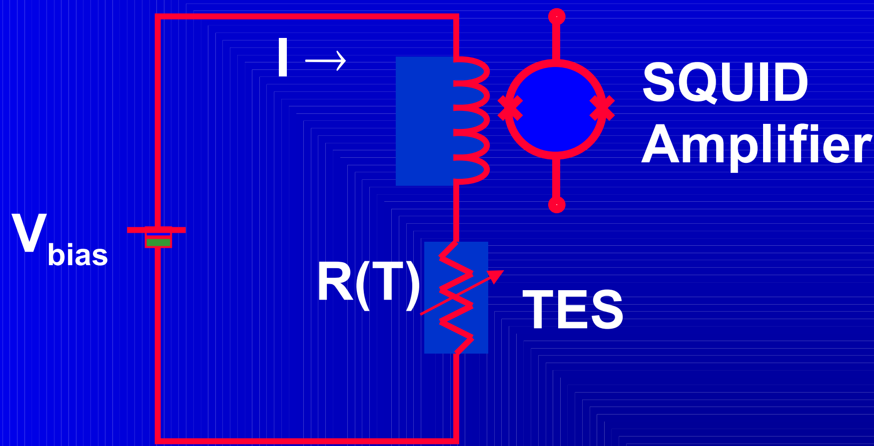

- **mK temperature**
- **resistive mode.**
- **constant voltage bias**
- **the TES is coupled to a SQUID amplifier.**

We can measure the current pulse and reconstruct the energy of the incident photon.

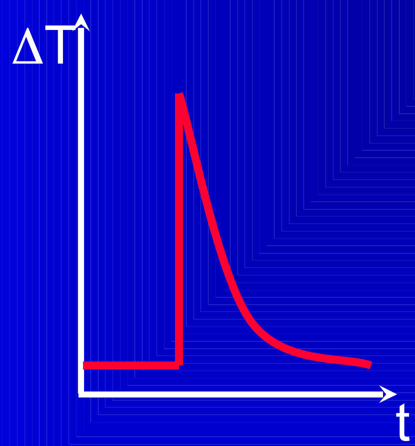

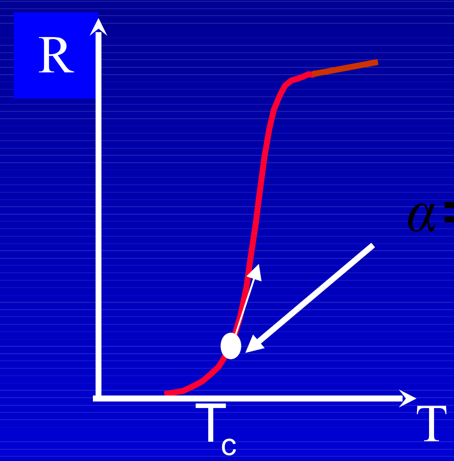

$$\alpha = \frac{T}{R}\frac{dR}{dT}$$

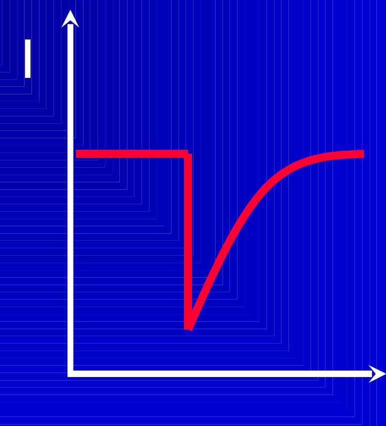

$$\Delta T = \frac{E}{C(T)}\exp\left(-\frac{t}{\tau_{eff}}\right)$$

$$\tau_{eff} = \frac{C(T)}{G(T)}$$

$$E = V_b \int \Delta I dt$$

$$\Delta E = 2.36\sqrt{4 k_B T^2 C / \alpha}$$

Examples of TES

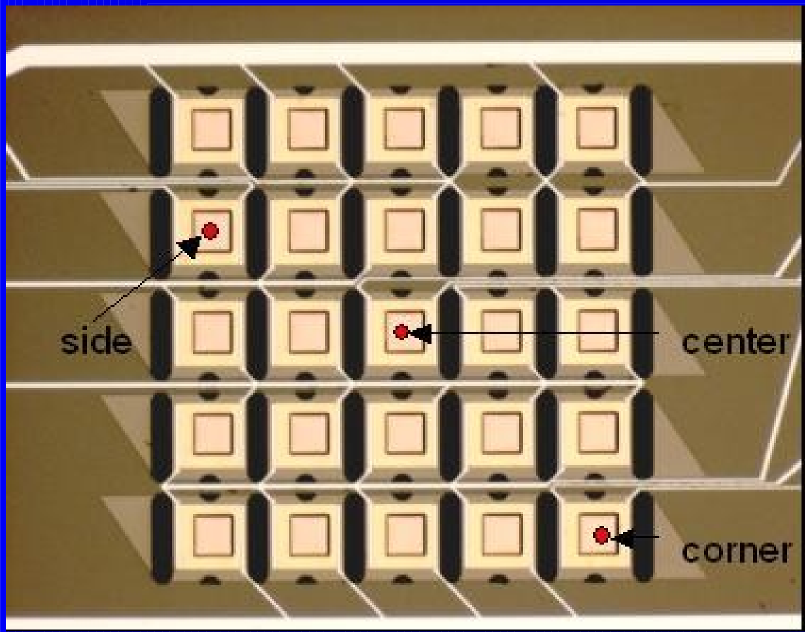

SRON (The Netherlands)

Ti/Au-TES on Cu/Bi absorber
ΔE = 4 eV at E=5.89 keV T=96mK

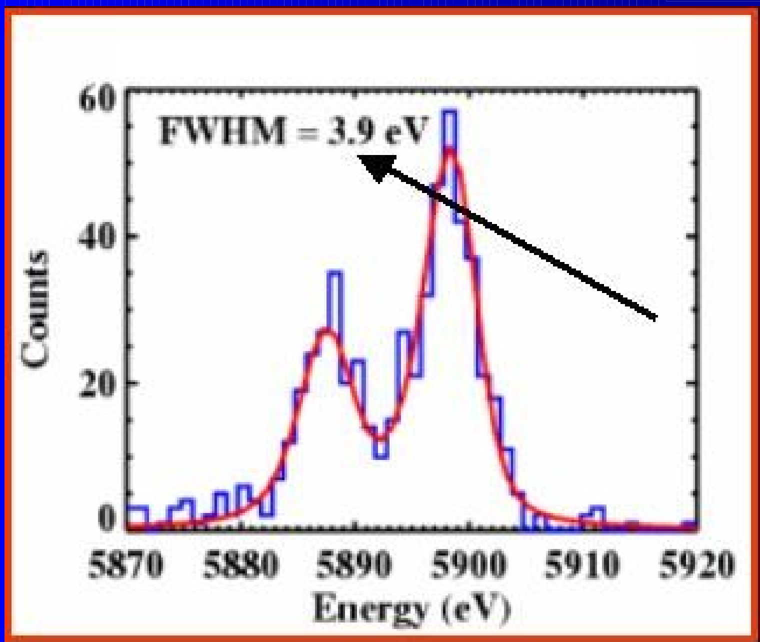

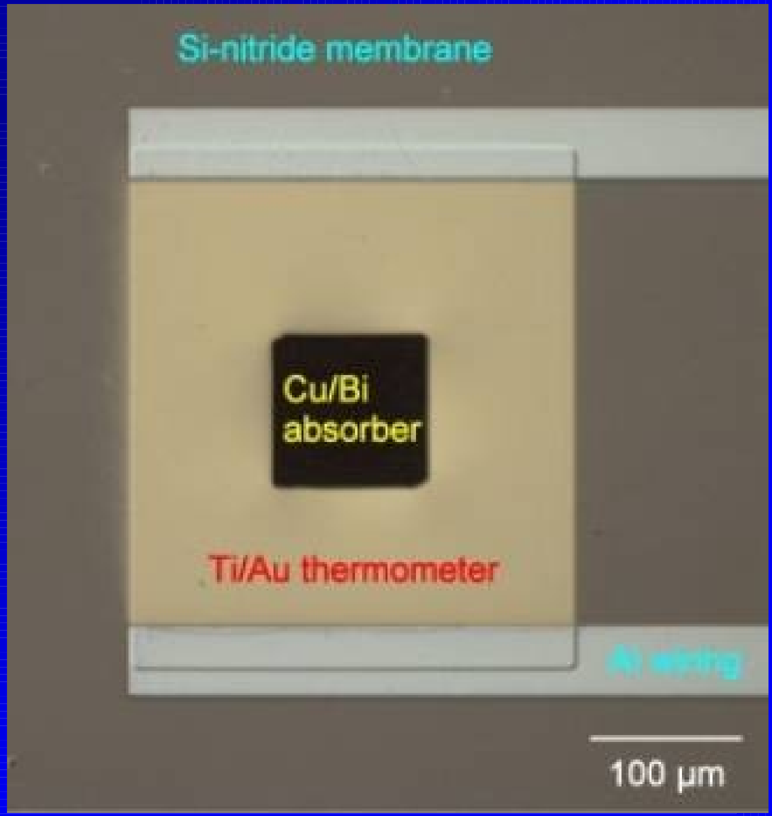

TES Performances

	TES	Absorber	T_c (mK)	ΔE(eV) @ 6keV	τ (μs)	Array
NASA/GSFC USA	Mo/Au W	None/TES	106	6.1	310	6x6, 400μm^2 pixel, 4 pixels per time
NIST Boulder USA	Mo/Cu Mo/Au	None/TES Bi	93	4.5	750	8x8, 20/64 pixels wired, TES tested without absorber
Tokio Univ.	Ti/Au	-		5.7		-
SRON The Netherlands	Ti/Au	Cu/Bi	96	4.0	100	5x5, 3 pixels wired
MPI-Munich	W	-	20	32		-

Hot Electron Superconducting Photodetector (HESP)

Ultra-thin, narrow films of NbN or YBCO

Operation temperatures 0.5 T_c or near T_c

Operation mode:

- resistive mode (TES-like)
- current assisted transition S/N transition
- kinetic inductance mode

Hot-spot formation & fast photodetection

$T<T_c$

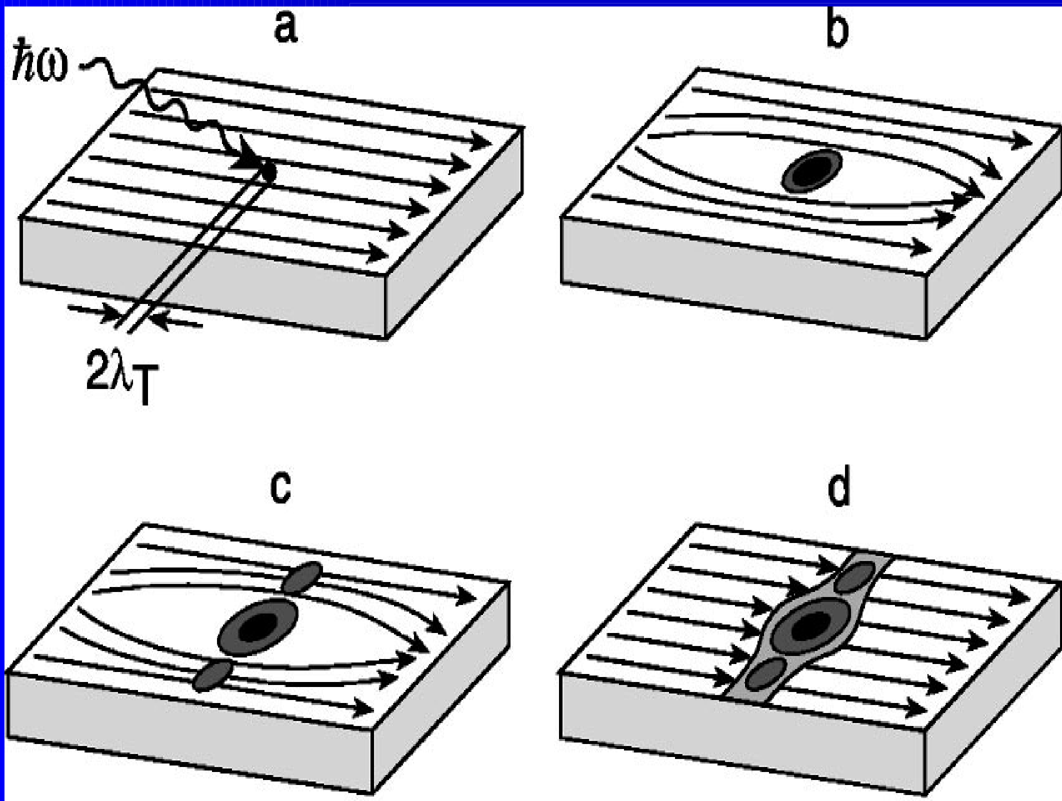

kinetic inductance

$J<J_c$ $\quad V = I\,(dL_{kin}/dt)$

current assisted S/N transition

$J>J_c$ $\quad V = I\,R$

Kinetic inductance of a stripline

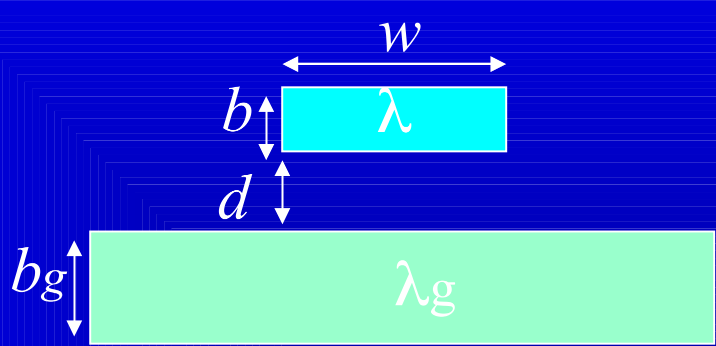

$$L = \frac{\mu_0 d}{kw}\left[1 + \frac{\lambda}{d}\coth\left(\frac{b}{\lambda}\right) + \frac{\lambda_g}{d}\coth\left(\frac{b_g}{\lambda_g}\right)\right]$$

if $b \ll \lambda$ and $bg > \lambda g$:

$$L = \frac{\mu_0}{kw}\left[d + \frac{\lambda^2}{b} + \lambda_g\right]$$

$$\lambda^2(x,t) = \frac{\lambda_0^2}{f_{sc}(x,t)}$$

$$f_{sc}(x,t) = \frac{n_0 - n_q - \Delta n(x,t)}{n_0}$$

$$n_q = N(0)\sqrt{\frac{\pi \Delta k_B T}{2}}\, e^{-\frac{\Delta}{k_B T}}$$

$n_0 = N(0)\,\Delta$

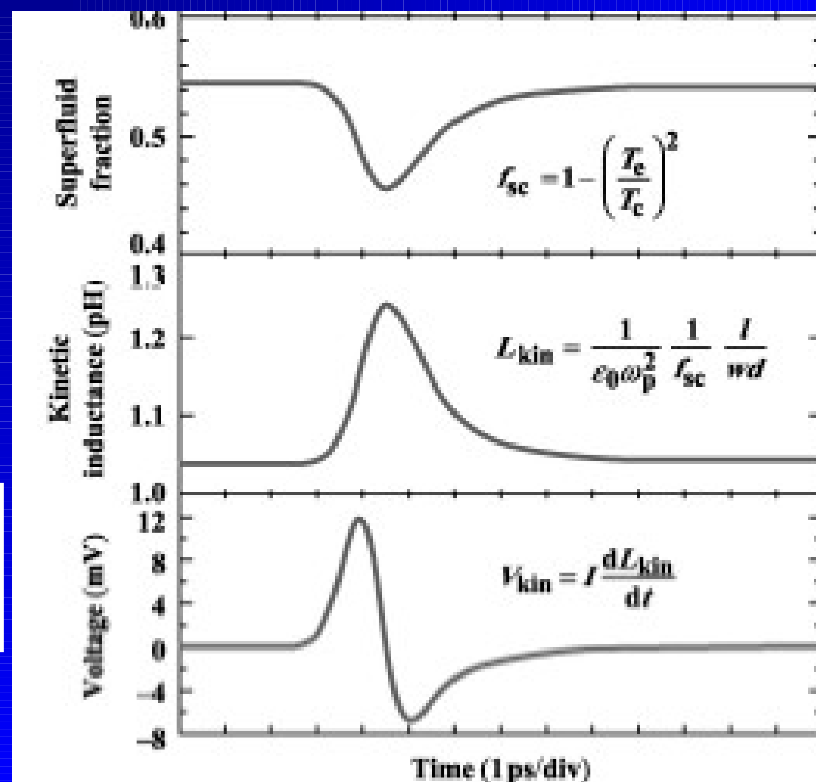

$\Delta n(x,t)$ is the non equilibrium quasiparticles density which is a solution of the RT equations

YBCO HESP

TES Mode

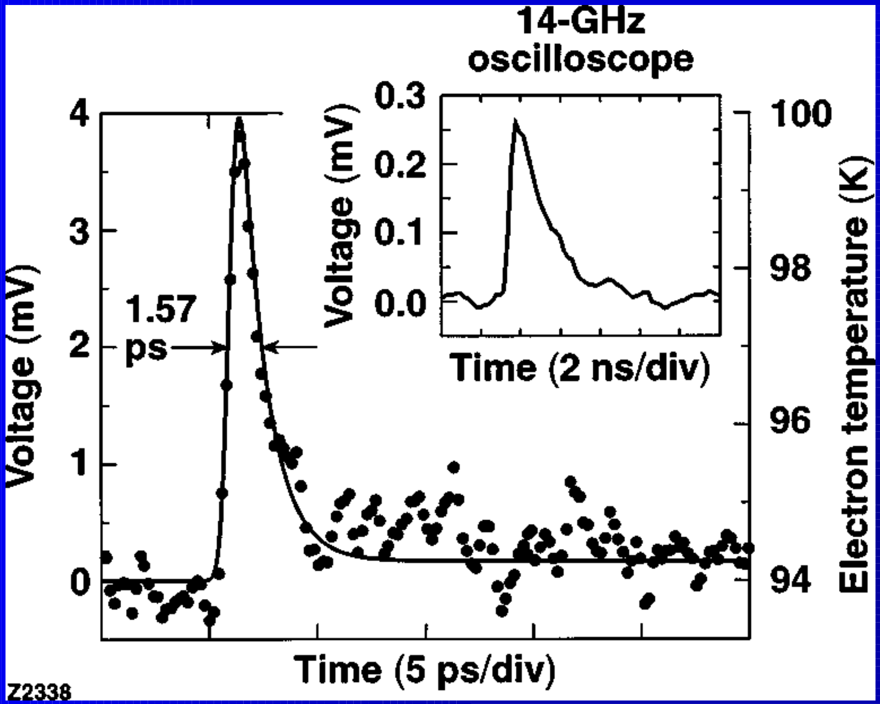

Kinetic Inductance Mode

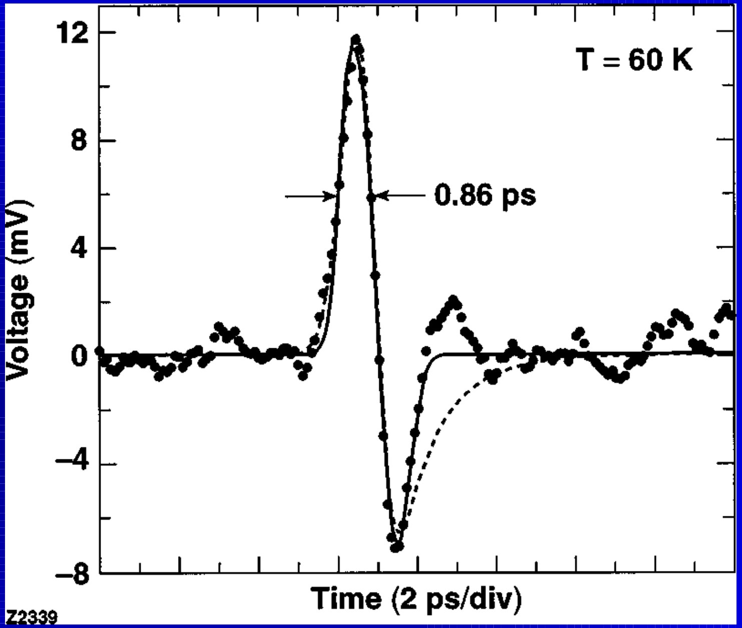

100 nm thick film
$T_c = 89$ K

M. Lindegren et al., APL 74. (1999) 853

UNIVERSITY OF ROCHESTER

HESP-the model

YBCO

NbN

$\tau_T = 0.56$ ps

$\tau_T = 6.5$ ps

$\tau_{e\text{-}ph} = 1.1$ ps

$\tau_{e\text{-}ph} = 10$ ps

$\tau_{es} = 3.5$ ns

$\tau_{es} = 38$ ps

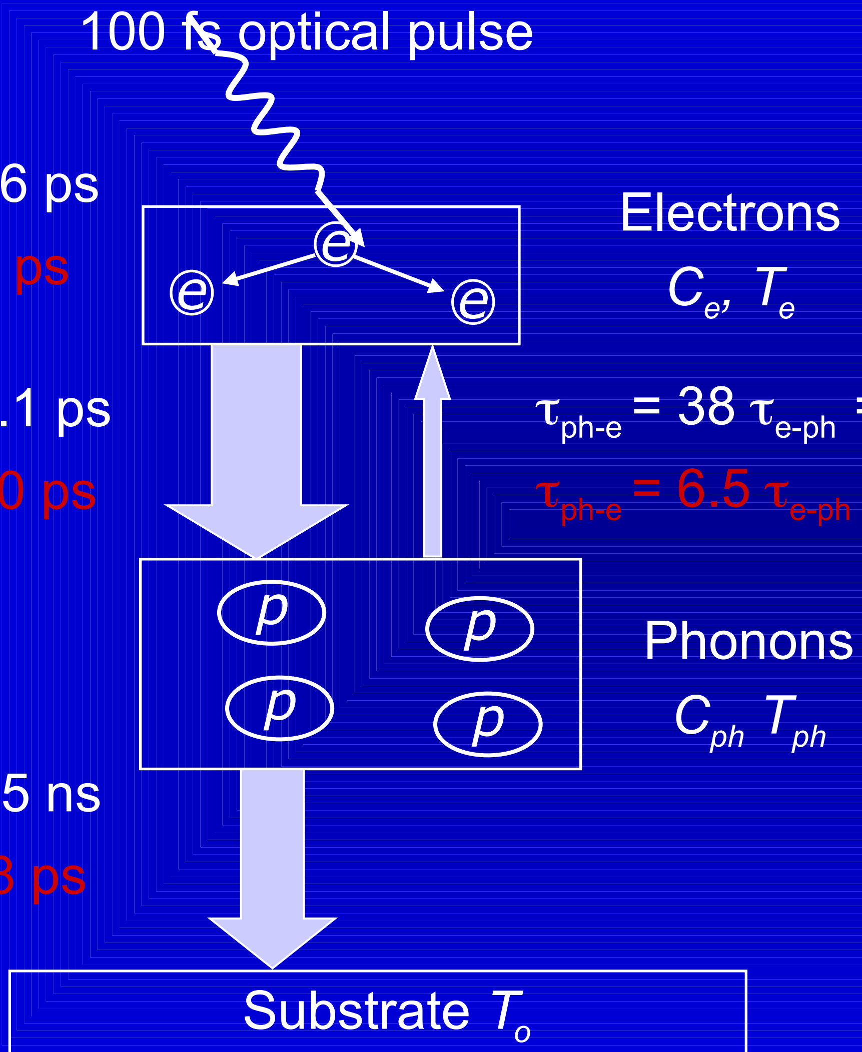

$\tau_{ph\text{-}e} = 38\ \tau_{e\text{-}ph} = 42$ ps

$\tau_{ph\text{-}e} = 6.5\ \tau_{e\text{-}ph} = 65$ ps

$$\frac{dT_e}{dt} = -\frac{T_e - T_p}{\tau_{e-ph}} + \frac{1}{C_e} W(t)$$

$$\frac{dT_p}{dt} = \frac{C_e}{C_p}\frac{T_e - T_p}{\tau_{e-ph}} - \frac{T_p - T_o}{\tau_{es}}$$

$$\tau_{ph-e} = \tau_{e-ph}\frac{C_p}{C_e}$$

M. Lindegren et al., APL 74. (1999) 853

K.S. Il'in et al APL 76 (2000) 2752

NbN-HESP

AFM Image of a 3.5 nm thick NbN-HESP (T_c>10 K)

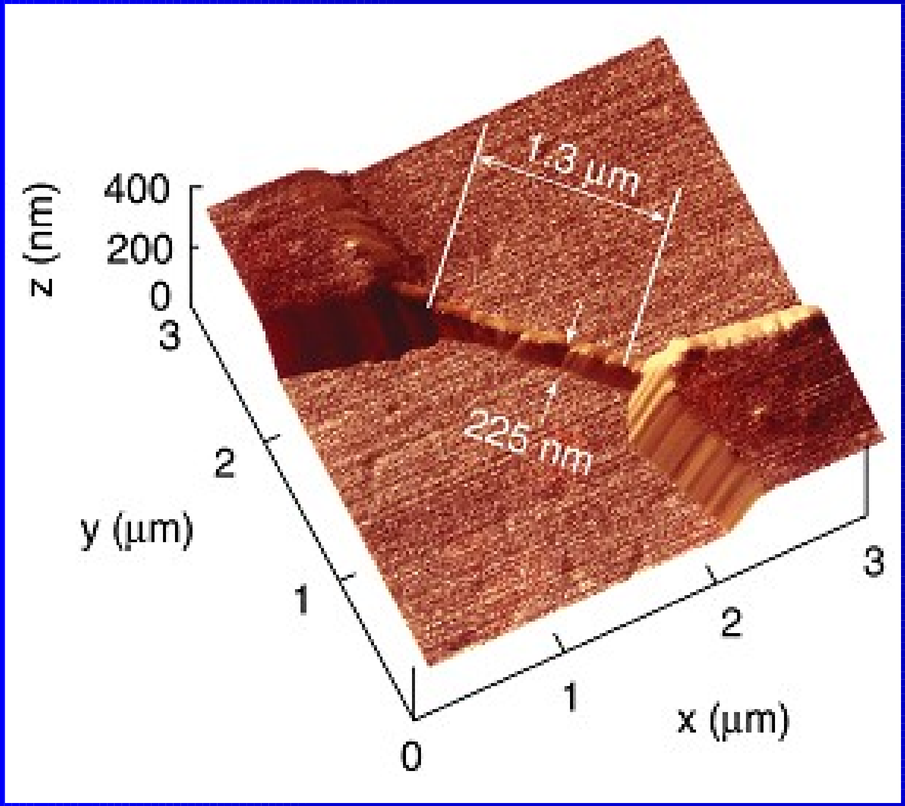

new-generation device for higher efficiency

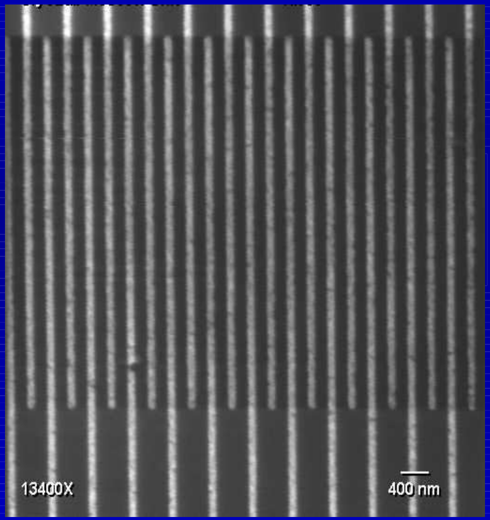

10 µm

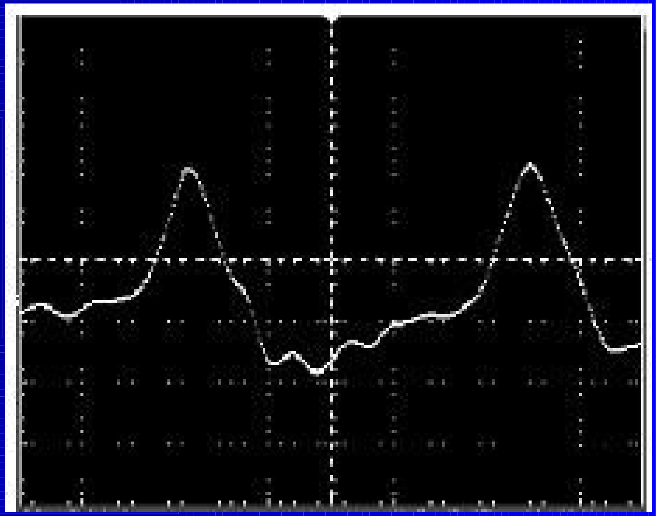

Response to two 810 nm photons x=200 ps Y=100mV

G. Gol'tsman et al., IEEE Trans. Appl. Supercon. (2001) 574
G. Gol'tsman et al., Proc. EUCAS 2003

UNIVERSITY OF ROCHESTER

NbN-HESP

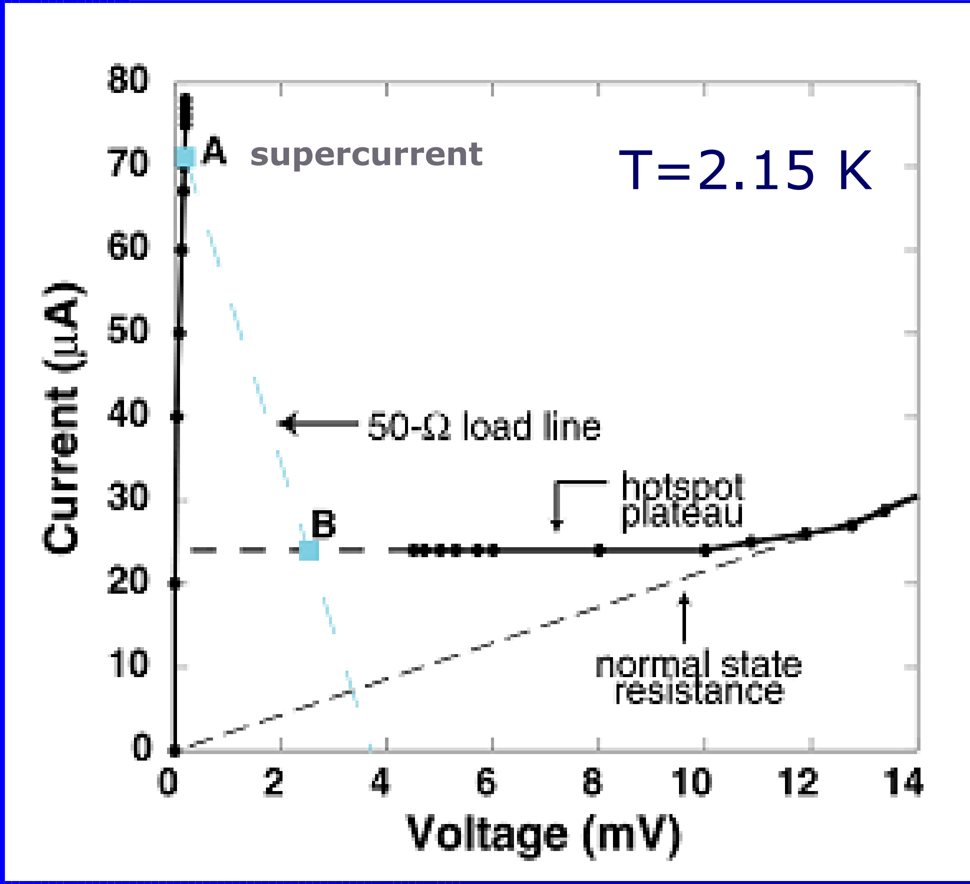

T=2.15 K
A supercurrent
50-Ω load line
B
hotspot plateau
normal state resistance
Current (µA)
Voltage (mV)

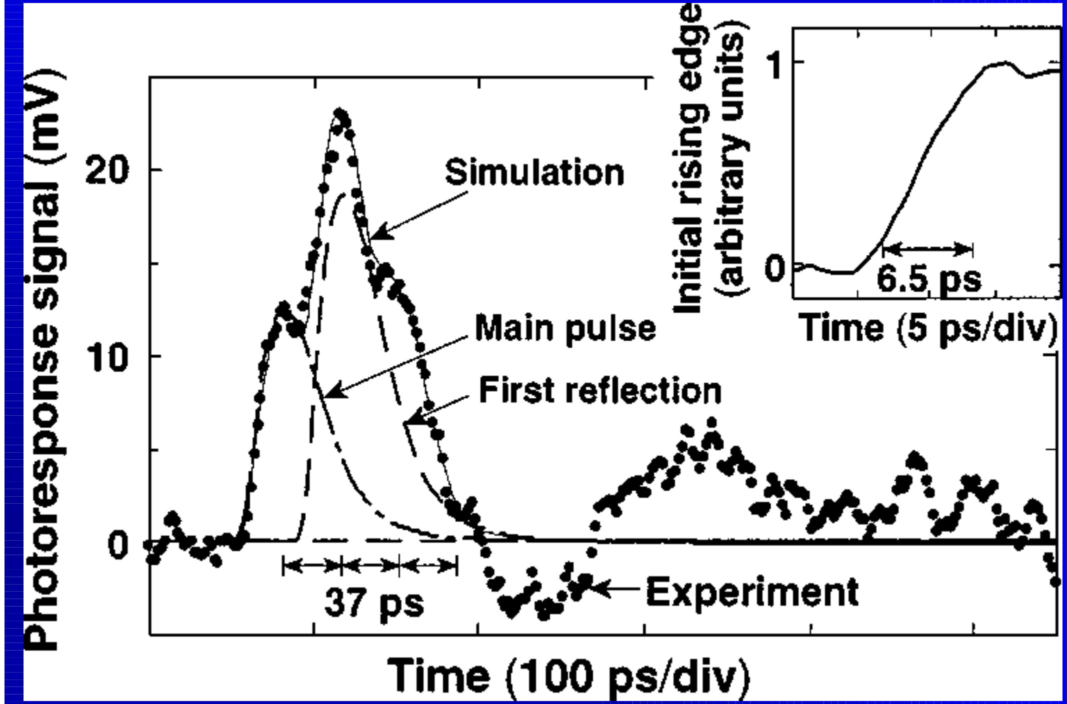

Photoresponse signal (mV)
Simulation
Main pulse
First reflection
Experiment
37 ps
Time (100 ps/div)
Initial rising edge (arbitrary units)
6.5 ps
Time (5 ps/div)

SSPD quantum efficiency

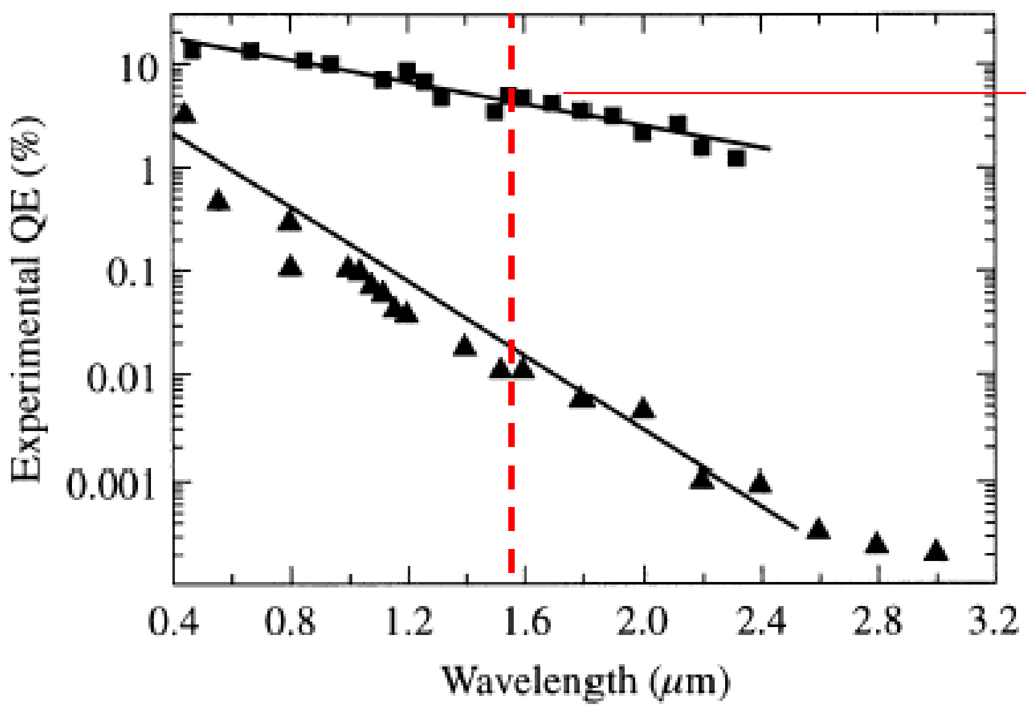

Fig. 7. Spectral dependences of QE for 10 × 10-μm² SSPD's, with NbN stripe thickness of 10 nm (triangles) and 3.5 nm (squares), respectively. The solid lines are guides to the eye, illustrating the exponential dependence of the QE on wavelength.

3% at 1550 nm

Sensitivity = **50 nW** at 10 Gbps

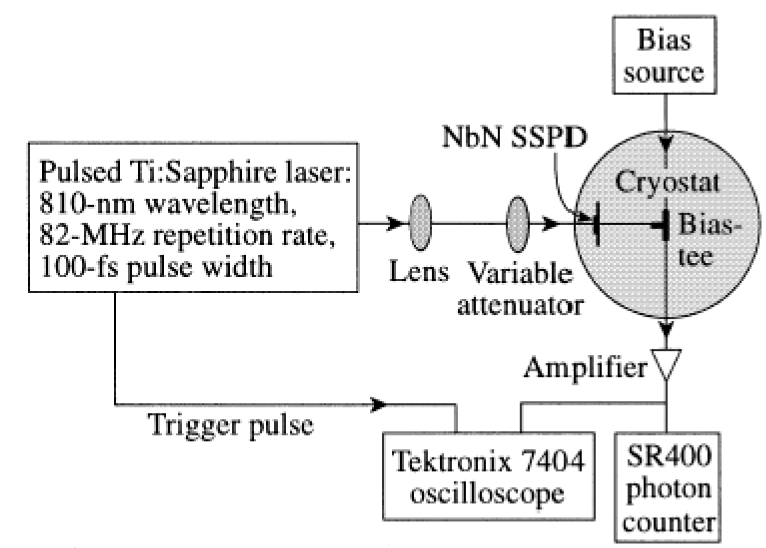

Fig. 4. Experimental setup for a free-space single-photon detection.

See: A. Korneev et al, Appl.Phys.Lett. Vol84,No26,pp.5338-5340 (2004)

Gigahertz Counting Rates of NbN Single-Photon Detectors for Quantum Communications

A. Pearlman, A. Cross, W. Słysz, J. Zhang, A. Verevkin, M. Currie, A. Korneev, P. Kouminov, K. Smirnov, B. Voronov, G. Gol'tsman, and Roman Sobolewski

IEEE TRANSACTIONS ON APPLIED SUPERCONDUCTIVITY, VOL. 15, NO. 2, JUNE 2005

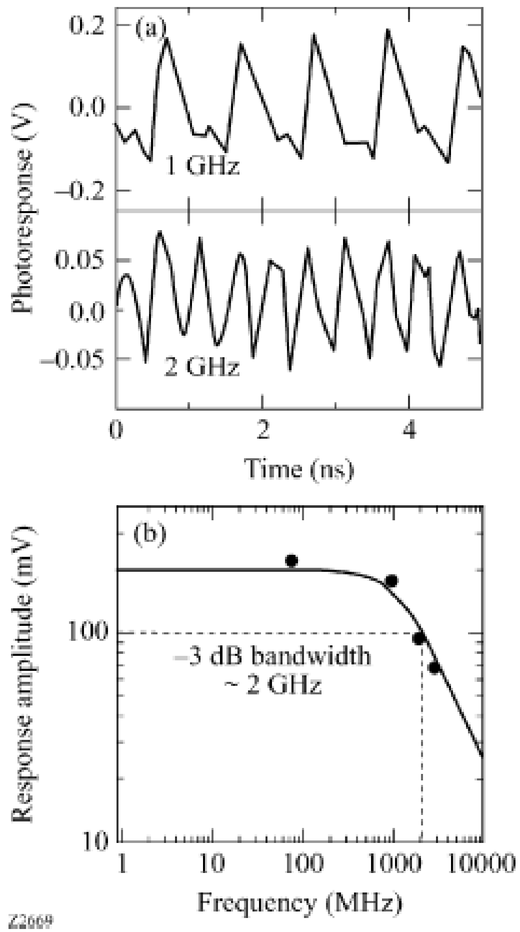

Fig. 1. (a) SSPD photoresponse real-time patterns at 1-GHz and 2-GHz laser pulse repetition rates. (b) Photoresponse amplitude after amplification (dots) at different counting speeds for a SSPD. The solid line represents the fit based on Eq. (1).

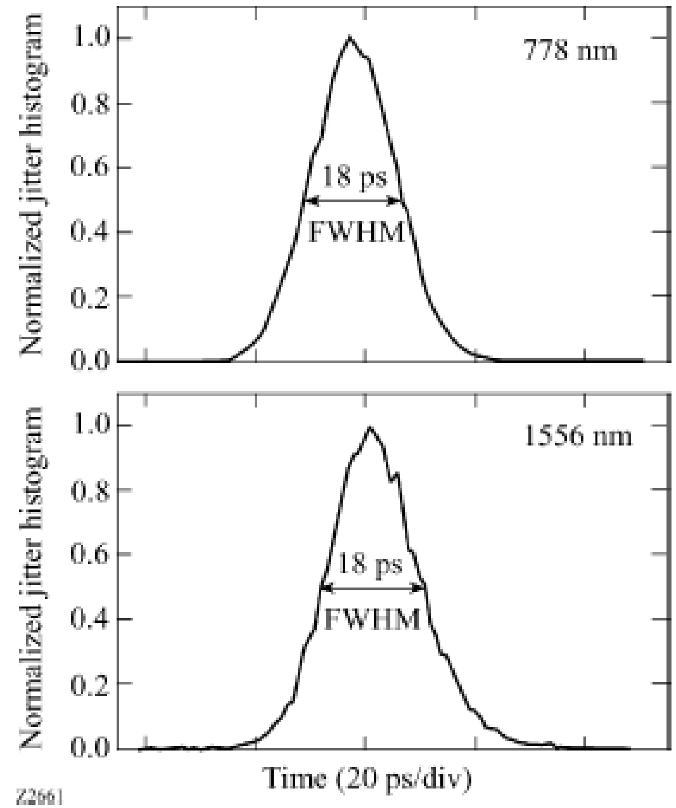

Fig. 2. Jitter measurements of an SSPD illuminated with 778-nm and 1556-nm wavelength optical pulses with 1-GHz repetition rate.

Tunneling between superconductors

Large distances d > 10 nm
no tunneling !!

Intermediate distances
2 < d < 20 nm
quasiparticle tunneling

Small distances
0.5 < d < 2 nm
pair (Josephson) tunneling

$I = I_o \sin\varphi$

$d\varphi/dt = 2e/\hbar\ V$

$d\varphi/dx \sim H$

$I_o(\Phi) = I_c \sin(\pi\Phi/\Phi_o)/(\pi\Phi/\Phi_o)$

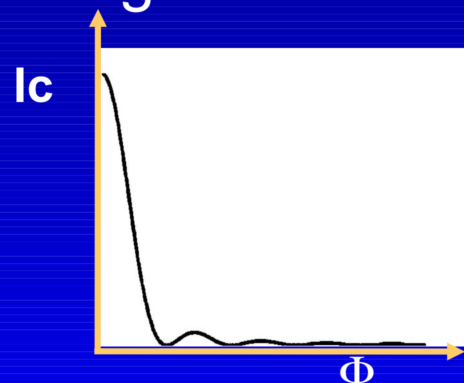

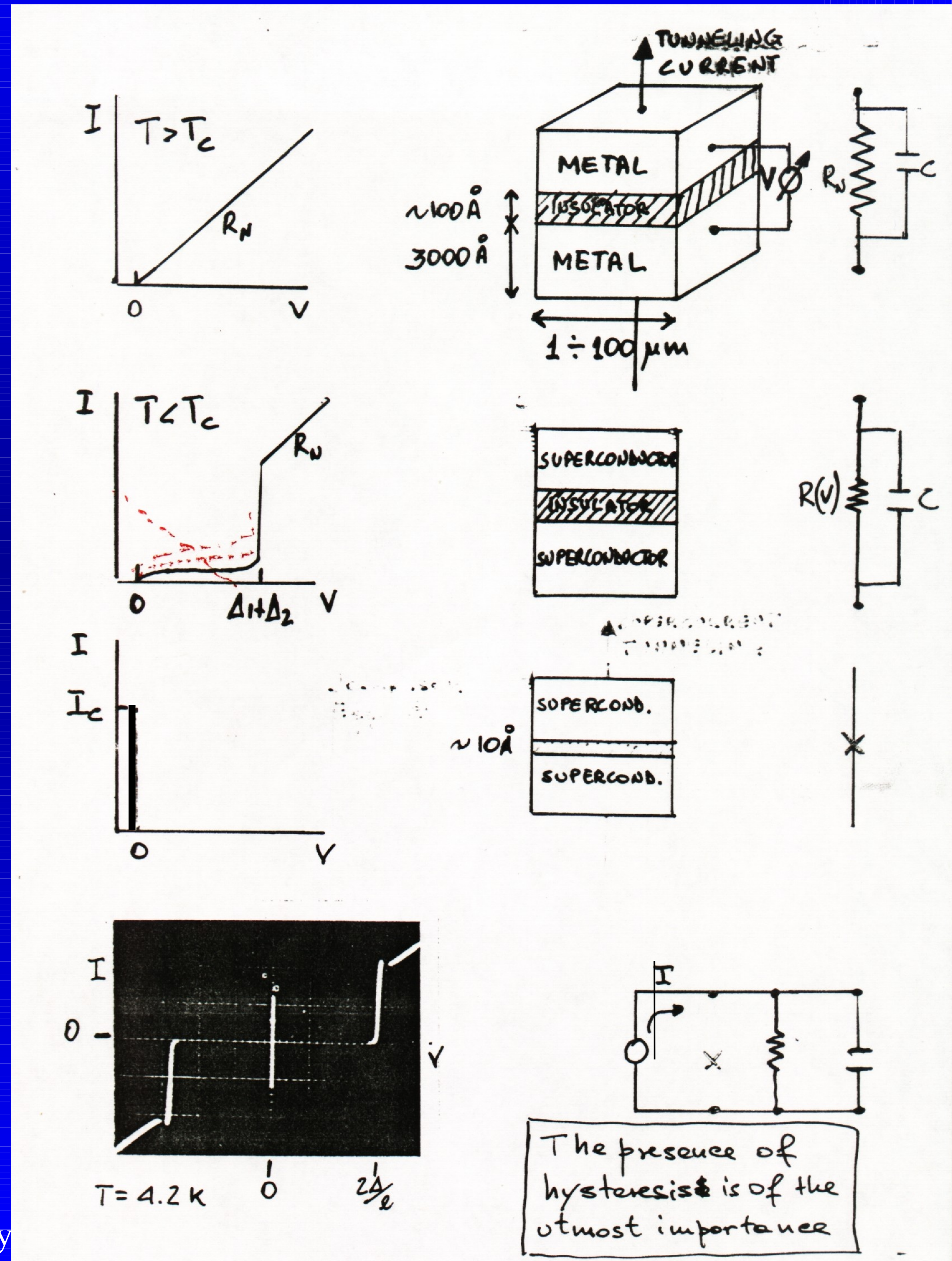

Superconducting Tunnel Junction Detectors

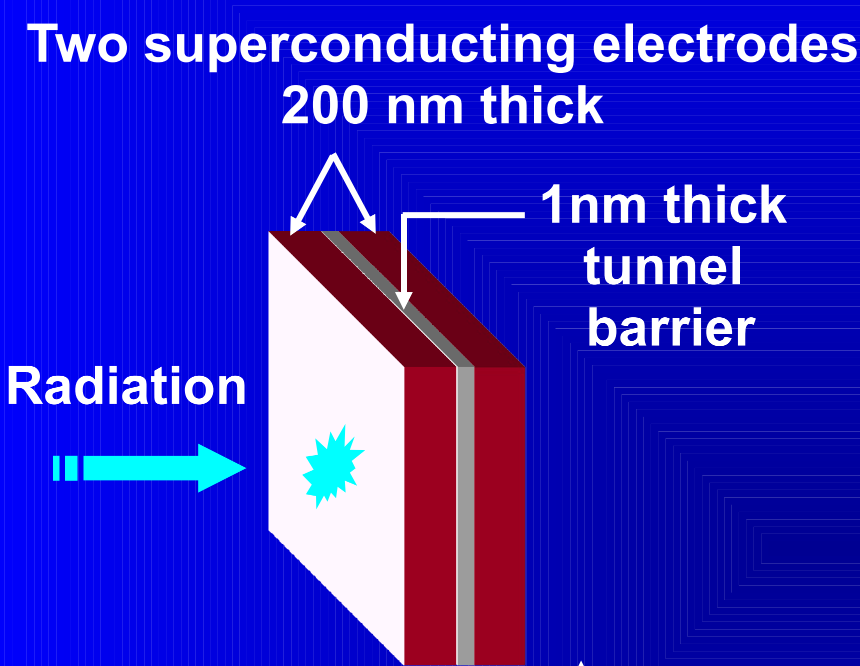

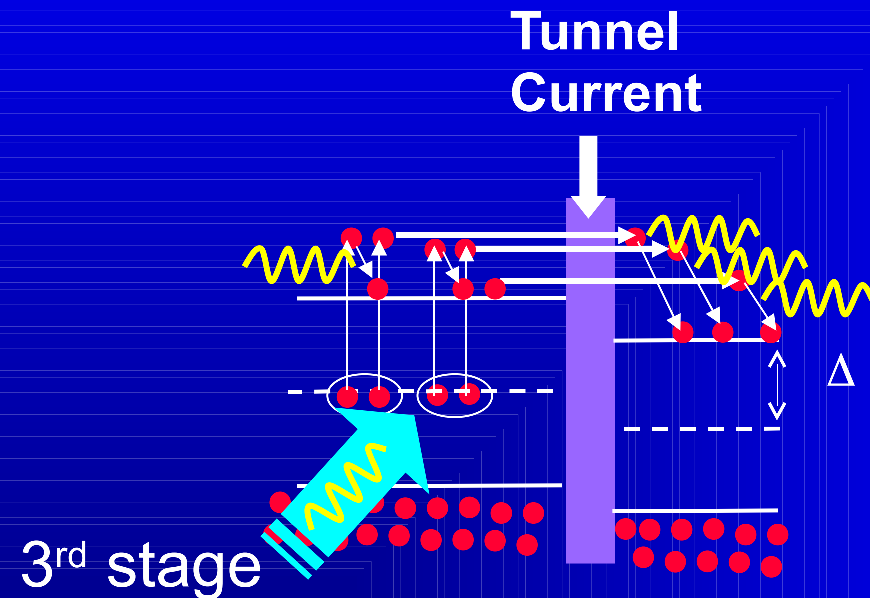

$$E \propto Q = \int I(t)\,dt$$

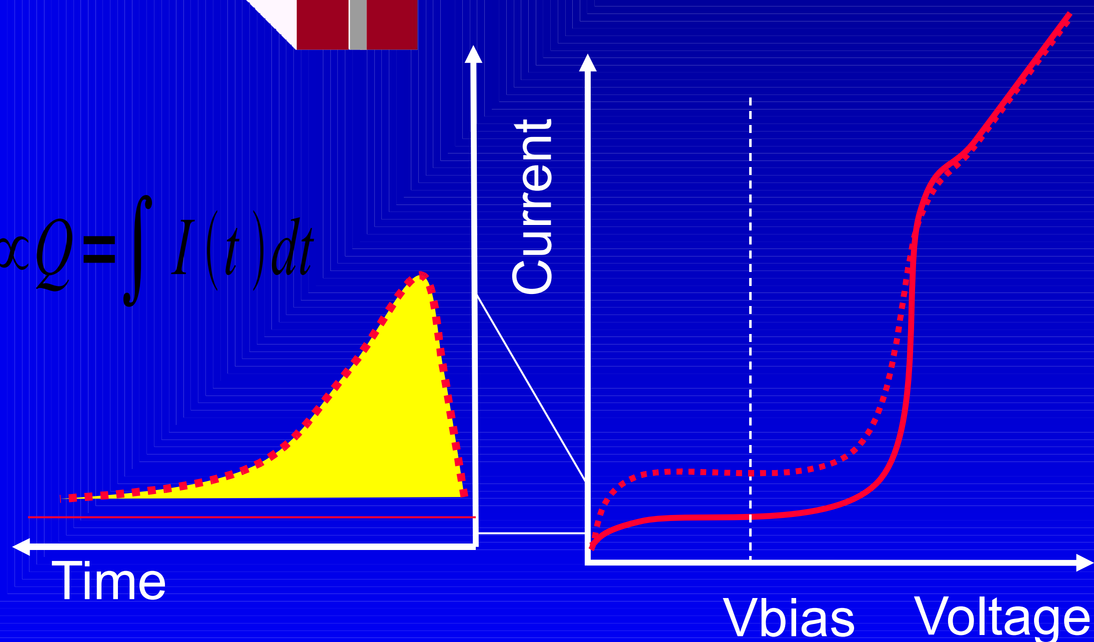

$Q = E/\varepsilon$

$\Delta E = 2.35\,\sqrt{\varepsilon F E}$

$\Delta \approx$ meV $\varepsilon \approx 1.7\,\Delta$

F (Fano Factor) ≈ 0.2

For $E \approx 1$ *keV* $Q \approx 10^6 e$

$\Delta E \approx 3\text{-}4$ eV

high energy resolution

Readout Circuit

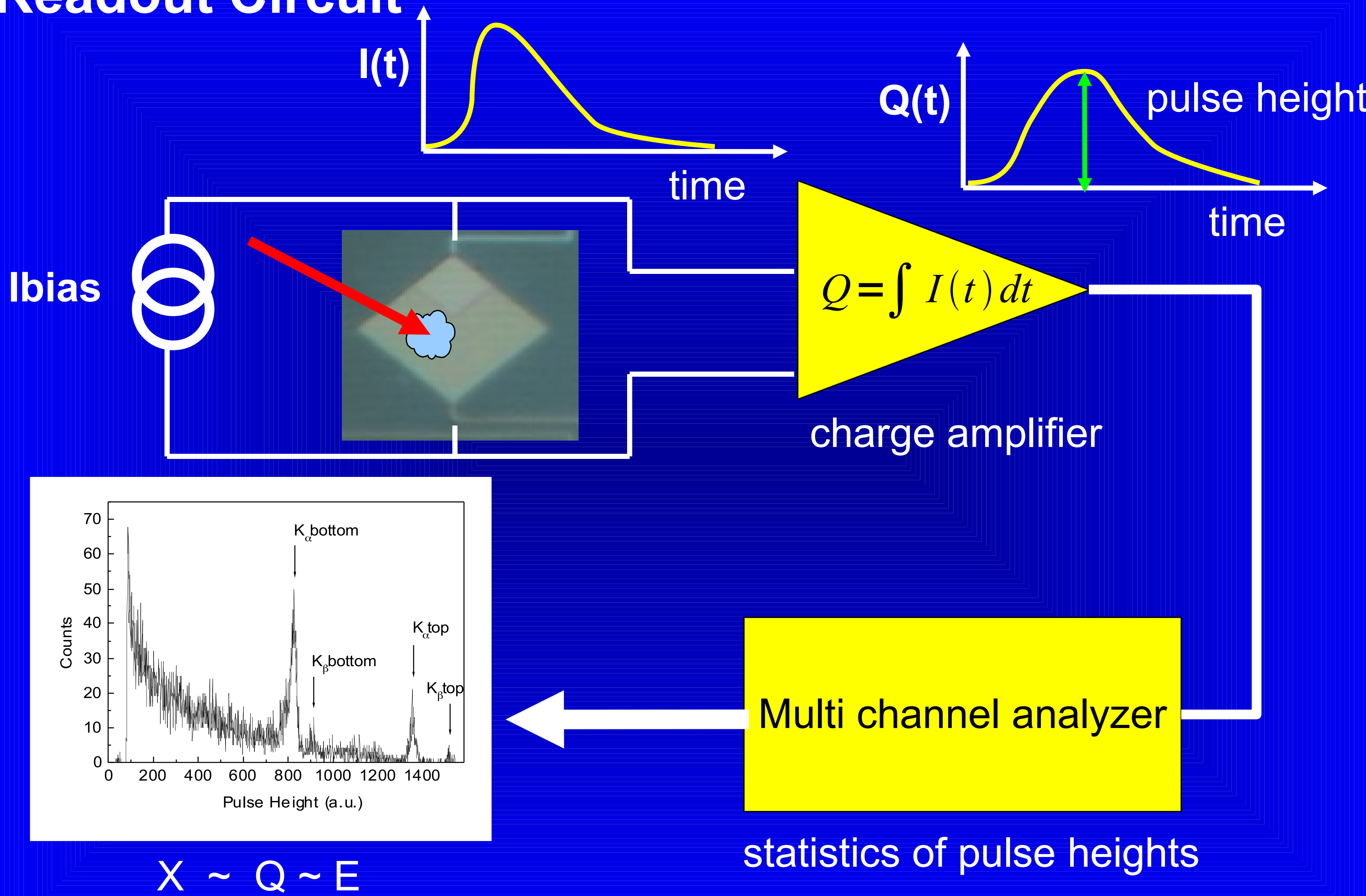

STJ: Suppression of the Josephson Effect

To perform as STJ-detector, the junction is polarized in the quasiparticle branch of the I-V curve.

The Josephson effect (Josephson current and resonances) in this context is a disturbing feature which has to be suppressed.

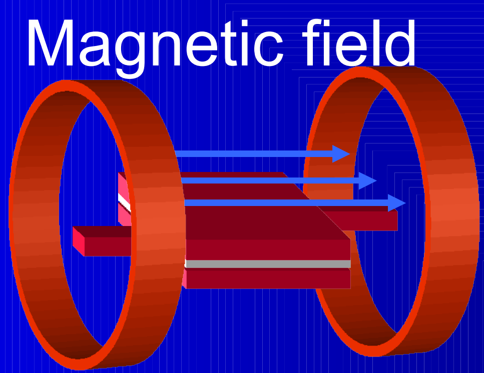

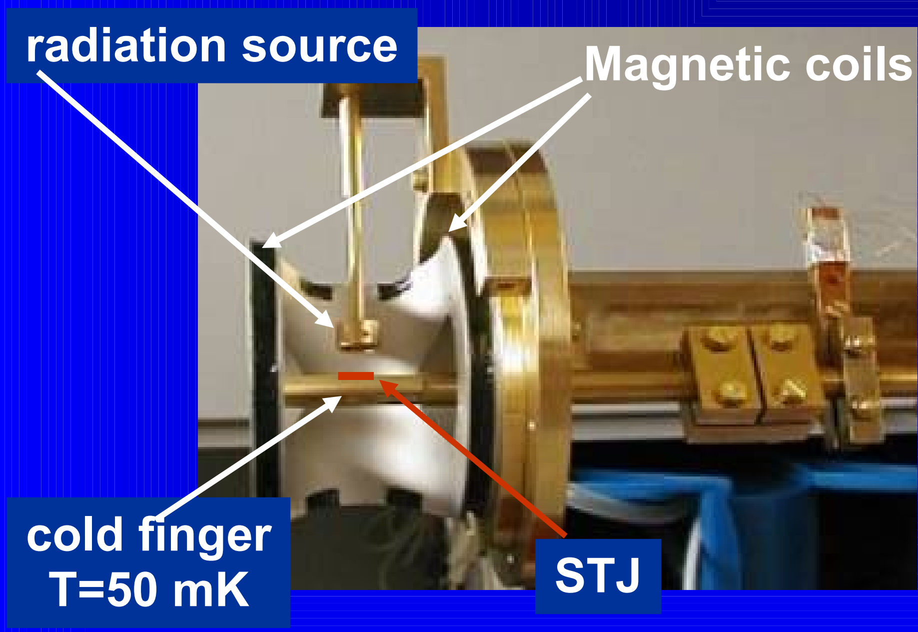

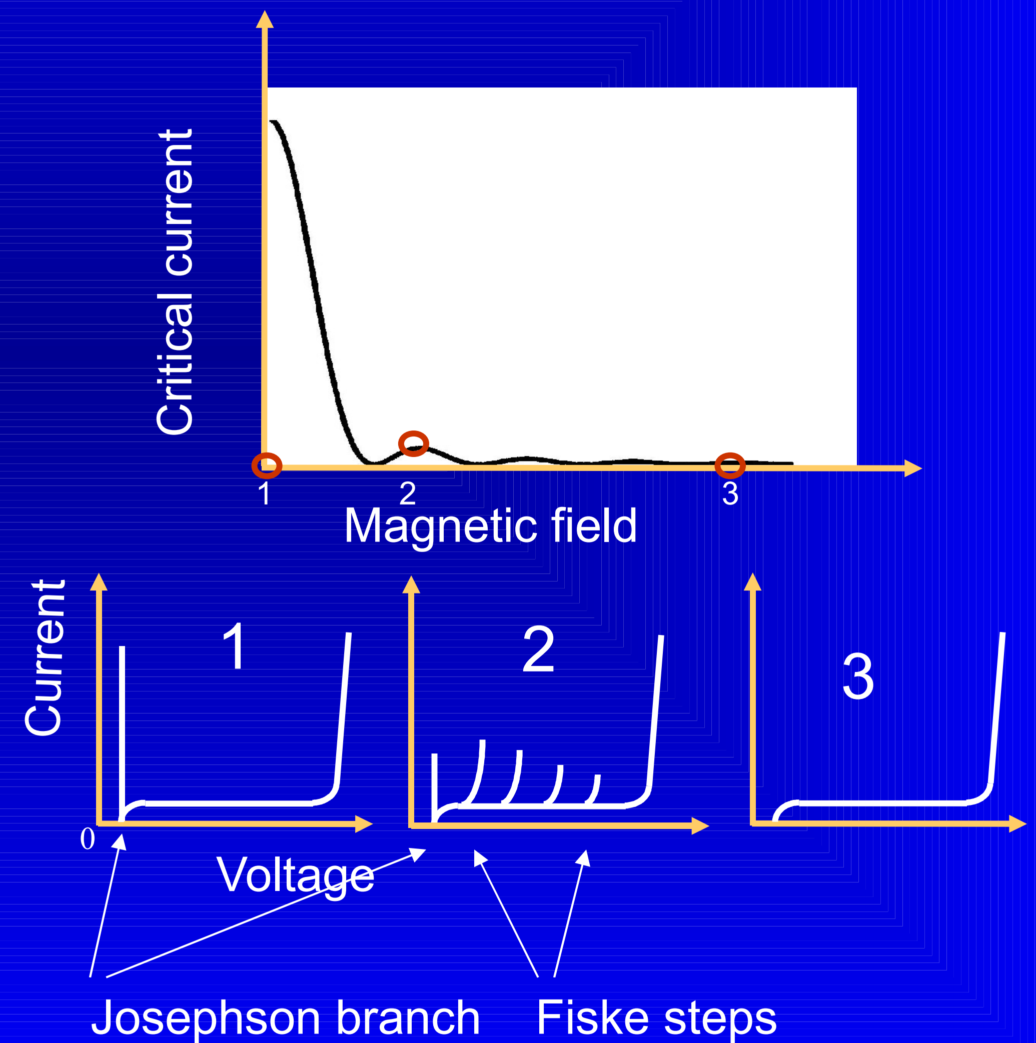

Detector Test Chip

Nb/AlOx/Nb technology
240 STJ detectors
2 x 100 juncion arrays
different geometries and sizes

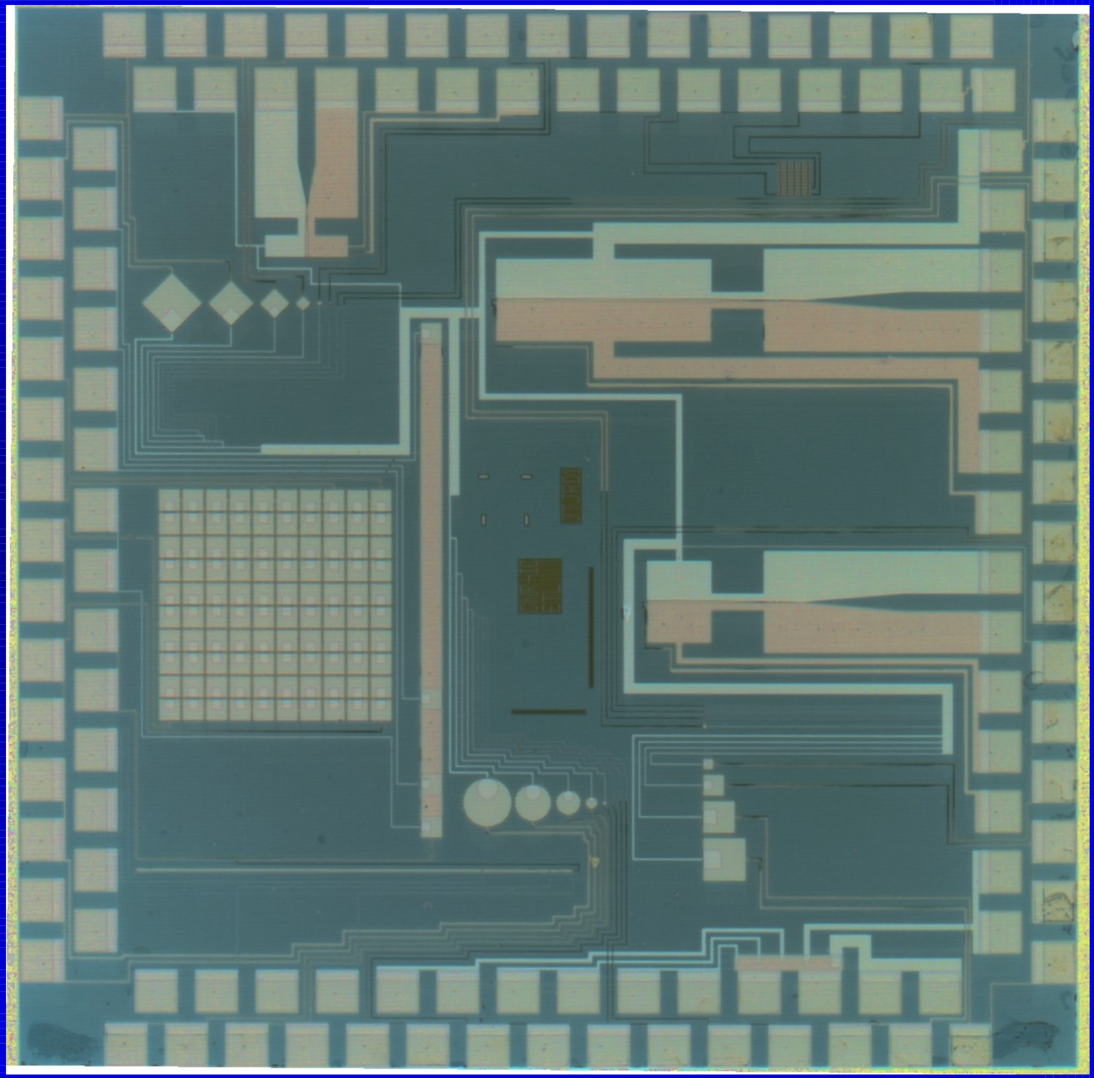

Naples-Tsukuba 1992

Annular STJ detector: results from CNR-ICIB and University of Naples

Suppression of the Josephson effect by trapped magnetic flux

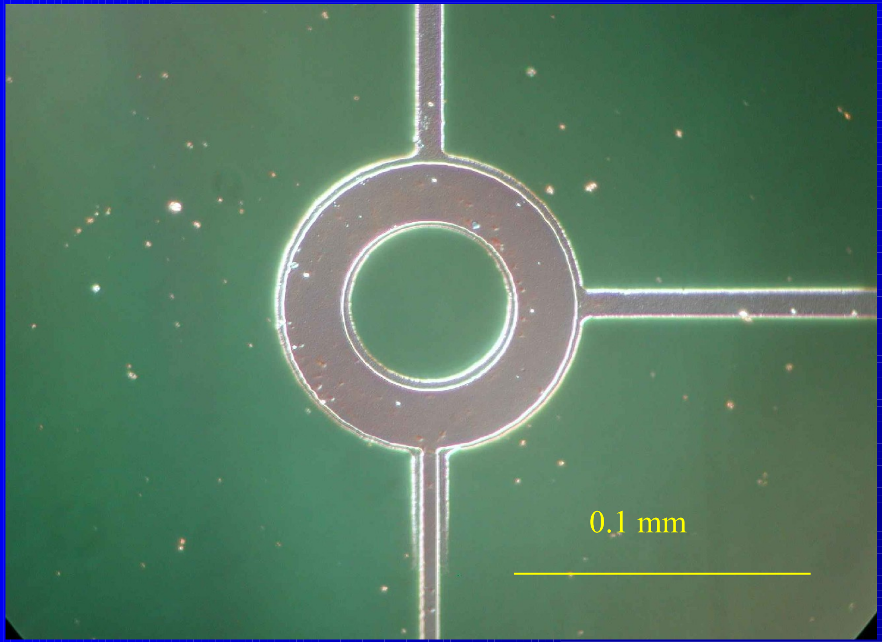

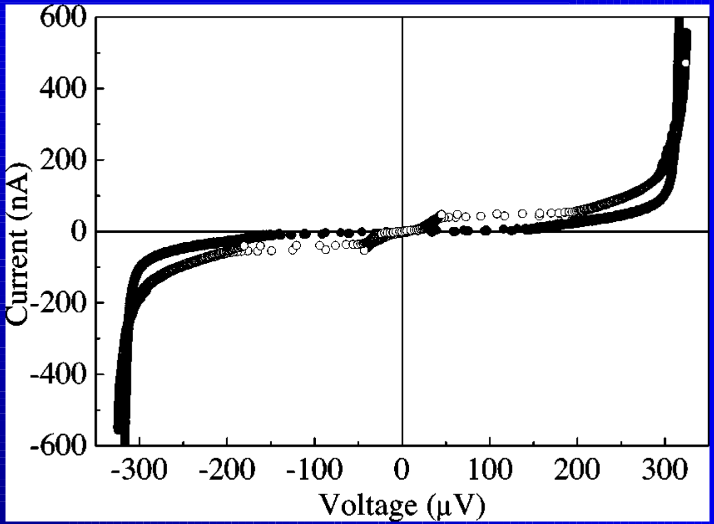

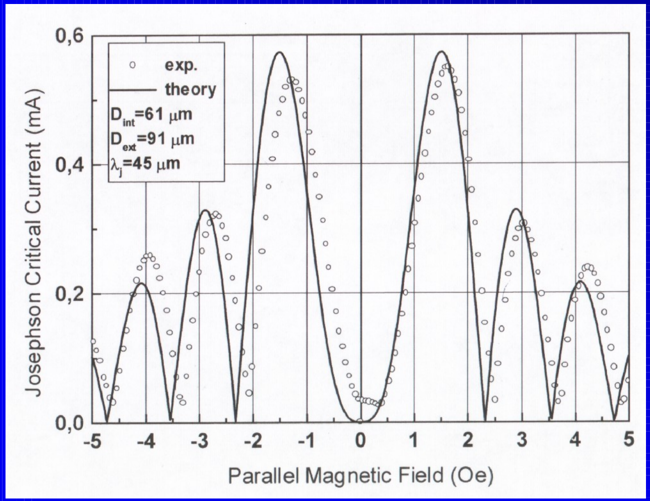

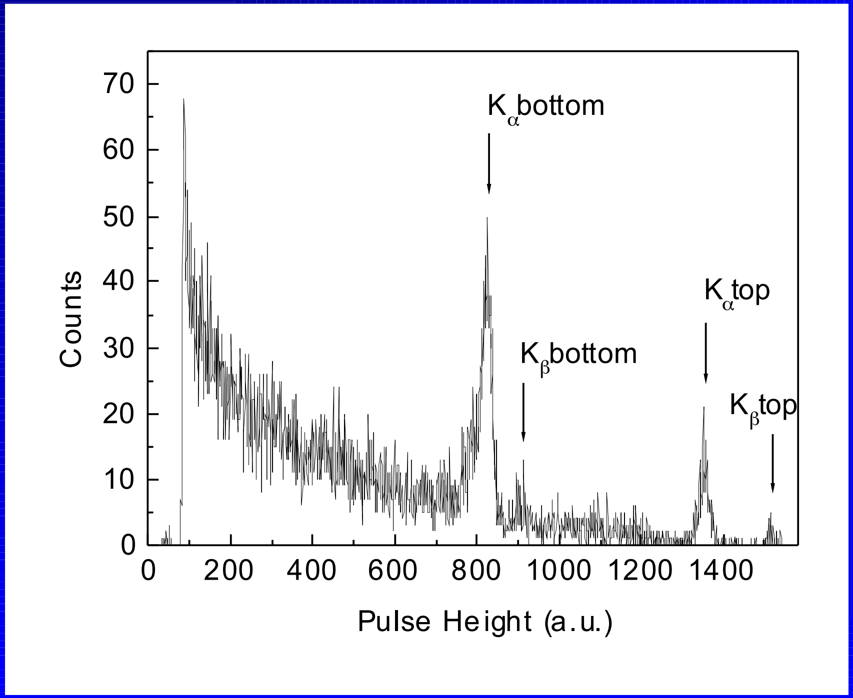

M.P. Lisitskiy et al., APL 84 (2004) 5464

STJ detectors: results from Technical University Munich

Al-STJ ΔE=12eV at E=5.89keV

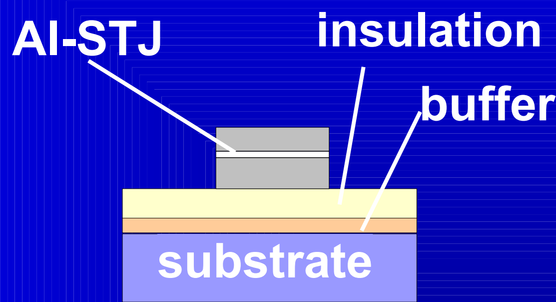

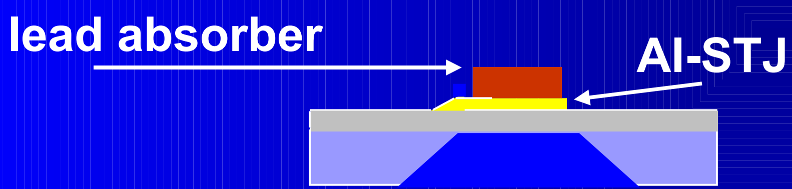

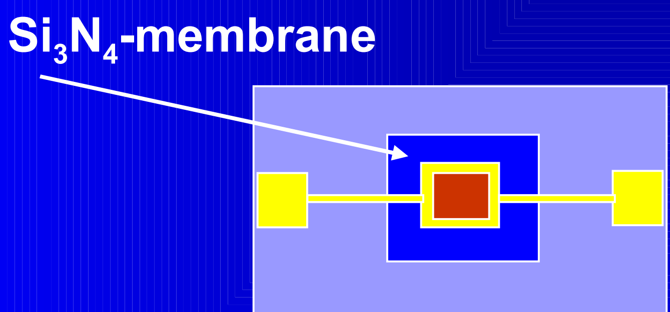

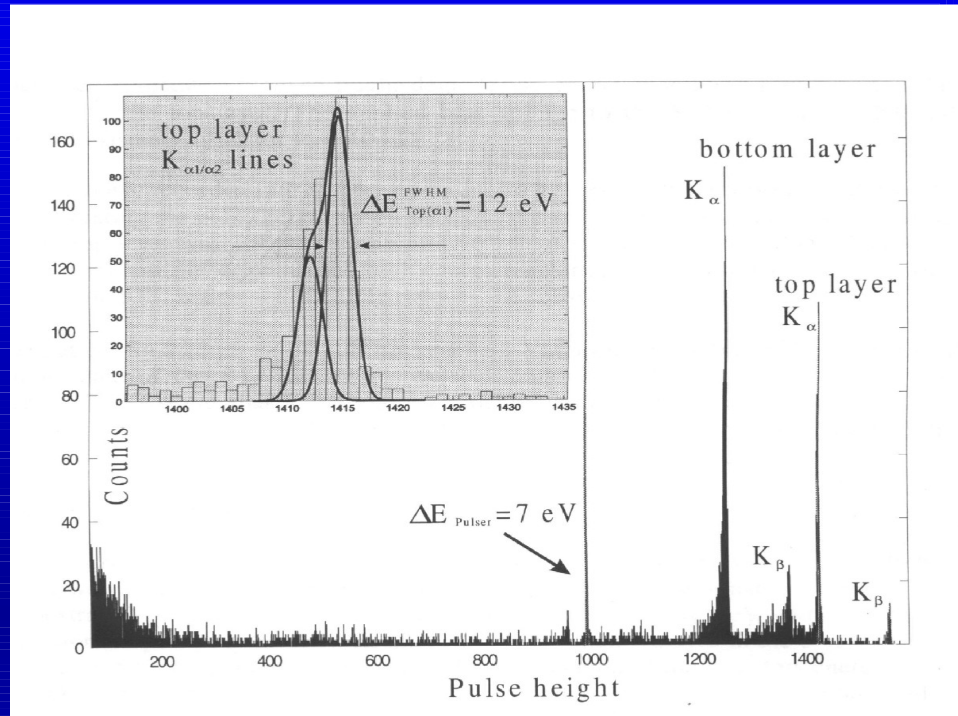

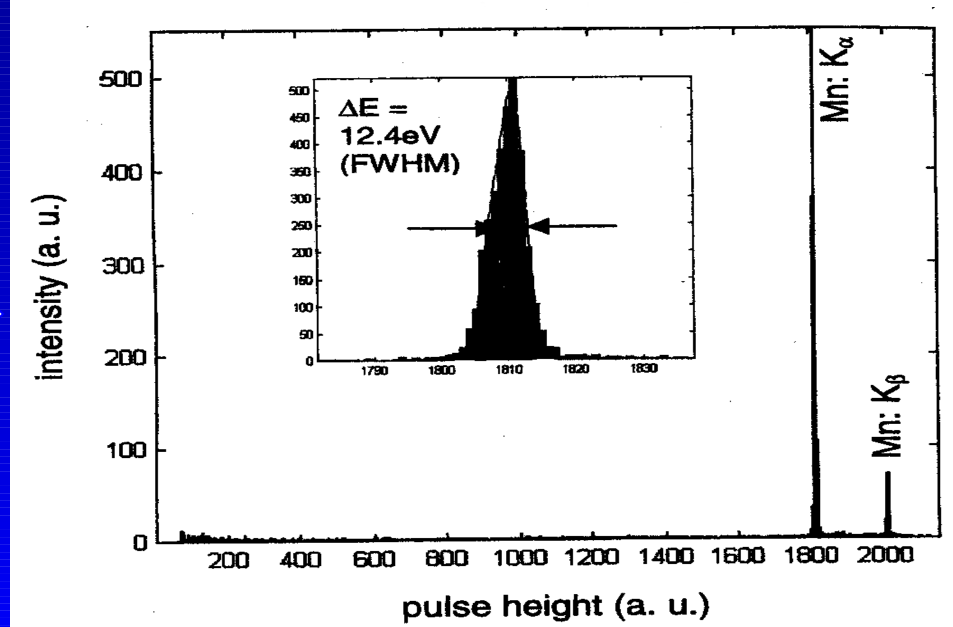

G. Angloher *et al.*, JAP 89 (2001) 1425

STJ Imaging devices: results from CNR-ICIB

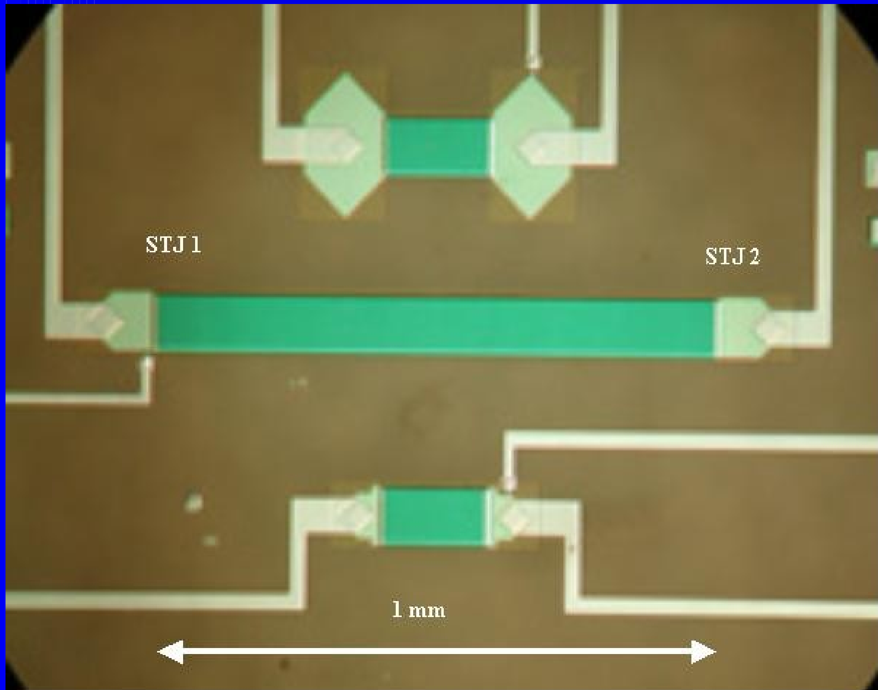

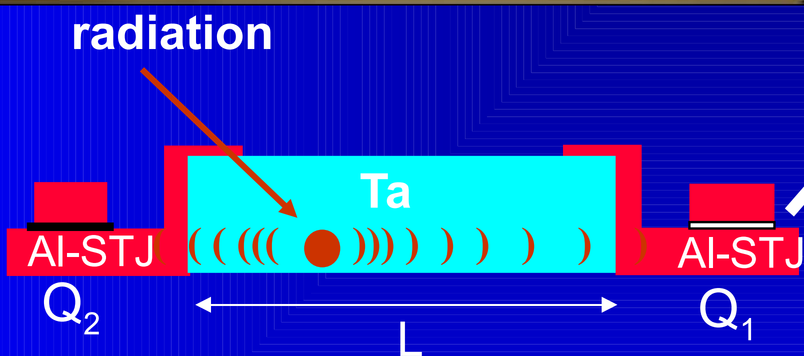

energy

$$Q_1 + Q_2 \propto \frac{E_{photon}}{\Delta_{Ta}}$$

position

$$\frac{Q_1}{Q_1 + Q_2} \sim x$$

Al-STJ with epitaxial Ta absorber

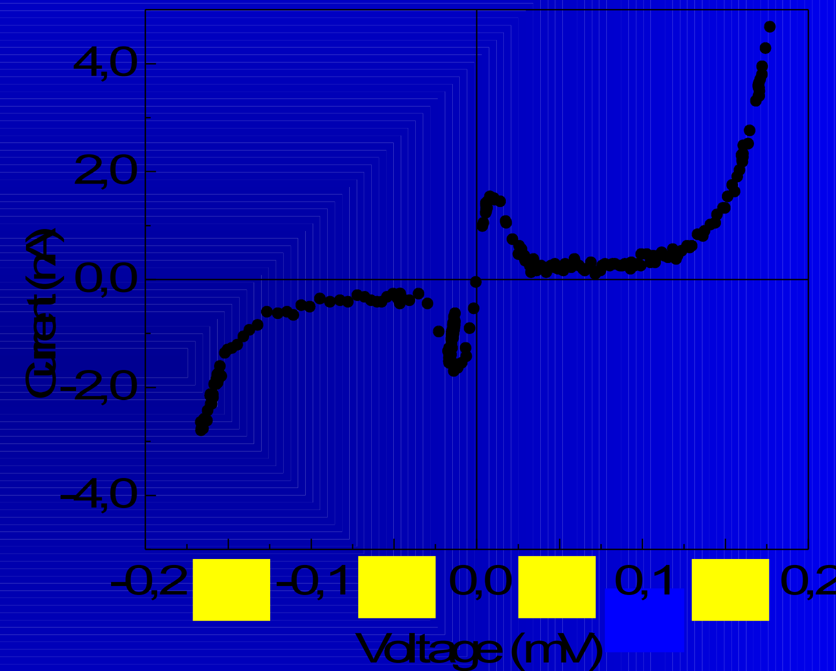

STJ Area = 64 μm²
J_c = 15 A/cm²
$R_N A$ = 1.65x10^{-5} Ω cm²
T = 50 mK
R_d = 370 k Ω

STJ Imaging devices: results from YALE University

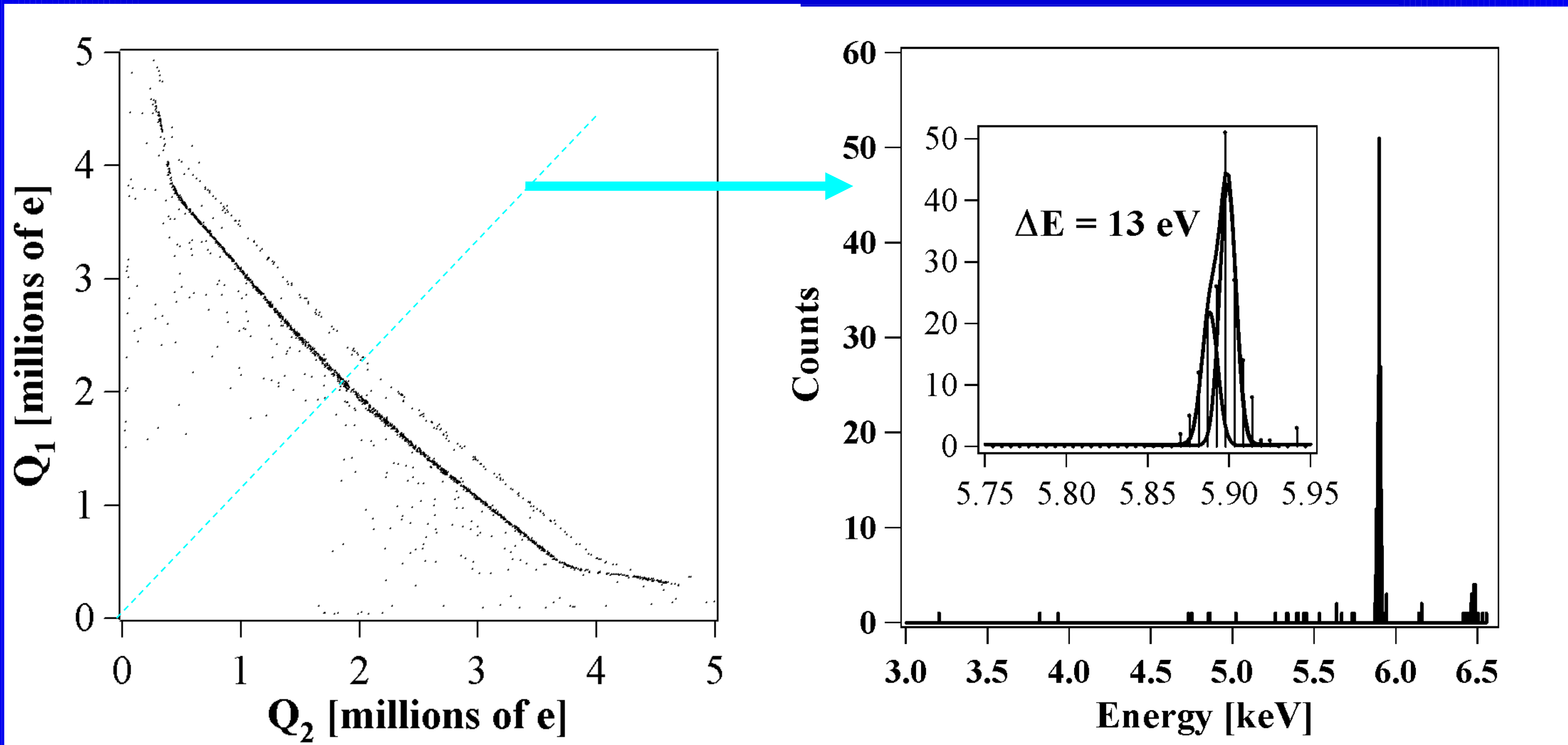

L.Li et al, IEEE on Appl. Supercon. 11(2001) 685

STJ Performances

group	STJ	Configuration	ΔE (eV) @ 6keV
TUM Munich	Al	Stacked Pb-absorber	12
Yale Univ. USA	Al	DROID with lateral STJ	13
LLNL USA	Nb/Al	Stacked STJ	23
ESA	Nb/Al Ta/Al	Stacked array and DROIDs	26
CNR Naples	Al Ta/Al	STJ and DROID with lateral STJ	40
Riken Saitama J	Nb	Stacked STJ	41
PSI Villigen CH	Ta/Al	Stacked DROIDs	60

Common characteristics

Response time few μsec

Counting rate > 10^4 cps

Temperature 100mK (1.2 K)

Josephson Fast Particle Detector

Application: (Barone & De Stefano – NIM 84)

LHC Interbunch ~ 25 ns

Others?

VIRTUES

- Fastest response $\tau_{sw} < 1$ psec
- Digital output 0 - 3 mV
- Simple interface with JJ circuitry RSFQ – LATCHING
- Low radiation damage

Permanent Tested with proton beam

E=6.5 MeV flux= 10^{16}p/cm^2 dose= 5 $\cdot 10^3$ M Rad

semiconductor damage threshold ~ 10 M Rad

FAULTS

- Energy Threshold → JJ dimension (~ 5x5 μm^2)

⇒ arrays ; J_c uniformity

- Magnetic field sensitivity (local shielding)

Radiation damage

Nb/ALOx/Nb detector chip
sequence of irradiations
with 6.5 MeV proton
max dose up 5 GRad

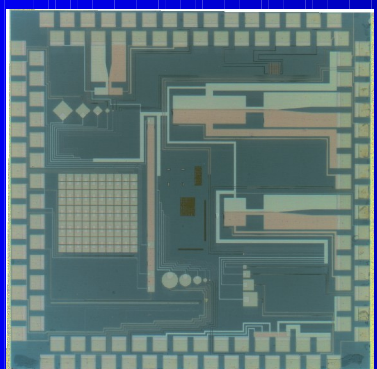

CNR ICIB – ETL Japan 1992

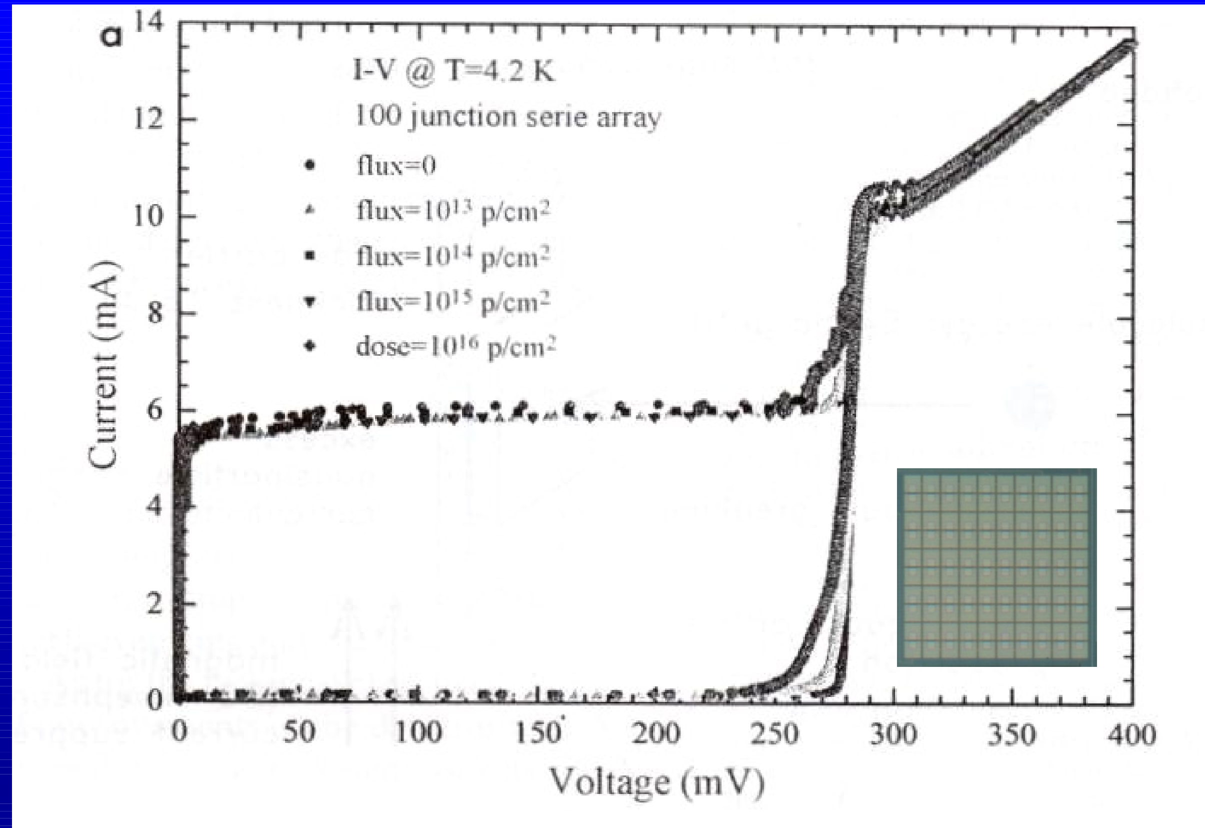

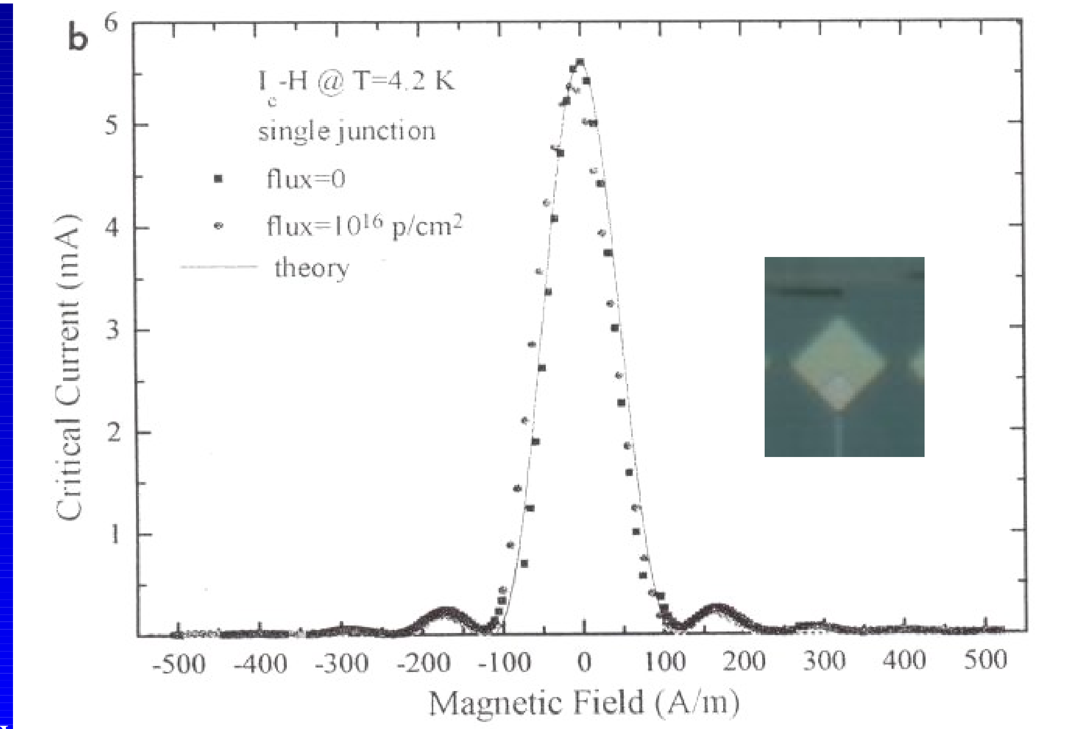

NO SIGNIFICANT DAMAGE

The Superconducting Single Photon Detector

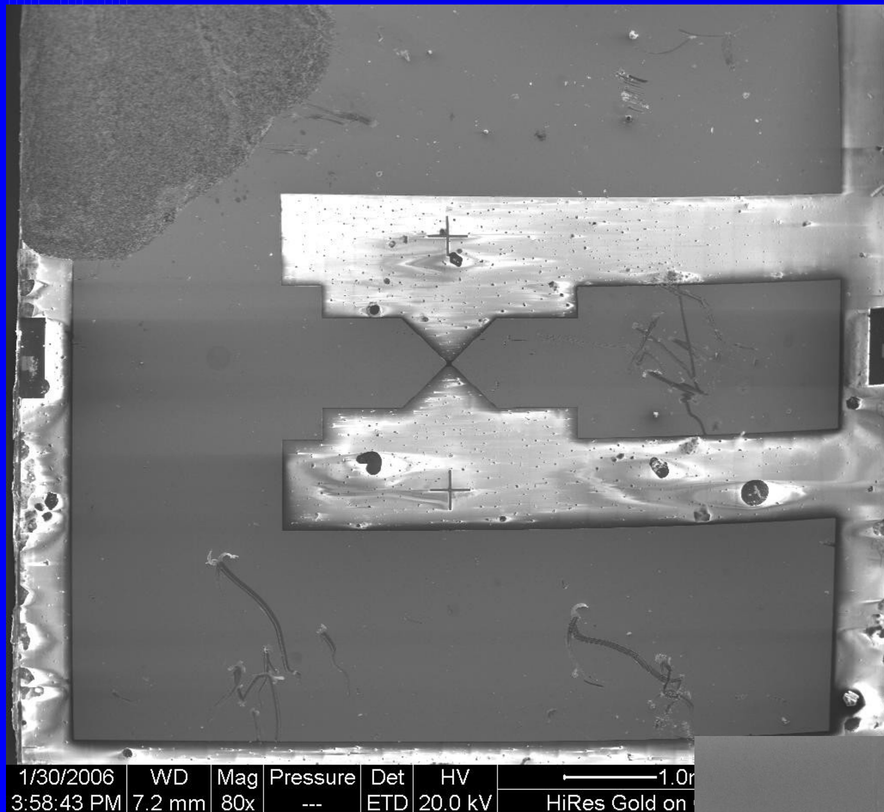

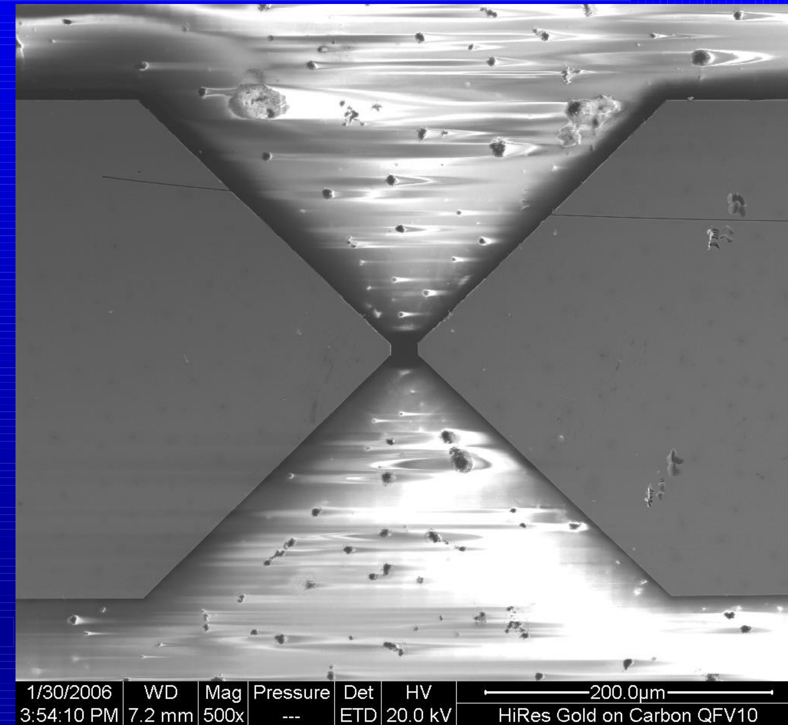

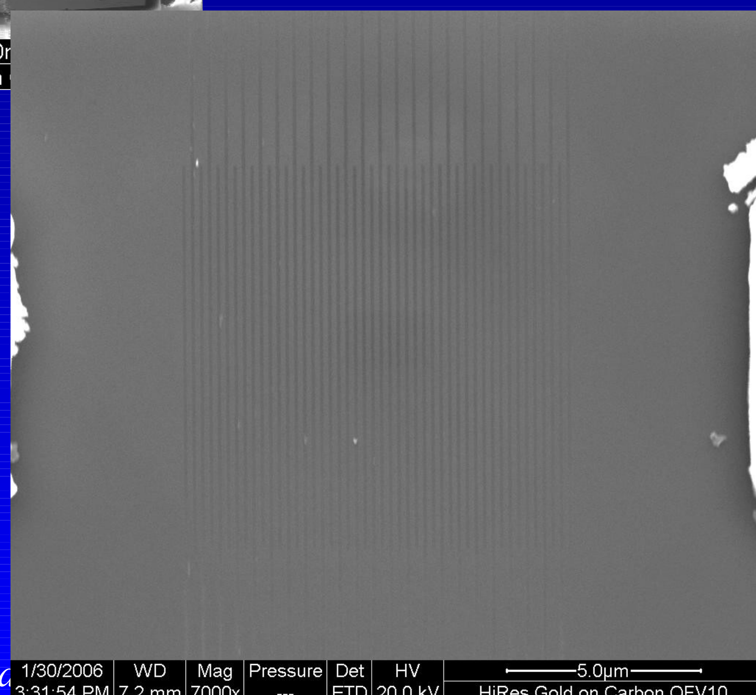

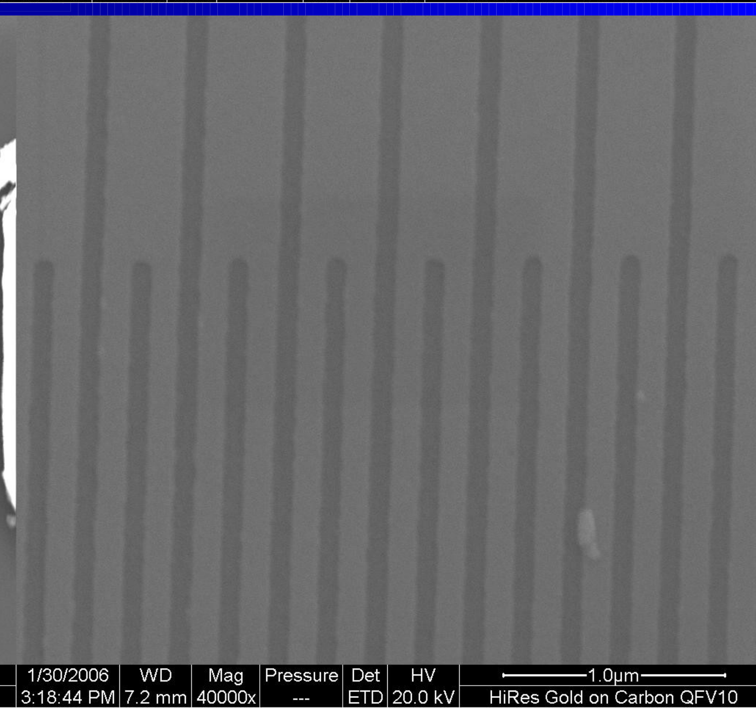

NbN strip detectors developed at CNR-ICIB

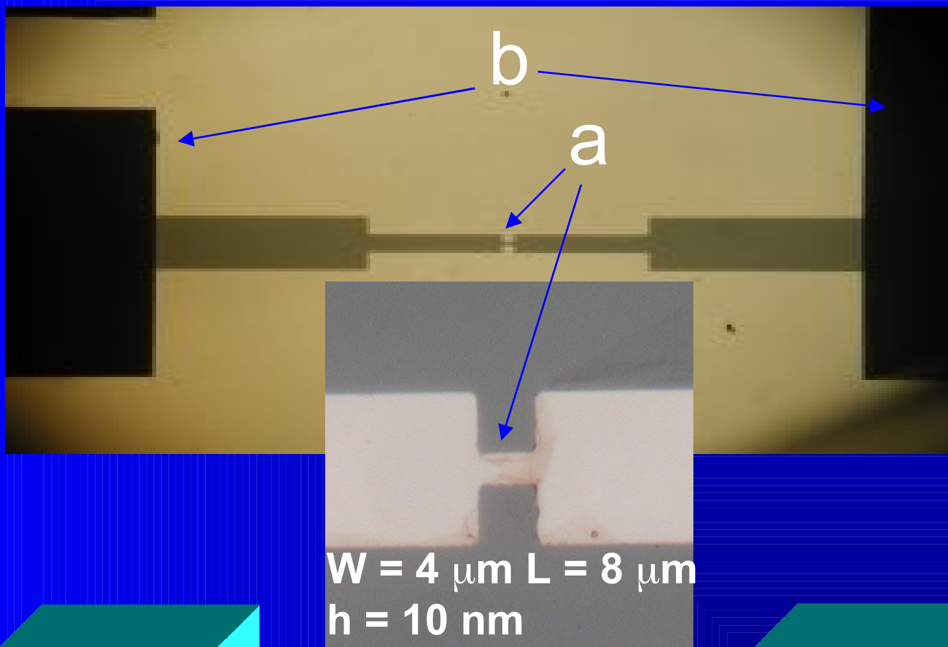

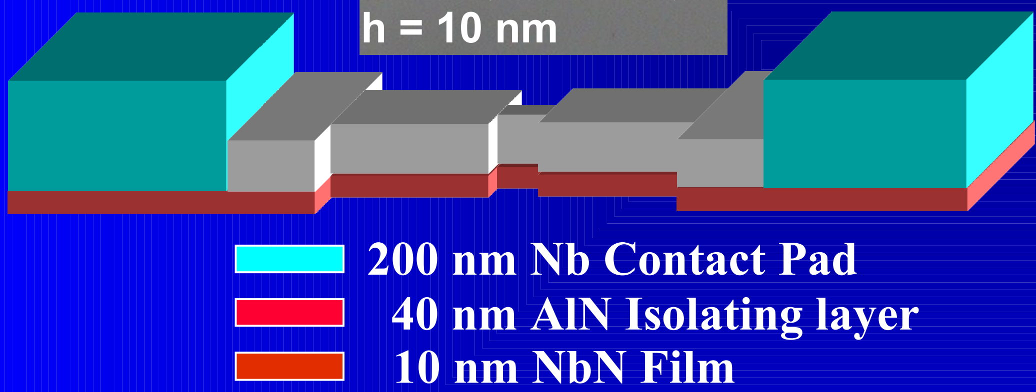

Photograph of a NbN strip detector:
(a) active part of the detector (W = 4 μm and L = 8 μm),
(b) (b) Nb contact pads

Room temperature deposition process

Substrate	Ptotal mtorr	P_{N2} %	Power W	Thick nm	Tc K	RRR
Al_2O_3	1.5	12	500	100	14.4	0.89
MgO	1.5	12	500	100	15.5	0.97

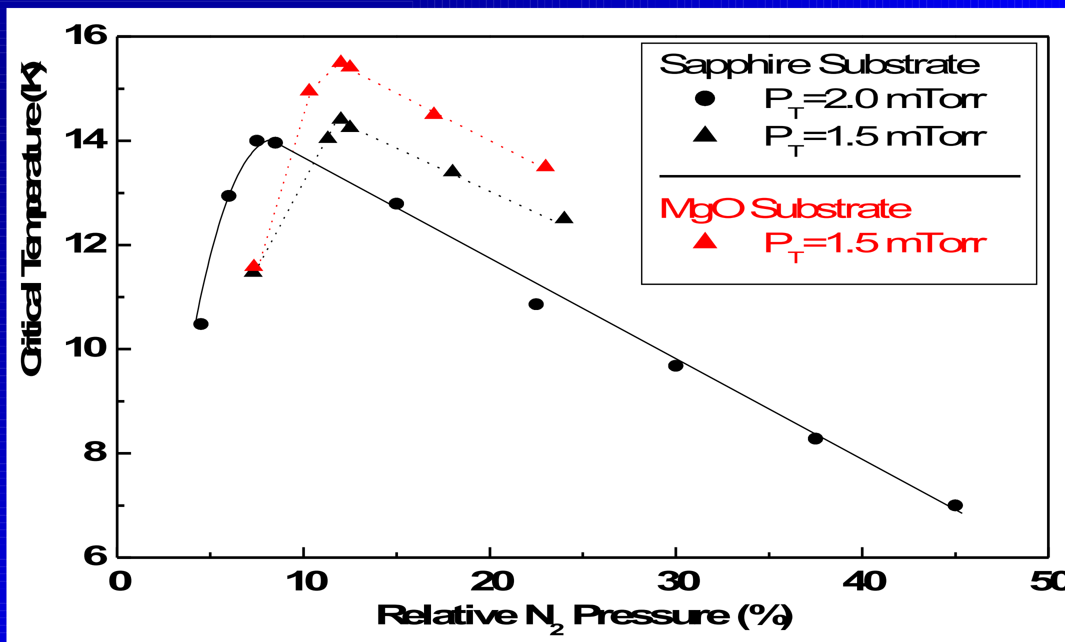

Critical temperature of 100 nm thick NbN films as a function of partial pressure of N_2 on substrates of Sapphire and MgO.

dc response

unshunted strip

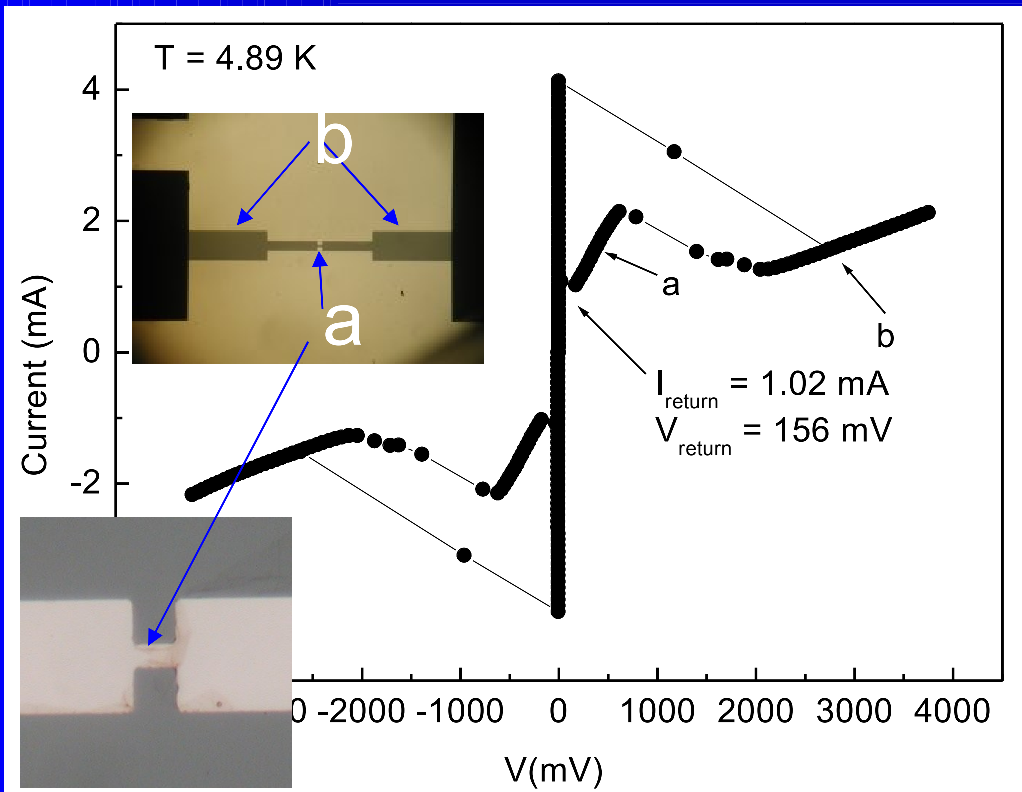

Current-voltage characteristics,
a) S/N the transition of the active part of the detector
b) S/N transition of the whole structure

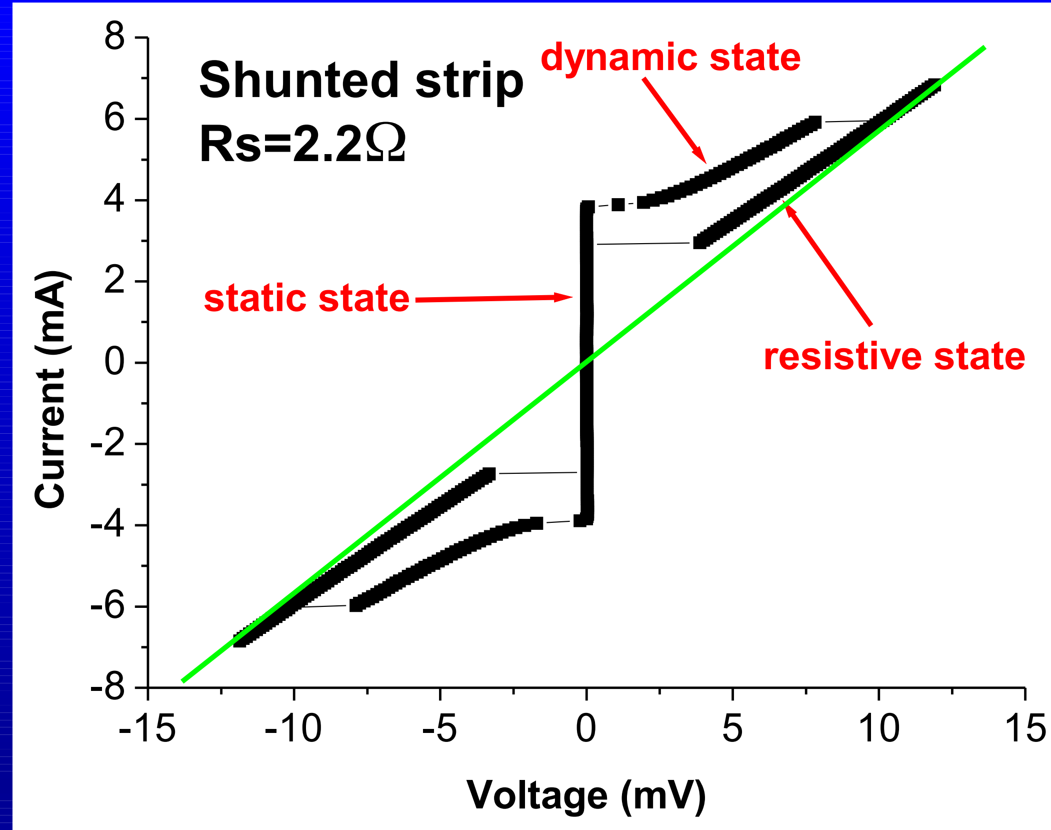

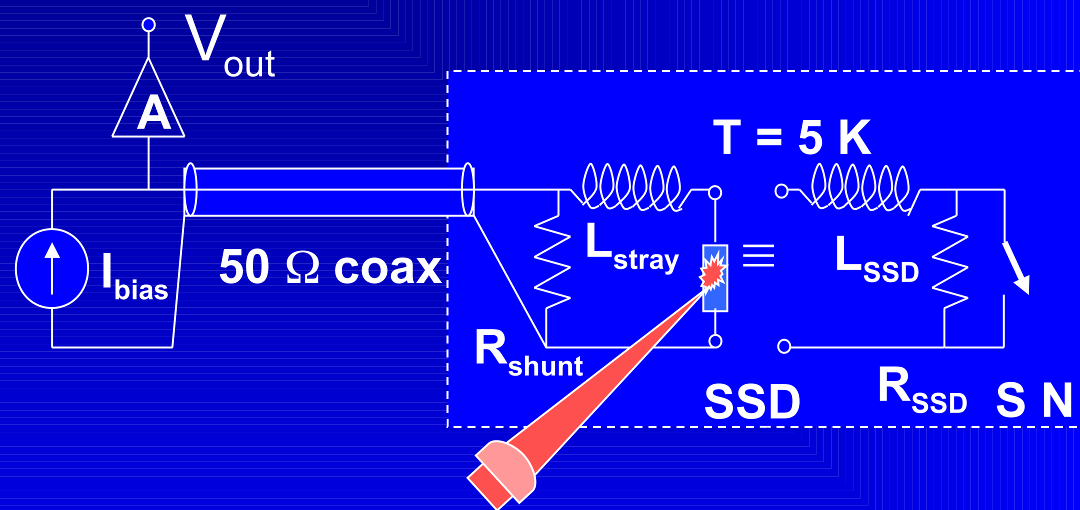

Optical pulse

Equivalent circuit of the detector and the bias read-out electronics

Laser induced response

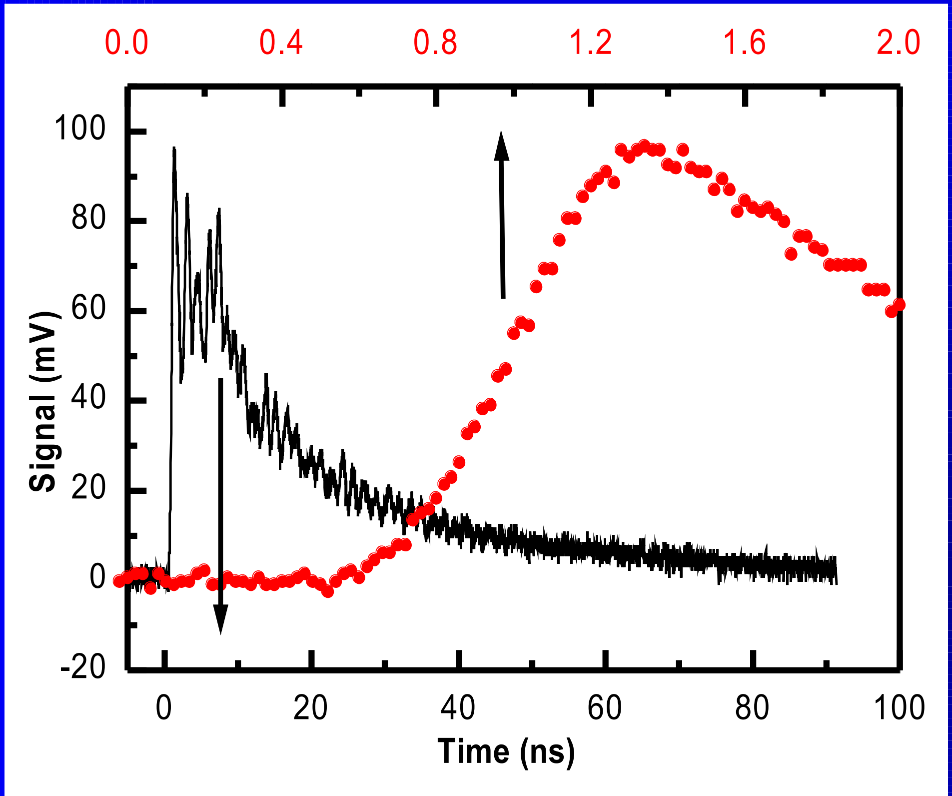

Light response of the SSD at T=4.93K. The measured response risetime is 490 ps, limited by the amplifiers and the oscilloscope bandwidths. The pulse duration is 20 ns and is determined by the time constant of the shunt resistor and the inductance of the wirebonds.

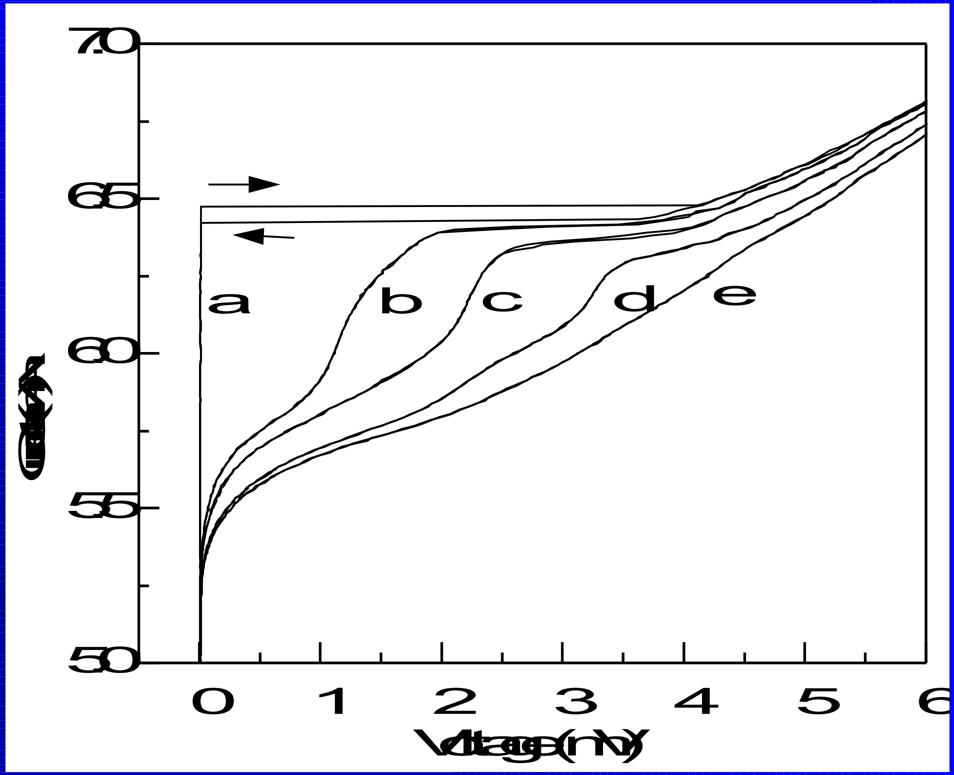

Current-Voltage characteristics of a 4 μm wide 10 nm thick NbN SSD under laser irradiation at 10 MHz repetition rate. The SSD is externally shunted with a 2.5 Ω resistor. The temperature is 4.89 K. The curve (a) corresponds to no laser irradiation. Curves (b) to (e) correspond to increasing duration (30,50,70, and 90 ns) of the light pulse.

Low Temperature Laser Scanning Microscope

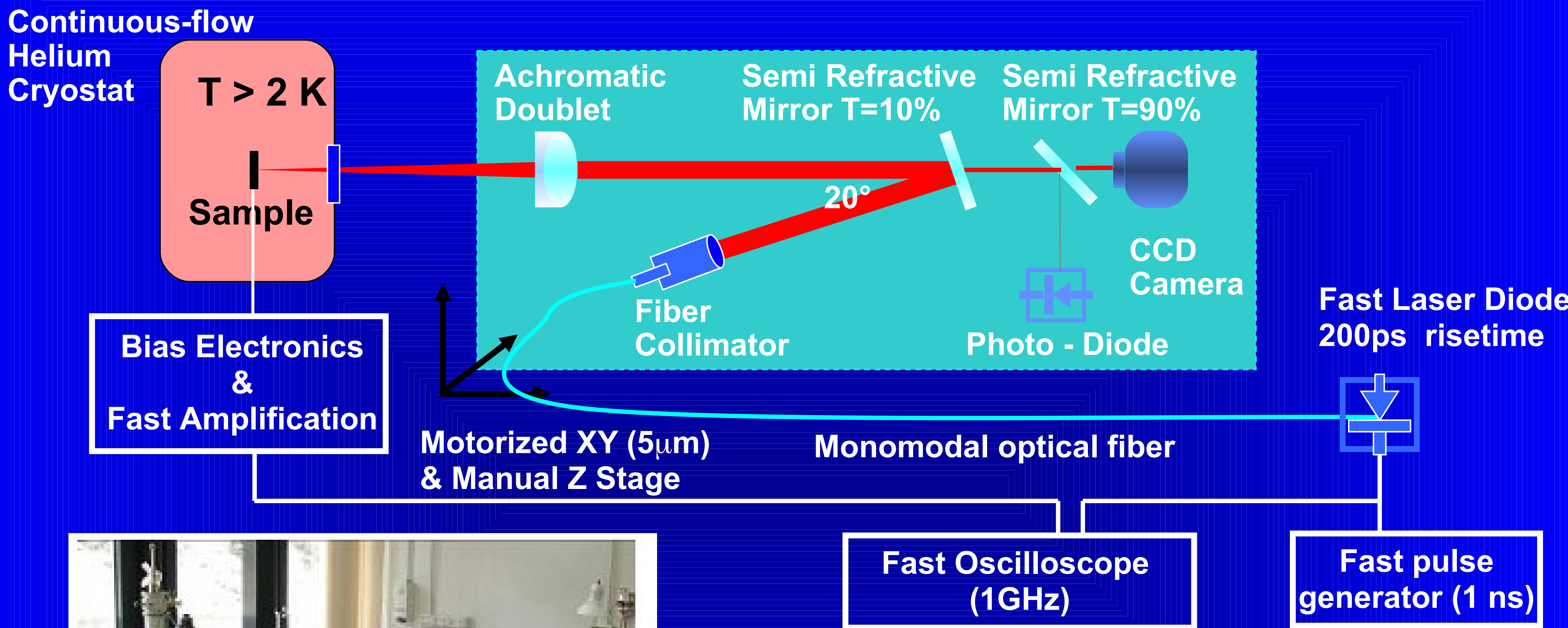

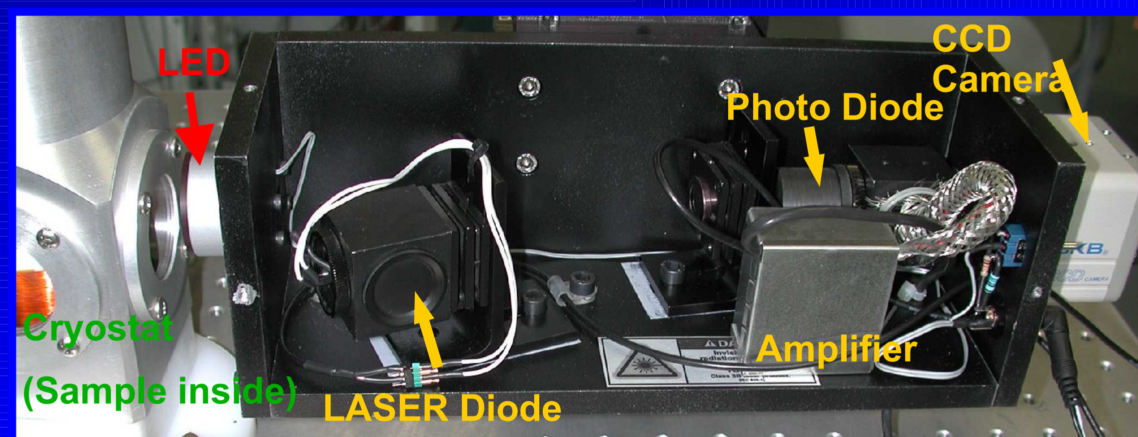

Nanoscale NbN Detectors (in collaboration with CNR-IFN)

Meander type SSPD.
Each stripe is 1000 nm wide

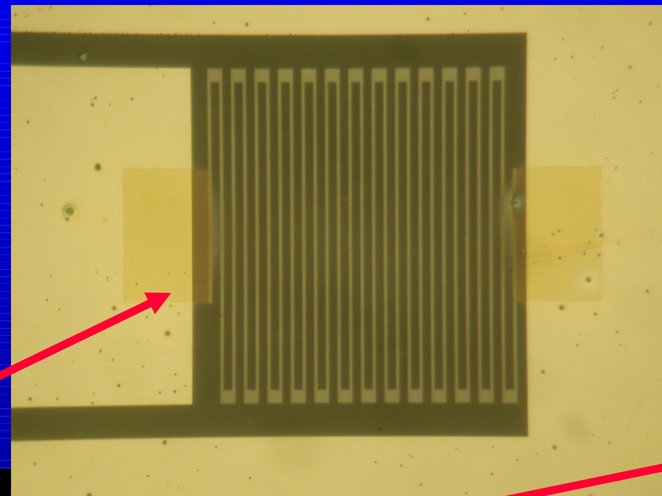

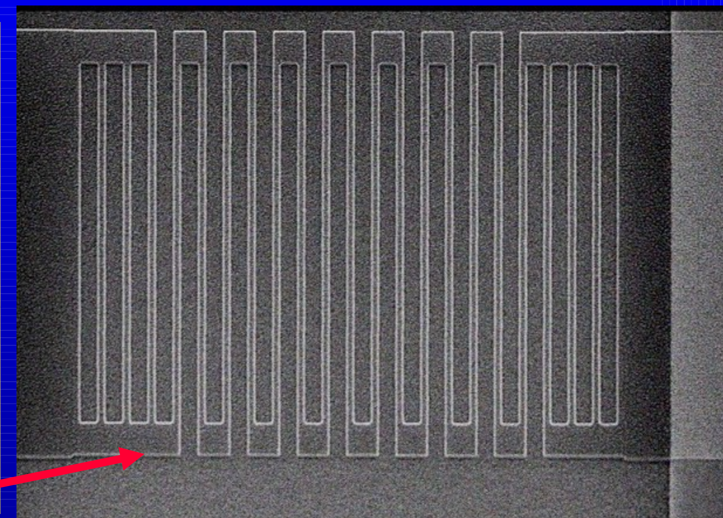

Meander-type SSPD.
Each stripe is 200nm wide

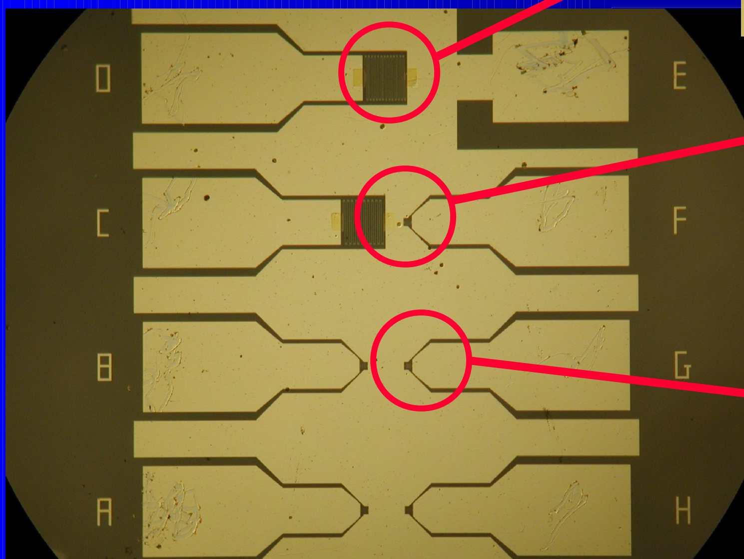

1.1.x1.2mm² area chip showing the Ti/Au pads on sapphire. Seven SSPDs structures are contacted.

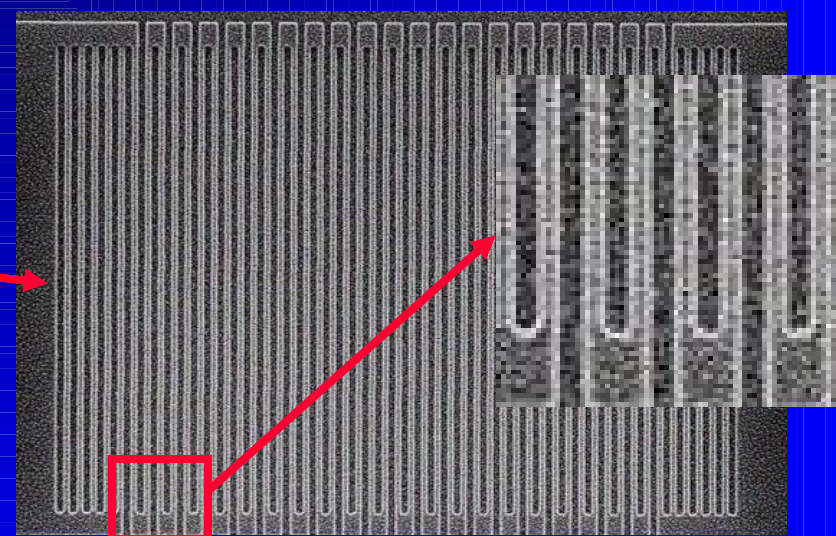

Meander-type SSPD.
Each stripe is 100nm wide with a line-to-space ratio about 1:3

100 nm NbN meander response to 850 nm Laser pulse

dc I-V characteristic

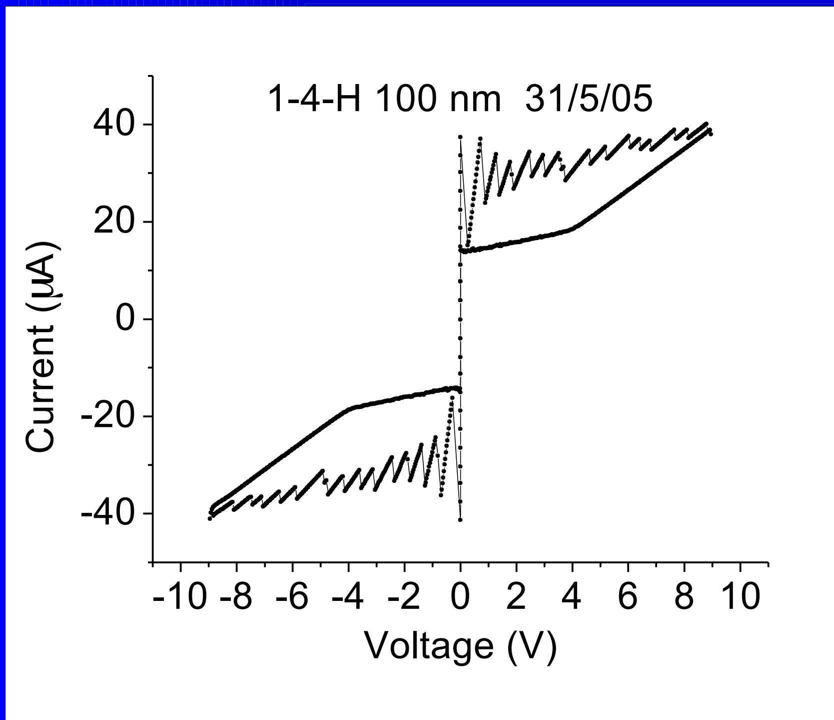

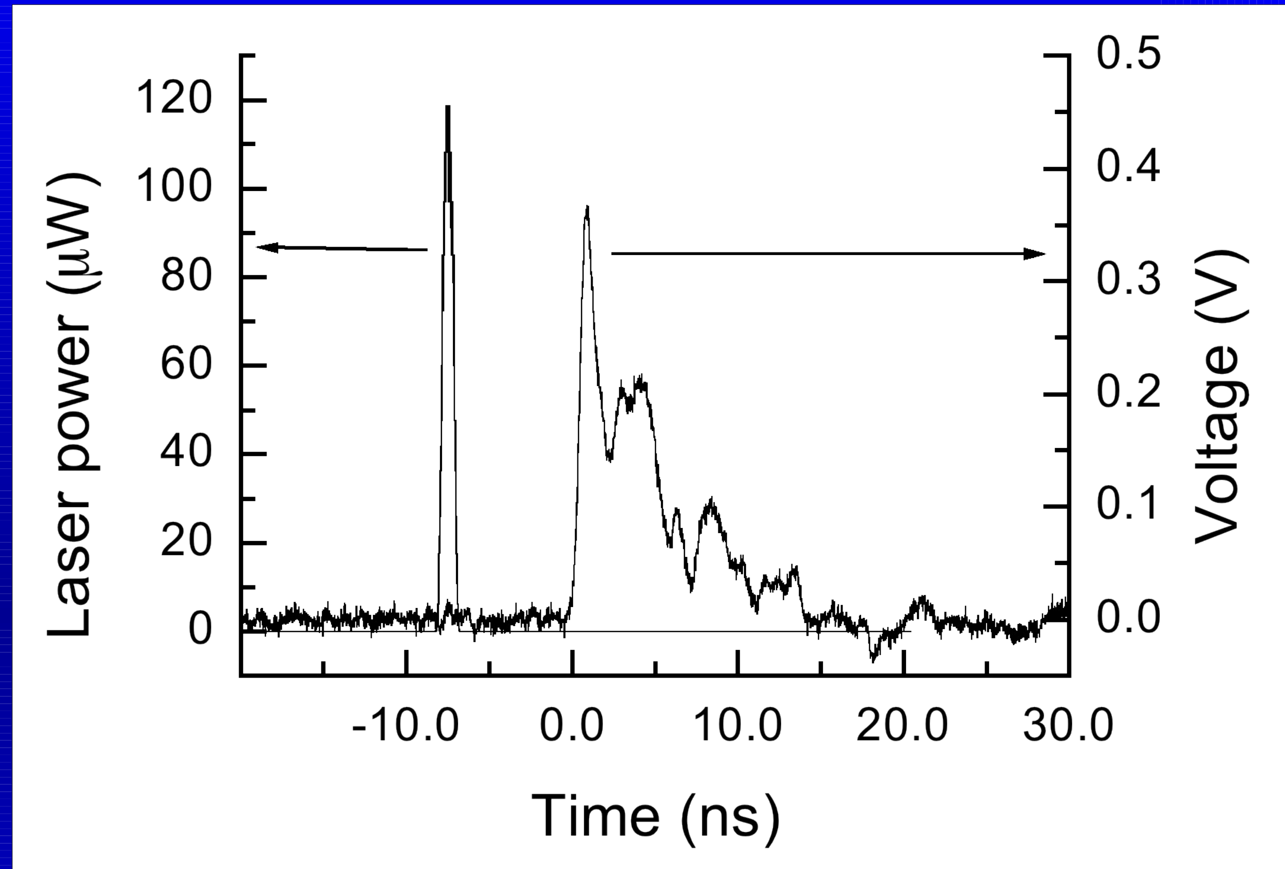

- **The two signal are artificially closer, the real time difference being about 40 ns**
- **The Laser pulse is 1 ns wide and has an energy of 84 fJ = 520 KeV on a 10 μm diameter spot**
- **The estimated absorbed energy is 5 photons each 100x100 nm square**
- **The voltage has been amplified of 52 dB with a bandwidth of 1 GHz**
- **The voltage pulse has a FWHM of 5 ns mainly determined by stray inductance**
- **The combination of the meander impedance and the 50 Ω coaxial line produces a self reset**
- **Ibias = 39.4 μA, T=5.12K**

The Superconductive Single Photon Detector

1. A superconductive nanowire is biased near its critical current
2. The arrival of one photon triggers a resistive transition
3. The bias current is diverted toward an external load generating a fast voltage pulse
4. The decrease of the current in the nanowire drives it back into the superconductive state

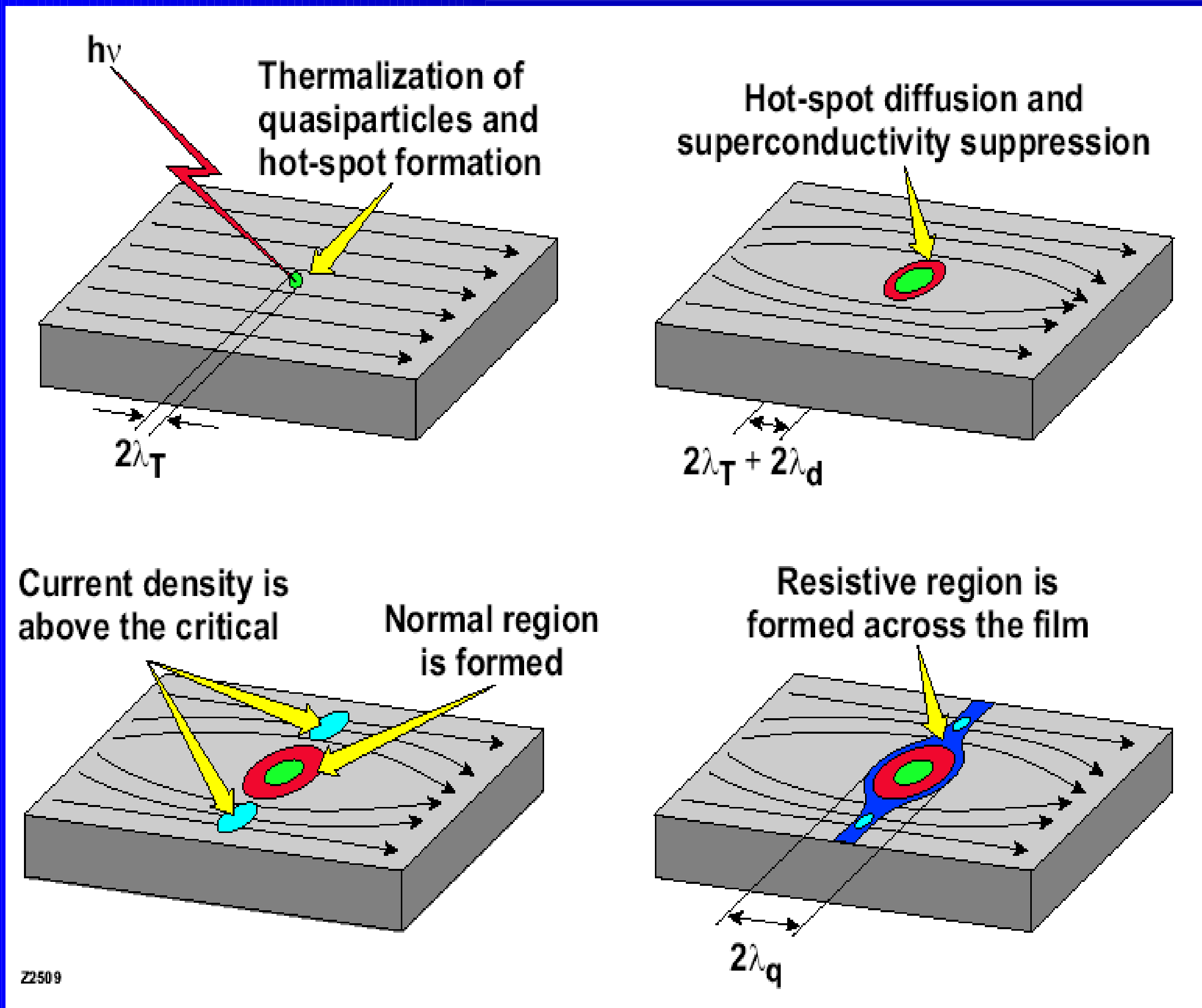

- To have single photon sensitivity the hot spot size must be comparable to the wire width.
- In the IR region (hν ≈1eV) this implies a width ≈ 100nm and a thickness ≈ 5 nm
- To cover a significative area the detector is shaped in the form of a meander

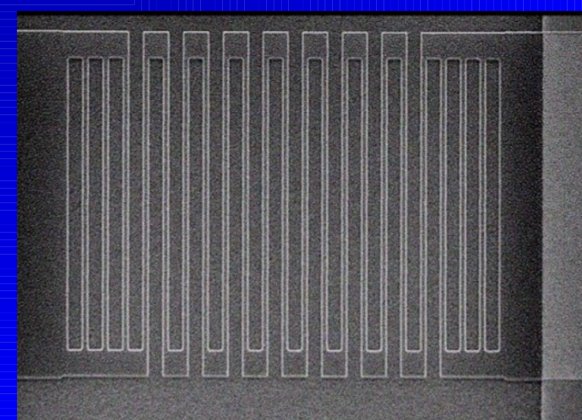

The SSPD detector

N wires in series
Large inductance
Small critical current

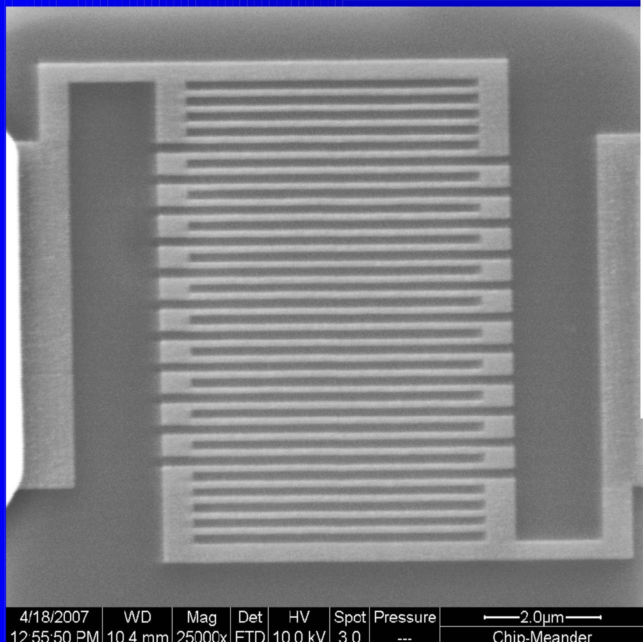

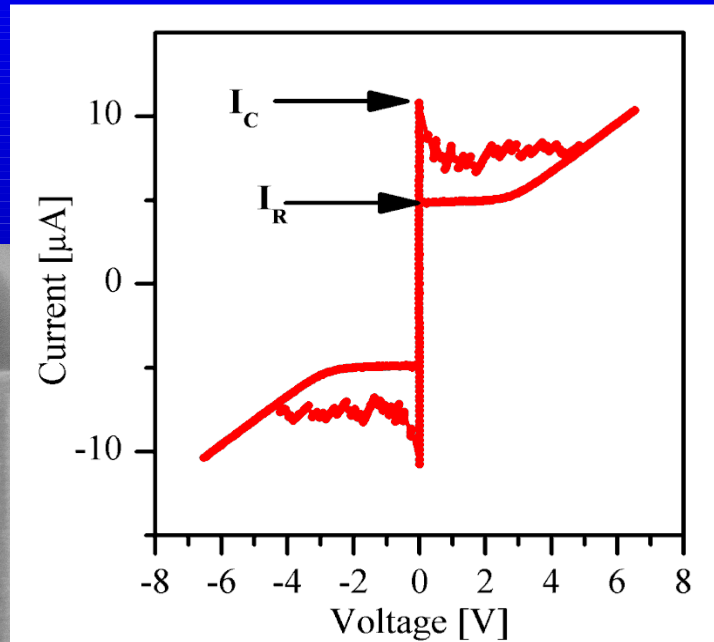

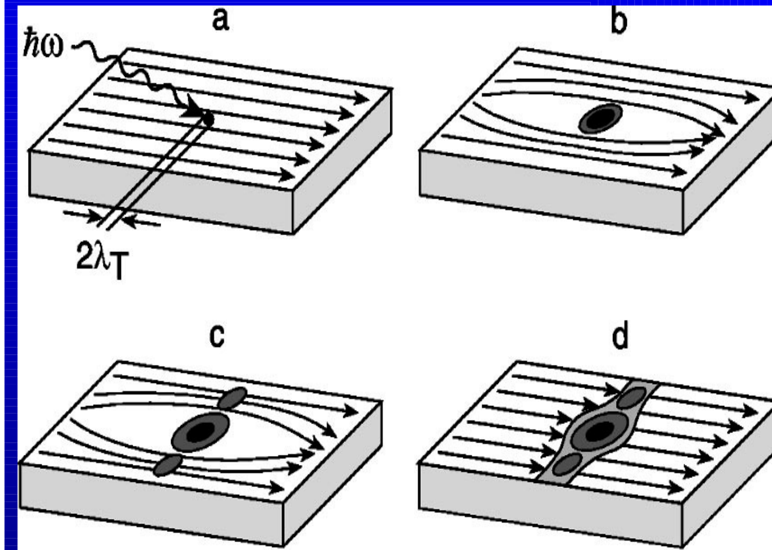

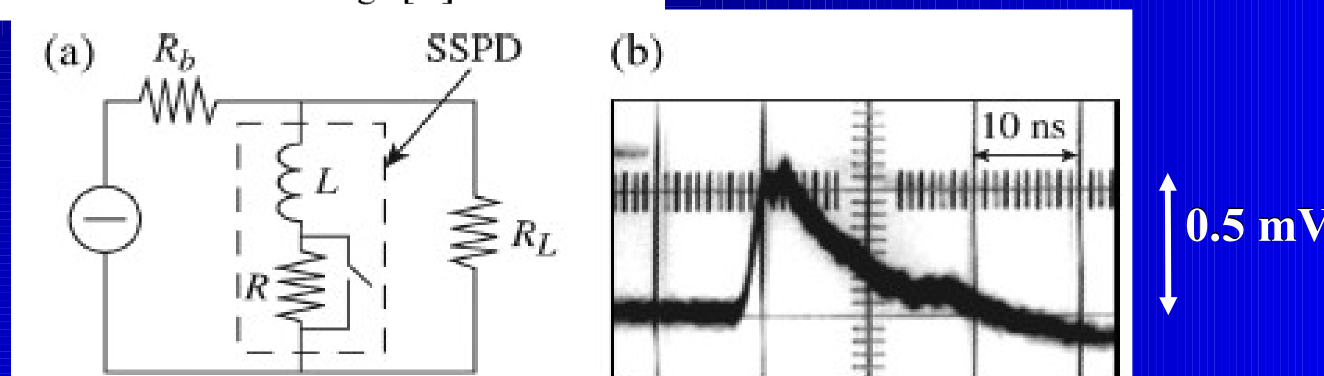

$L = N L_W$

$\tau_R = L/(R+R_L)$

$\tau_D = L/R_L >> \tau_R$

$Vs = (I_C - I_R)*R_L$

$R_L<R<R_b$

detection efficiency up to 57% at 1550 nm

K. M. Rosfjord, et al., Optics Express 74, 527 (2006)

Physical model of the SSPD

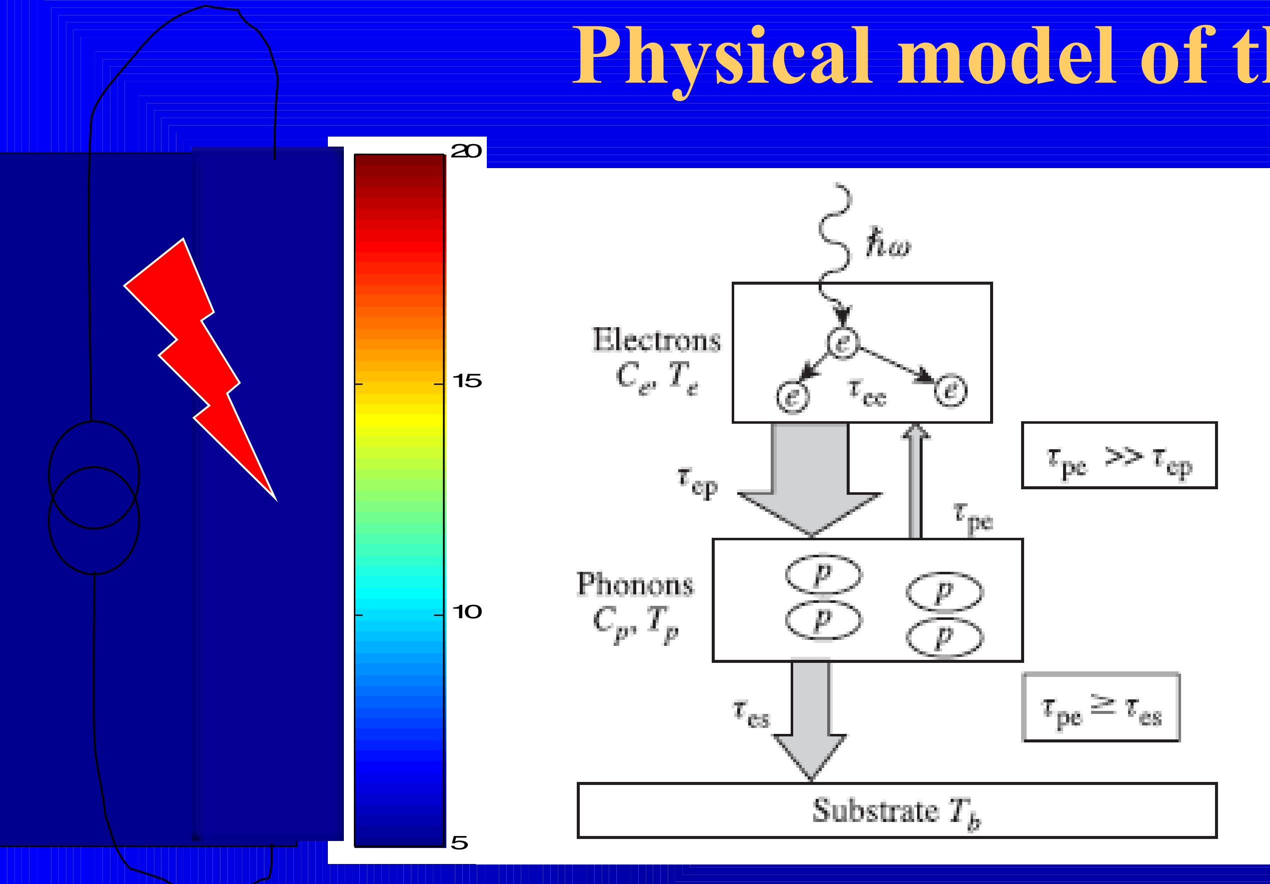

$$\dot{T}_e = -\frac{1}{\tau_{ep}}\left(T_e - T_p\right) + \frac{1}{C_e} W(x,y,t) + D_e \nabla^2 T_e$$

$$\dot{T}_p = \frac{1}{\tau_{ep}} \frac{C_e}{C_p}\left(T_e - T_p\right) - \frac{1}{\tau_{es}}\left(T_p - T_0\right) + D_p \nabla^2 T_p$$

$$W(x,y,t) = \frac{\rho}{V \cdot h} I_N^2(x,y,t)$$

$$I(t) = \int_0^w \left(I_N + I_S\right) dx$$

$$\dot{I} = -\frac{1}{L \cdot \tau_{ep}}\left(R(t) + \frac{R_s \cdot R_L}{R_s + R_L}\right) I + \frac{R_L}{R_s + R_L}\frac{V_B}{L}$$

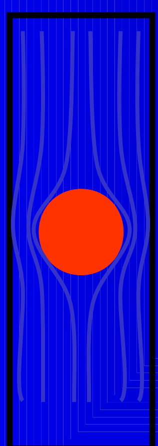

Is > 0 In = 0

Is >> 0 In = 0

Is > 0 In = 0

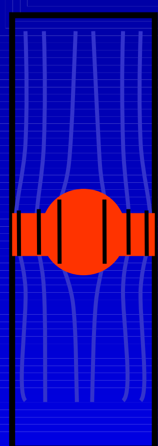

Is > 0

Is = 0 In > 0

Is = 0

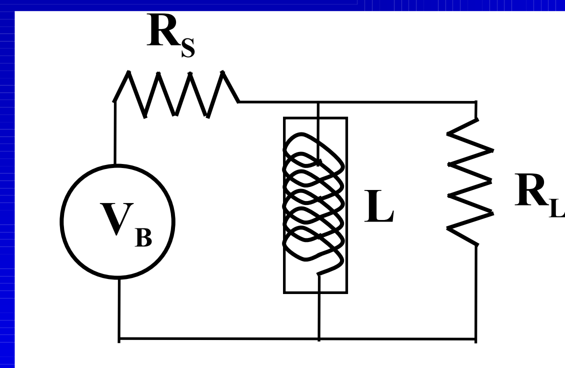

Electrical model of SSPD

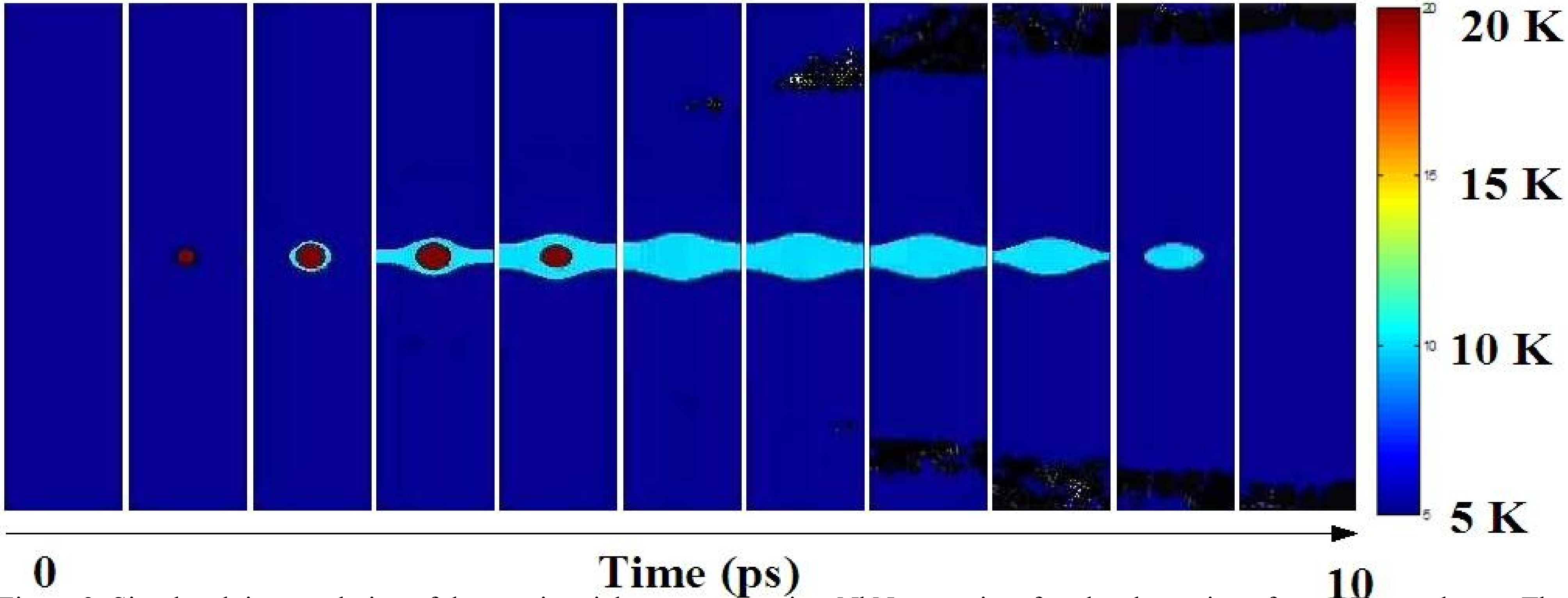

Figure 3: Simulated time evolution of the quasiparticle temperature in a NbN nanowire after the absorption of one 850 nm photon. The strip is 100nm wide and 5 nm thick.

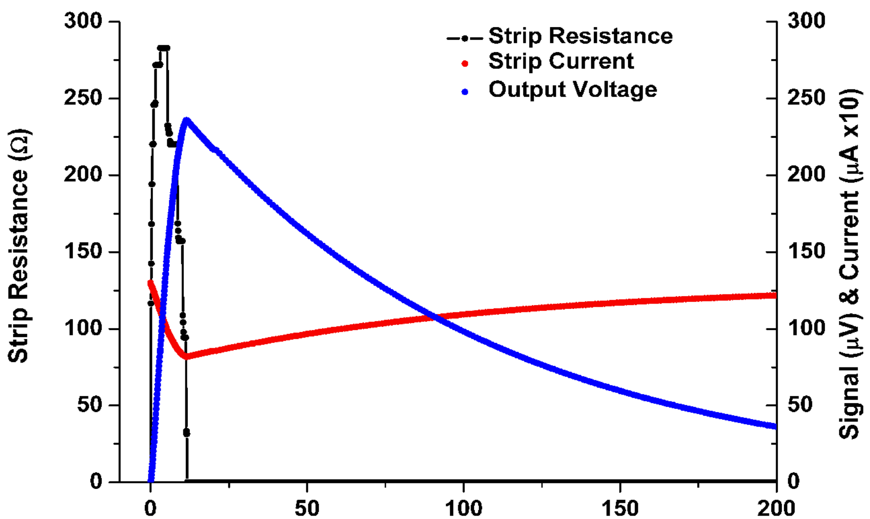

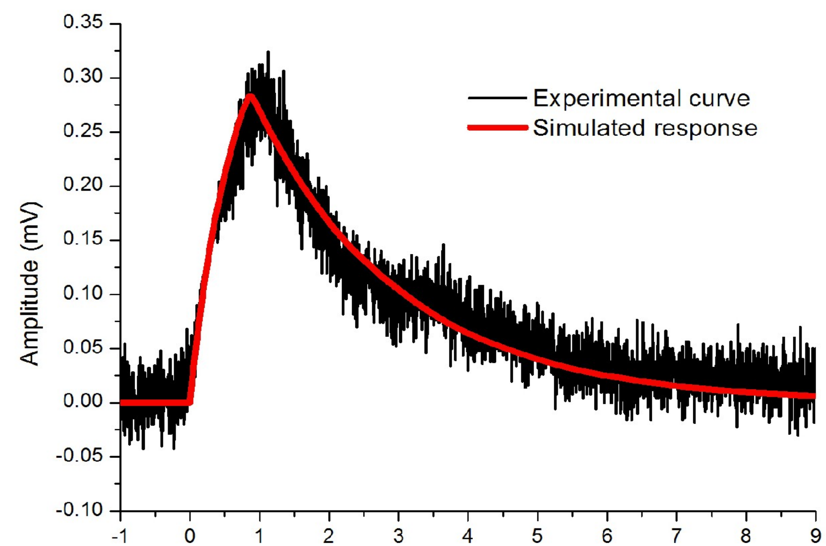

Figure 4: Left) Simulated time evolution of the strip resistance, current and output voltage after the absorption of one 850 nm photon. Right) Comparison of experimentally measured single photon response from SSPD and results from our simulation of hot spot dynamics

Comparison of existing single-photon detectors

	SEMICONDUCTING APDs		SUPERCONDUCTING SPDs	
Detectors	**Si**	**InGaAs**	**SSPD (NbN)**	**TES (W)**
Temperature (K)	300	200	2	0.1
Wavelength (μm)	0.25-1.1	1.1-1.8	0.4-5.6	0.1-5
Time resolution (ps)	50	~300	20	$3\text{x}10^5$
Quantum efficiency	25%@0.7μm	14%@1.54μm	**20%@1.55μm**	>80%@1.5μm
Apertures (μm)	200	30-80	SM fiber	SM fiber
Dark count rates (cps)	$<10^4$	$>3\text{x}10^4$	$\mathbf{<10^{-4}}$	<0.001
Data rate	< 10 MHz	<15MHz	>2 GHz	20 kHz
Dynamic range(# *h*)	1-3000	NA	$>10^8$	50
Electrical quenching	Yes (0.3 ns)	Yes (0.3 ns)	No	No
Photon number resolution	Limited	No	**Yes**	Yes
Ruggedness	Very high	High	High	Low
Availability	Yes	Limited	Limited	Very limited

NbN nanowires can also detect the number of photons

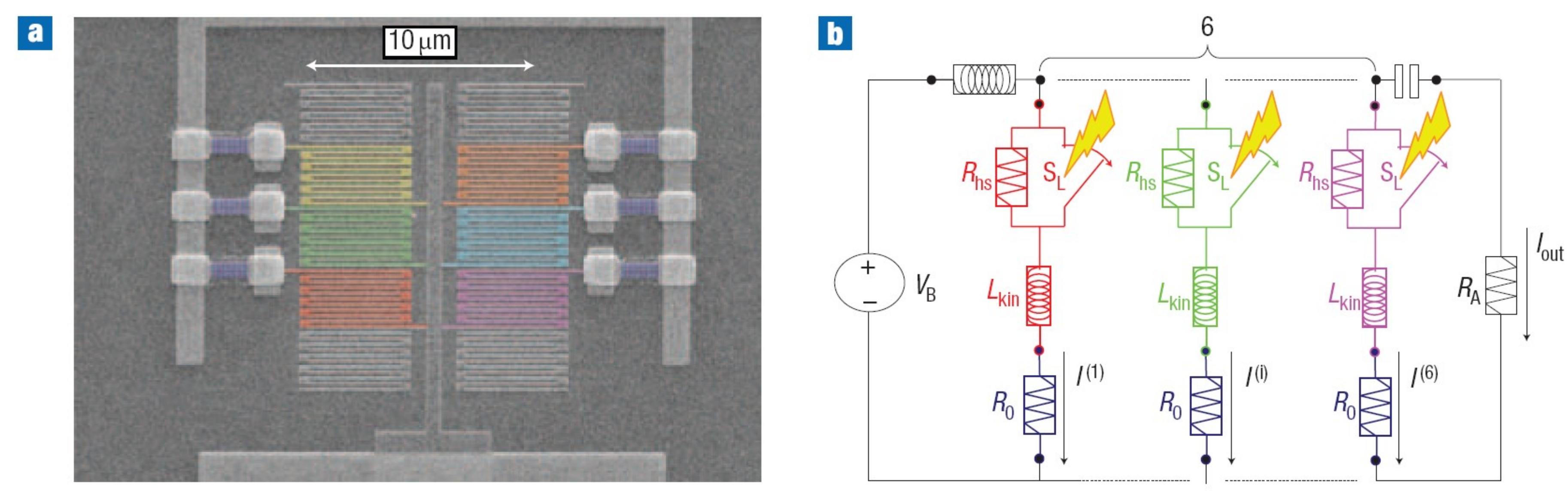

Table 1 Reported performance for detectors with PNR functionality.

	Repetition rate (Hz)	DK (Hz)	η (%)	NEP (W Hz$^{-1/2}$)	λ (nm)	M_{noise}	M_{max}	T (K)	Readout
CIPD (ref. 3)	40	NR	80	NR	1,550	Yes	NR	4.2	Cryo JFET
QD-FET (refs 4,5)	2×10^5	0.4	1.3	2×10^{-17}	684	Yes	3	4.2	Cryo MESFET
TES (ref. 6*)	5×10^4	400	89	4×10^{-18}	1,550	Yes	11	<0.1	SQUID array
PMT (ref. 7)	6.7×10^5	400	7	1×10^{-16}	523	Yes	9	Room T	Room T amp.
VLPC (refs 8,9)	1.5×10^4	2×10^4	85	9×10^{-17}	543	Yes	10	6–7	Cryo preamp.
MPPC (ref. 10)	1×10^4	1.4×10^5	25–65	7×10^{-16}	400	Yes	100–1,600	Room T	Room T amp.
APD array[11]	2×10^4	1.6×10^8	33	1×10^{-14}	1,064	No	1,024	246	Multichannel
Time multiplexed[12,24]	1×10^4	NR	66	NR	700–800	No	8–16	Room T	Two-channel
PND	8×10^7	0.15	2	4×10^{-18}	1,300	No	4	2	Room T amp.

CIPD, charge integration photodiode, QD-FET, quantum dot field-effect transistor; TES, transition edge sensor; PMT, photomultiplier; VLPC, visible-light photon counter; MPPC, multi-pixel photon counter; APD, avalanche photodiode; λ, optical excitation wavelength; M_{noise}, device affected by multiplication noise; M_{max}, maximum number of detected photons; NR, not reported; Cryo JFET: cryogenic junction gate field-effect transistor; Cryo MESFET: cryogenic metal epitaxial semiconductor field-effect transistor; SQUID: superconducting quantum interference device; amp.: amplifier; preamp.: preamplifier.
Repetition stands for the repetition frequency used in reported experiments (does not necessarily represent the maximum possible rate).
*A better NEP (1×10^{-19} W Hz$^{-1/2}$), with a lower quantum efficiency ($\eta = 20\%$) was reported in ref. 25.

From: A. Divochiy et al., "Superconducting nanowire photonnumber-resolving detector at telecommunication wavelengths", Nature Photonics, 2008

Applications of SSPD

Quantum cryptography
(single-photon communication ensures unconditional security)
Long distance telecommunications
(high sensitivity and speed allows longer unamplified fiber links)
Silicon CMOS IC device debug
(Time-correlated near IR photon (0.9-1.4μm) emission from nMOS transistors)
Non-quantum optical tomography (transmission)
(to discriminate "line-of-sight" propagated photons from those scattered or diffused by tissues).
Quantum Entanglement tomography
(additional resolution)
Coherence tomography
(increase in the scanning depth, fully 3D scanning)
Optical Quantum computers
(quantum detector of propagating entangled photons)
RSFQ chip level I/O interface
(Optical input to SFQ pulse, SFQ pulse amplifier)

Bit Error Rate requirements for telecommunications

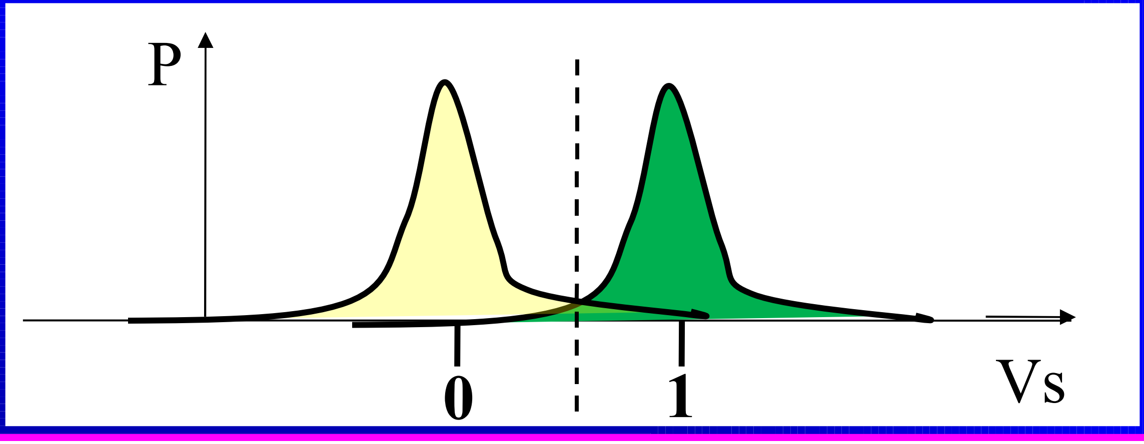

Goal: BER=10^{-12} @ 10 Gbps

Amplifier Noise Power

$Pn := B \cdot T \cdot Kb \qquad Pn = 20.363 \times 10^{-12}\,W$

$F := 5$ noise figure of the amplifier in dB

$L := 2$ cryostat loss in dB

$Pntot := Pn \cdot 10^{\frac{(F+L)}{10}} \qquad Pntot = 102.059 \times 10^{-12}\,W$

$Vntot := \sqrt{Pntot \cdot 50 \cdot ohm} \qquad Vntot = 71.435 \times 10^{-6}\,V$

$Vs := 0, 0.0001 .. 0.001$

$$BER = 0.5 * erfc\left\{\frac{\mu_1 - \mu_0}{\sqrt{2}(\sigma_1 - \sigma_0)}\right|$$

$$BER = 0.5 * erfc\left\{\frac{Vs}{2\sqrt{2} * Vntot}\right.$$

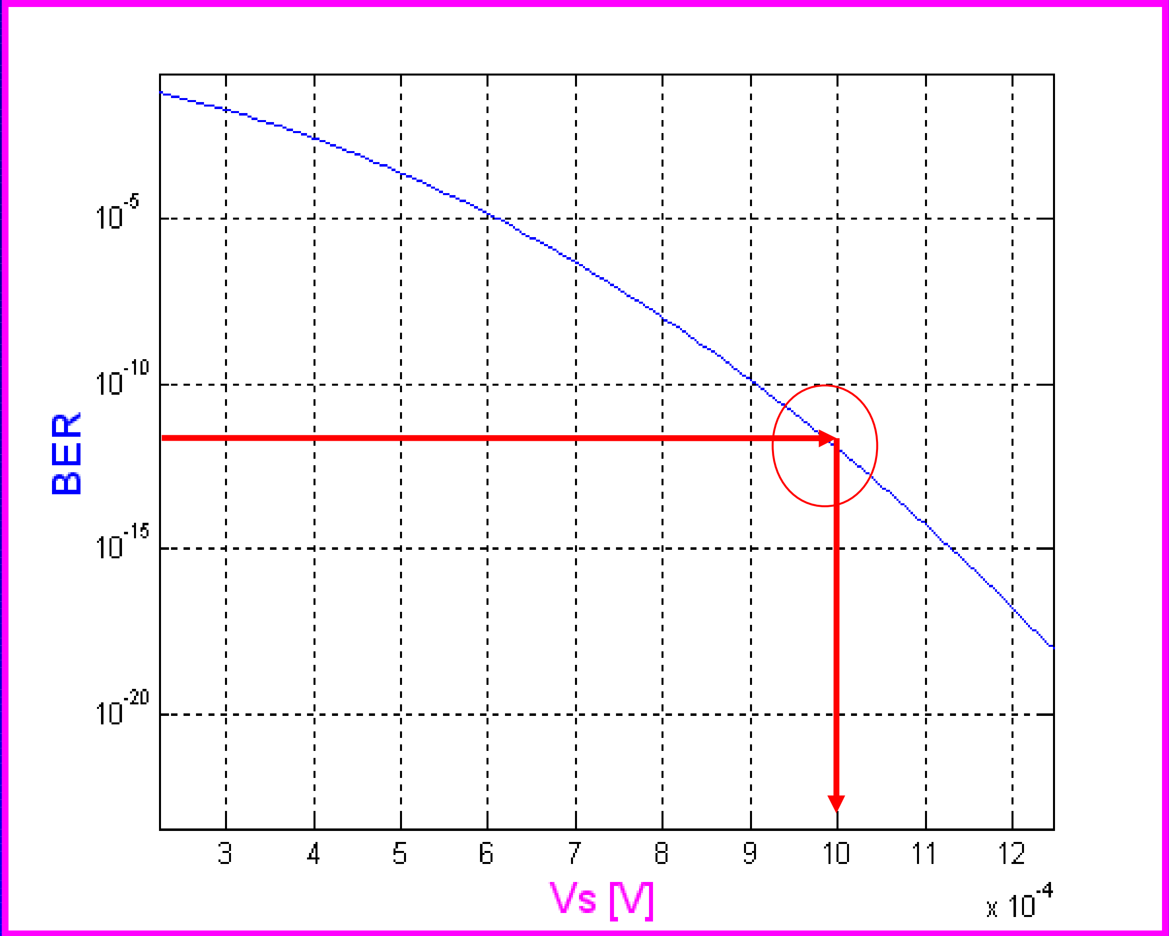

The parallel array SSPD

To increase both speed and signal amplitude we have proposed a parallel array configuration instead of the meander one

The photon induced transition of one of the wires in the parallel array induces a transition of all the other wires with a cascade mechanism.

To achieve a synchronus switching an additional inductor L_S has to be introduced such that $L_S \geq L_W$

$$L = L_S + L_W / N \approx \mathbf{L_{meander}\ /N}$$

$$\tau_R = L/(R+Z_0) \approx \tau_{\mathbf{Rmeander}}\ \mathbf{/N}$$

$$\tau_D = L/Z_0 >> \tau_R$$

$$Vs = N\ (I_C\text{-}I_R)*Z_0 \approx \mathbf{N\ Vs_{meander}}$$

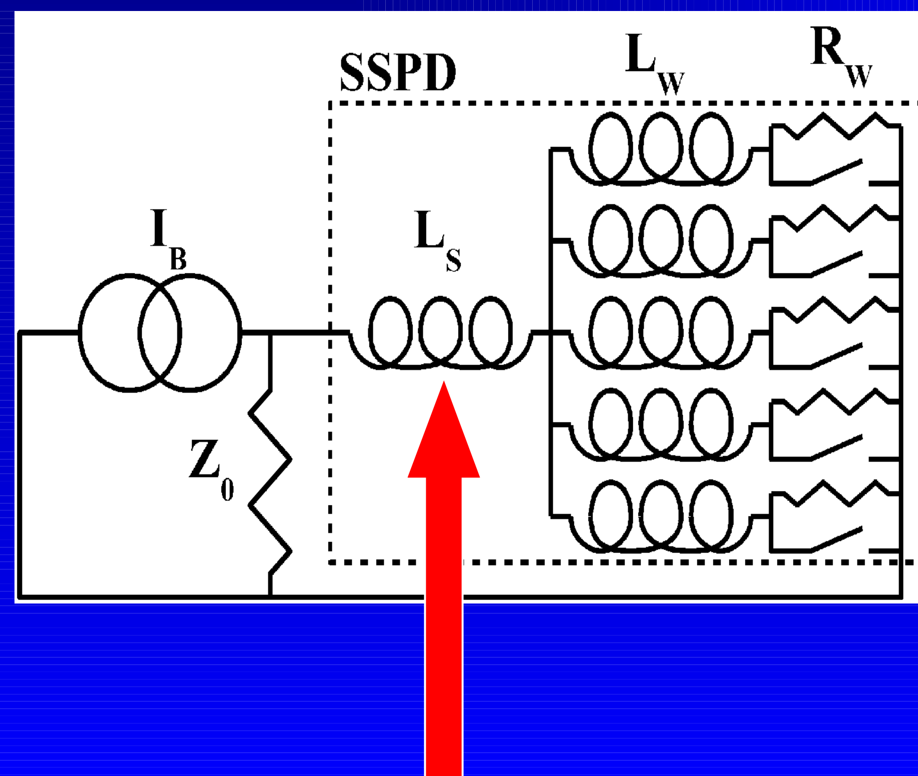

Circuit response simulation

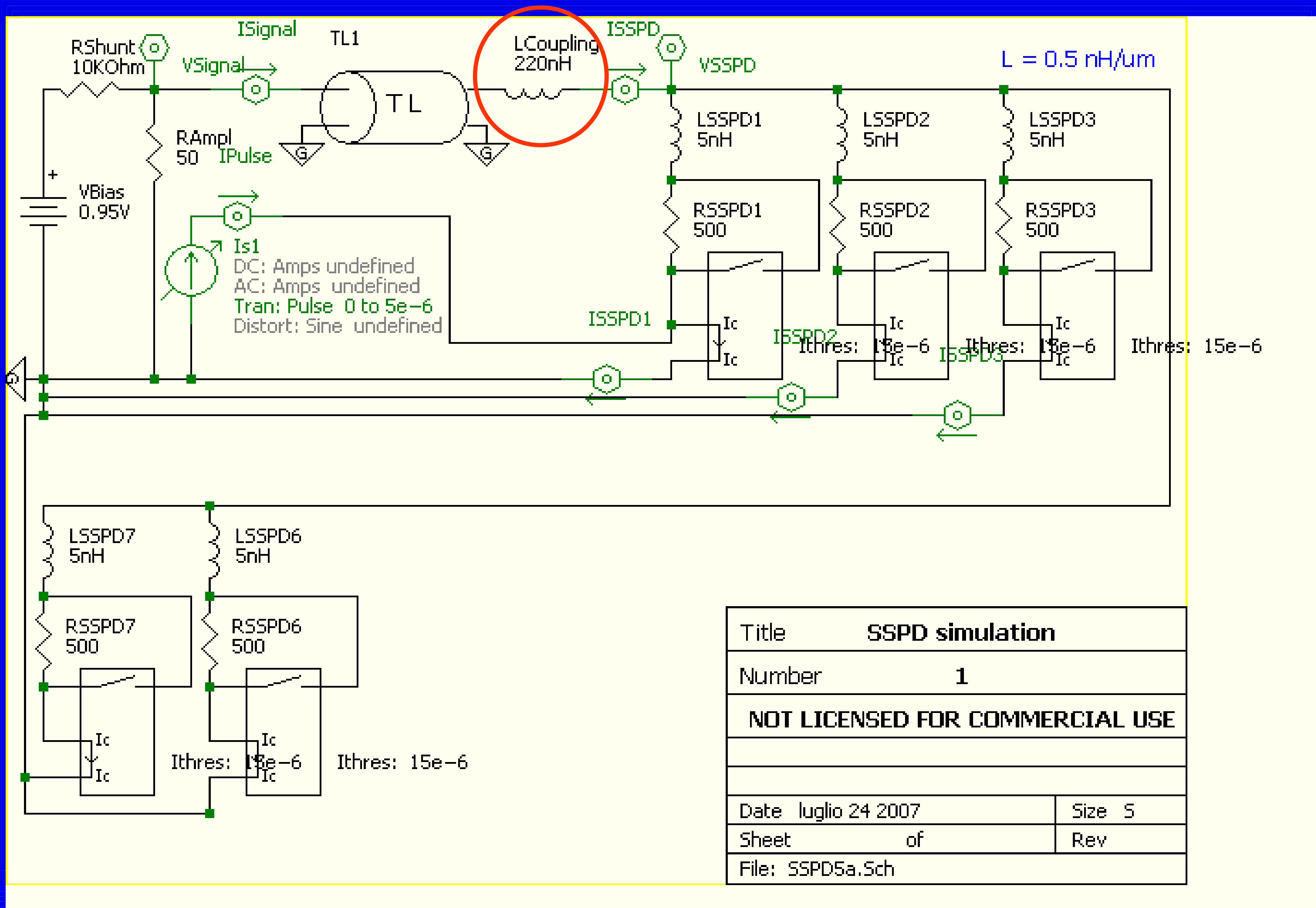

Results from circuit simulations

$L_S = 5$ nH

$L_S = 220$ nH

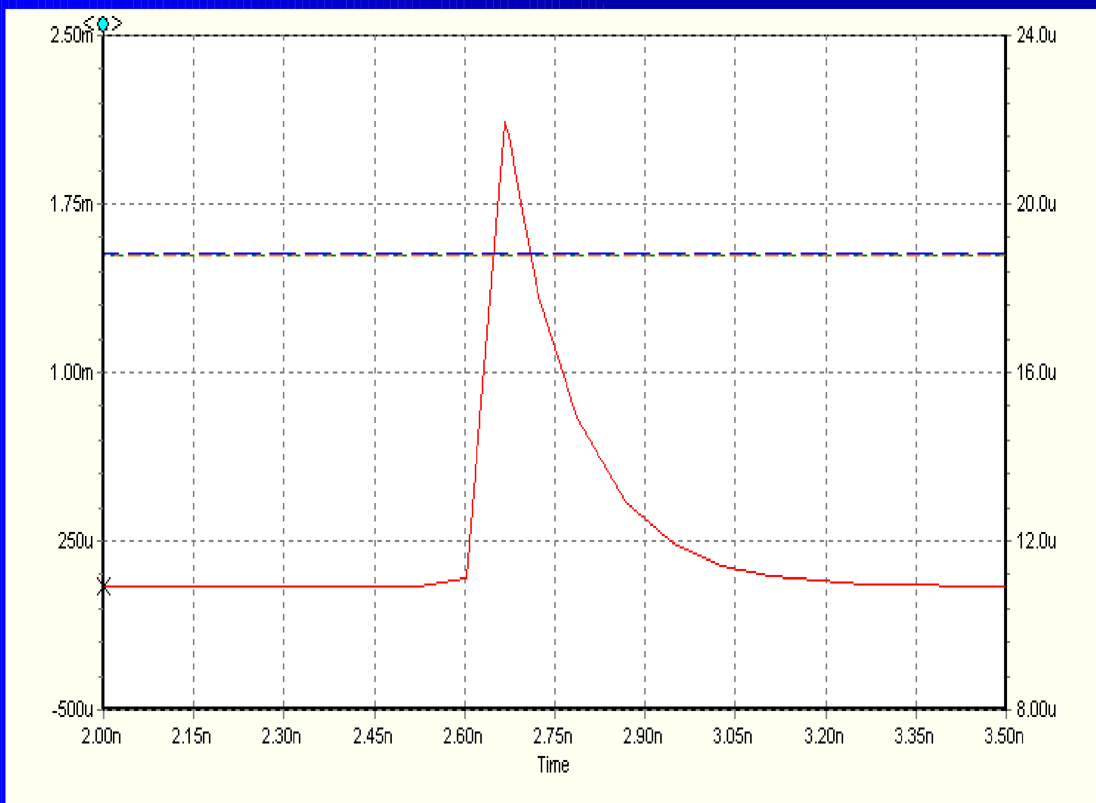

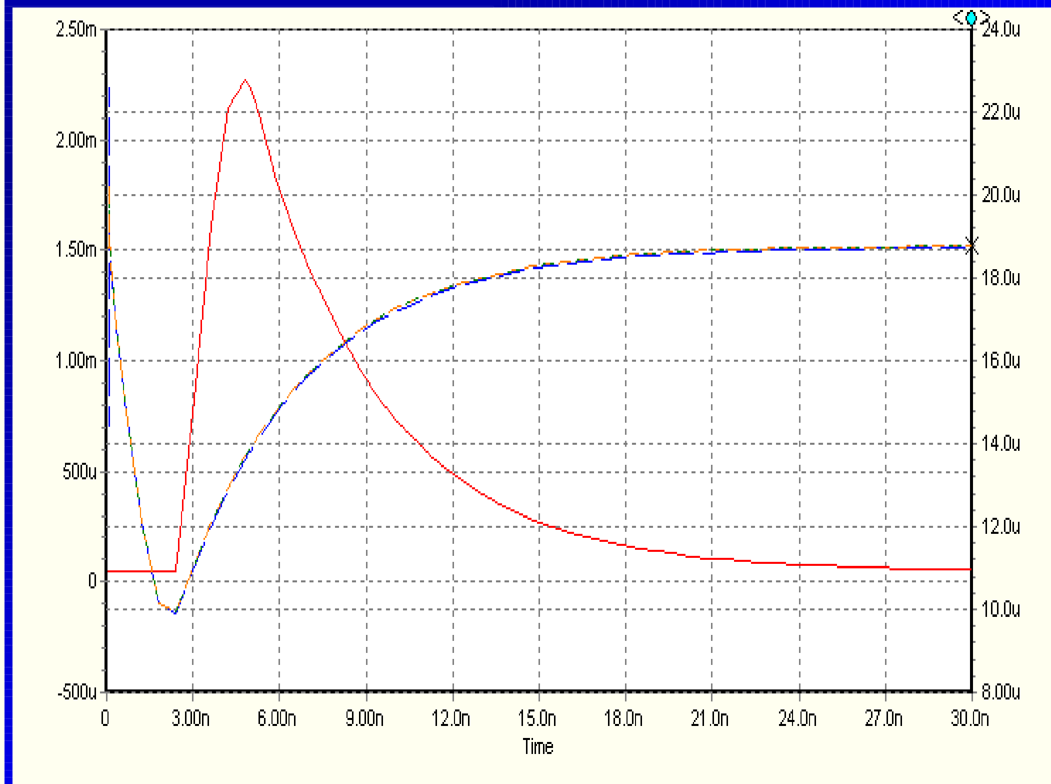

Device Design and Fabrication I

NbN deposited on 2” sapphire wafer at 900K:

- thickness $t \approx 3\text{-}5$ nm
- surface resistance $R_S \approx 150–500\ \Omega/\square$,
- critical temperature $T_C \approx 10–11$ K, $\Delta T_C \approx 0.3$K,
- critical current density $J_c \approx 6\ 10^6\ A/cm^2$ at 4.2 K

2-step process electron beam lithography

60nm Ti/Au film e-gun for stripline circuit

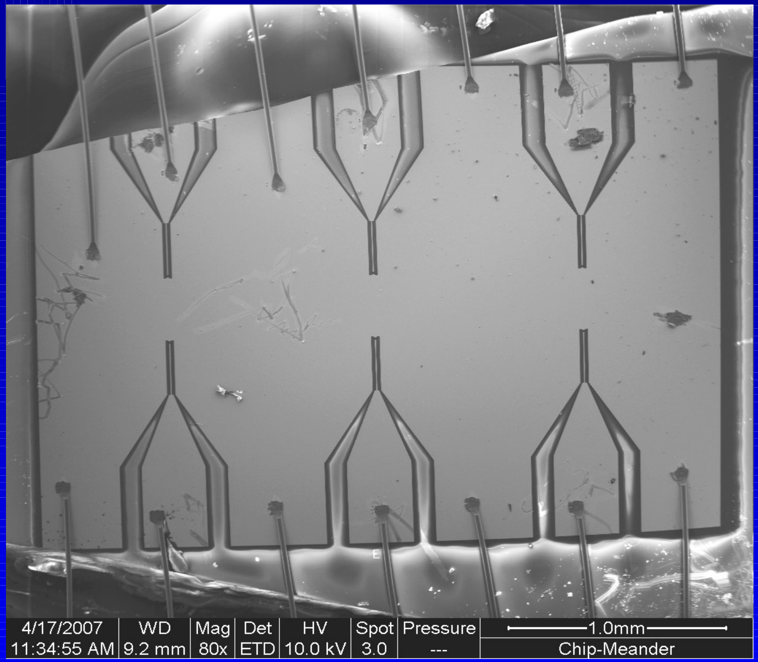

one chip with 6 devices

Device Design and Fabrication II

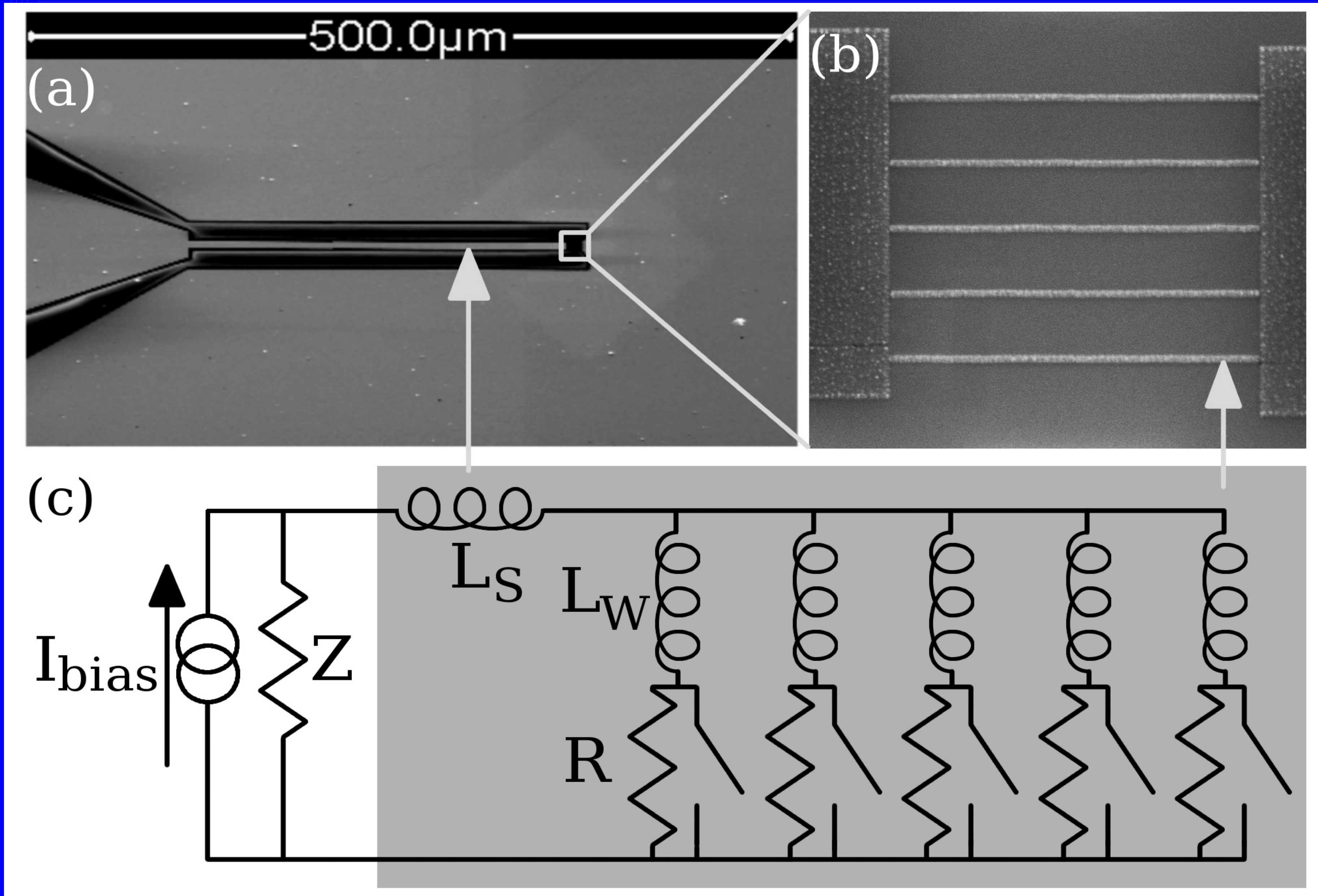

Device Design and Fabrication III

series inductor Ls

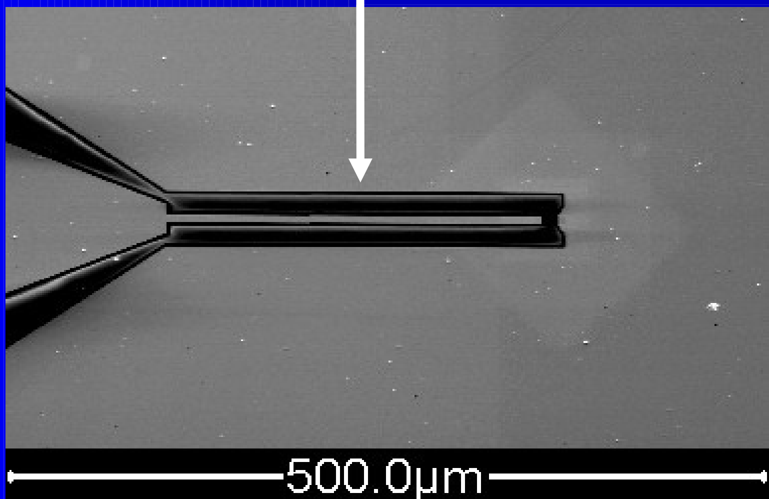

SSPD area

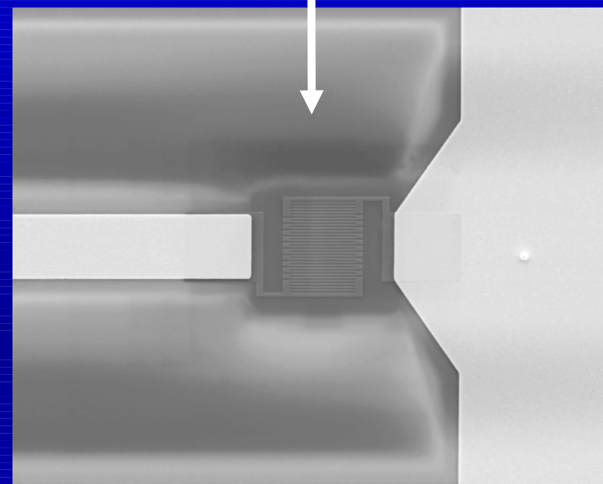

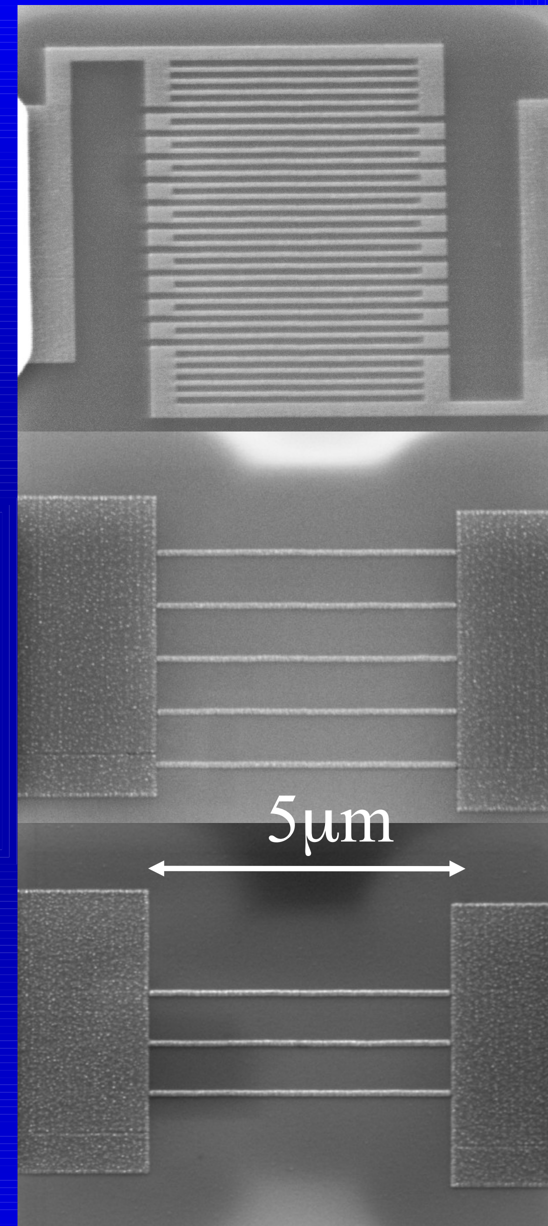

all wires are 5 μm long, 100 nm wide and 5 nm thick

Electro-Optical Characterization with a LTLSM

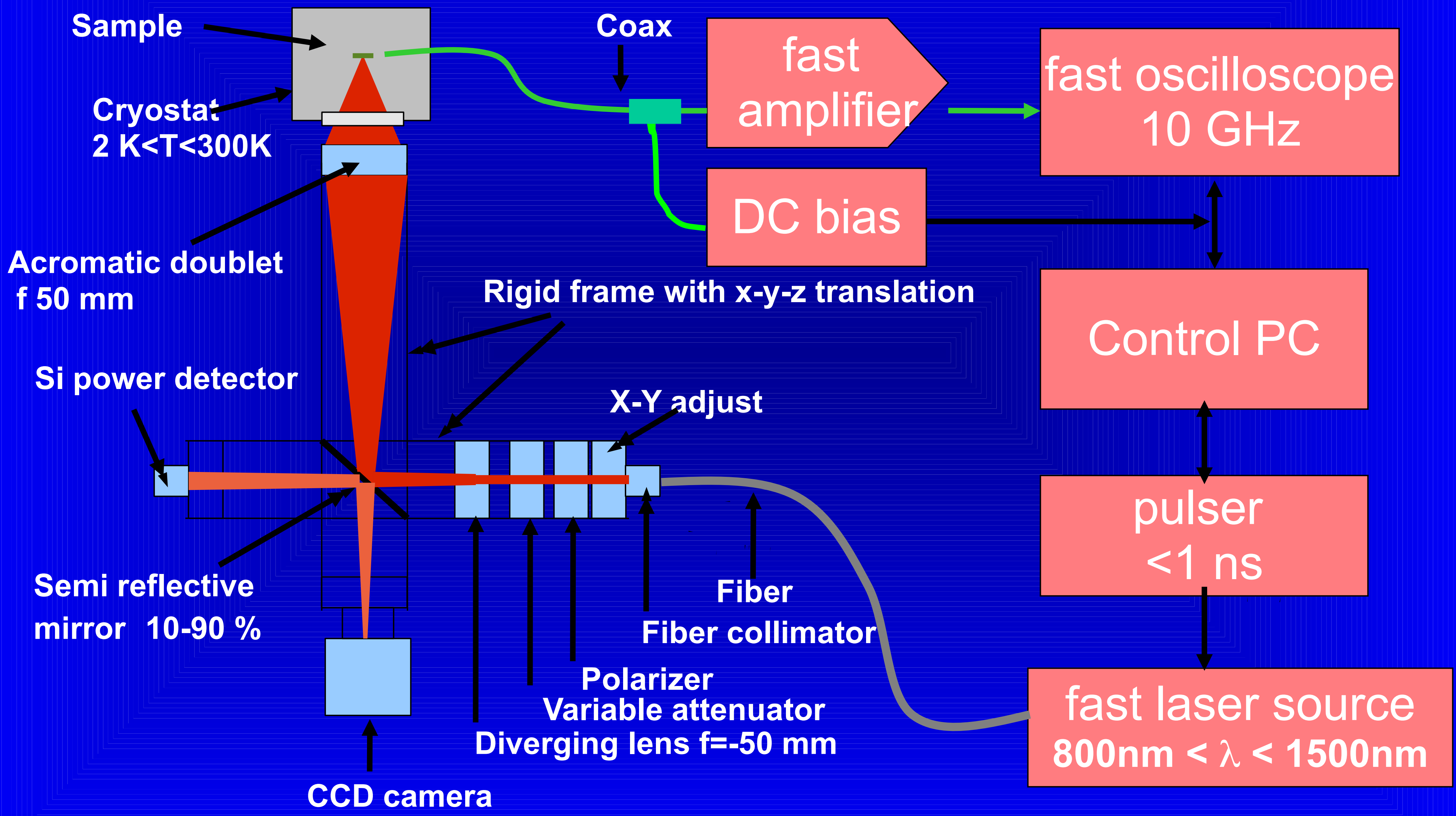

Electro-optical test bed for SSPDs

New generation Low Temperature Laser Scanning Microscope

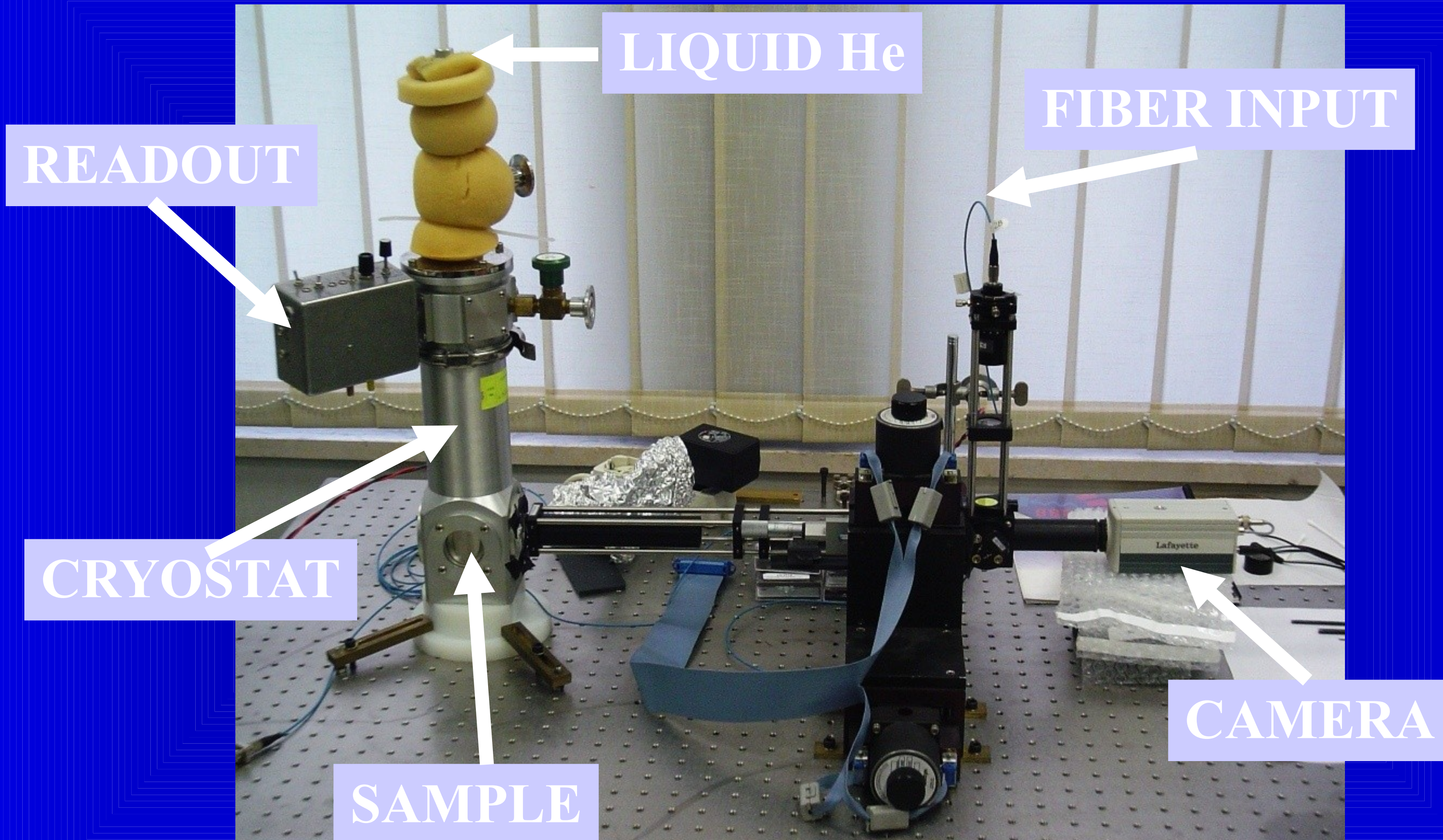

$3 < T < 300$ K, spot size: 5 μm, wavelengths: 850, 1300, 1550 nm, pulses $<$ 1ns
xyz positioning, 1 cm^2 addressable detector area

The parallel SSPD: experimental results

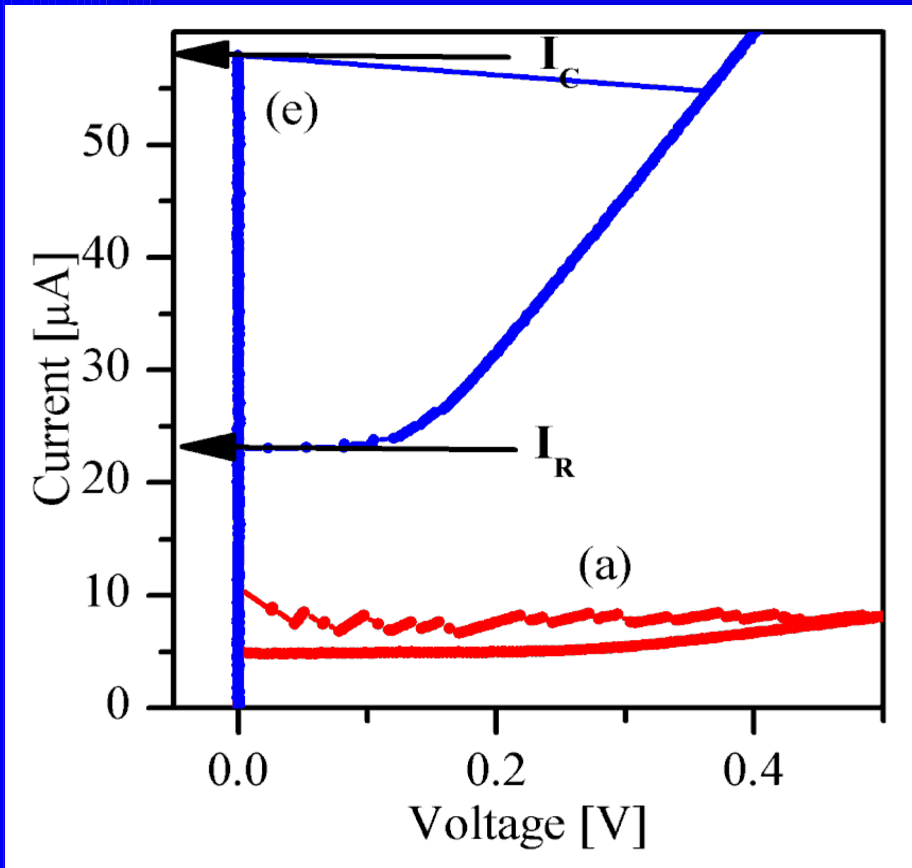

I-V curve of a meander (**red**) and a parallel (**blue**) SSPD

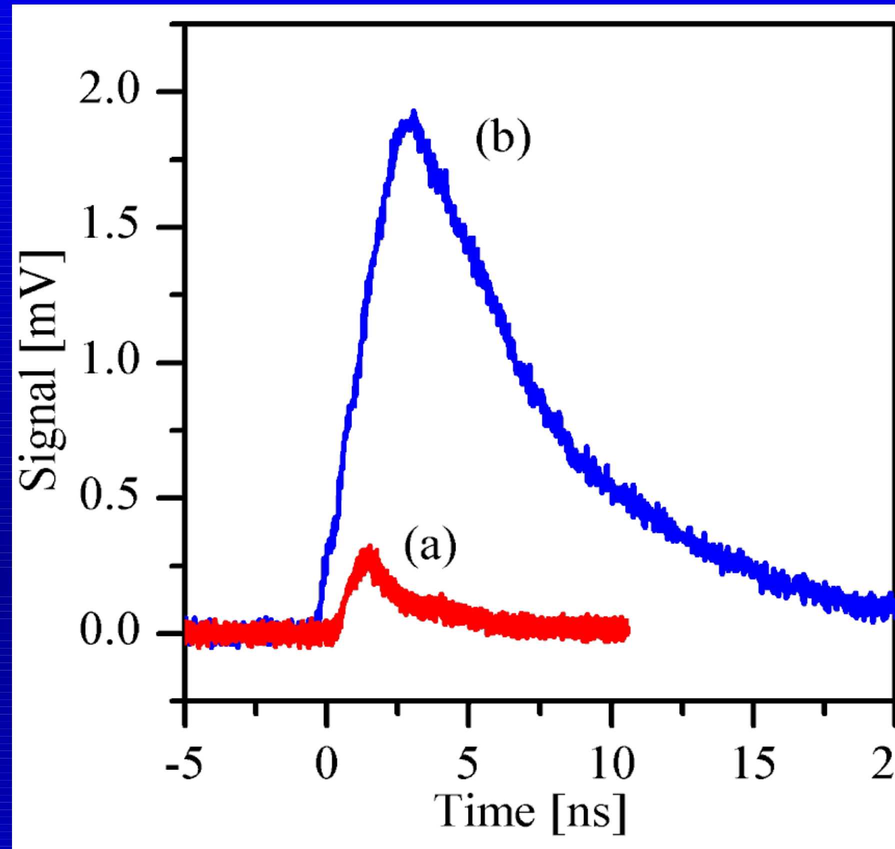

Single photon response from meander (**red**) and parallel (**blue**) SSPD

note: pulse duration of parallel SSPD has been artificially stretched (LS = 200nH). The intrinsic duration is < 100ps

Optical characterization

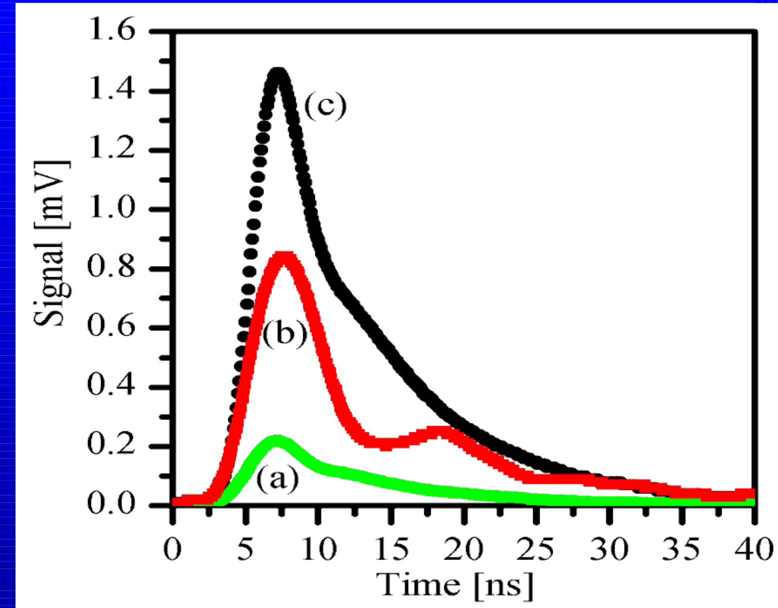

response from 1,3 and 5 wires

L_S increased to 200 nH to stretch pulses

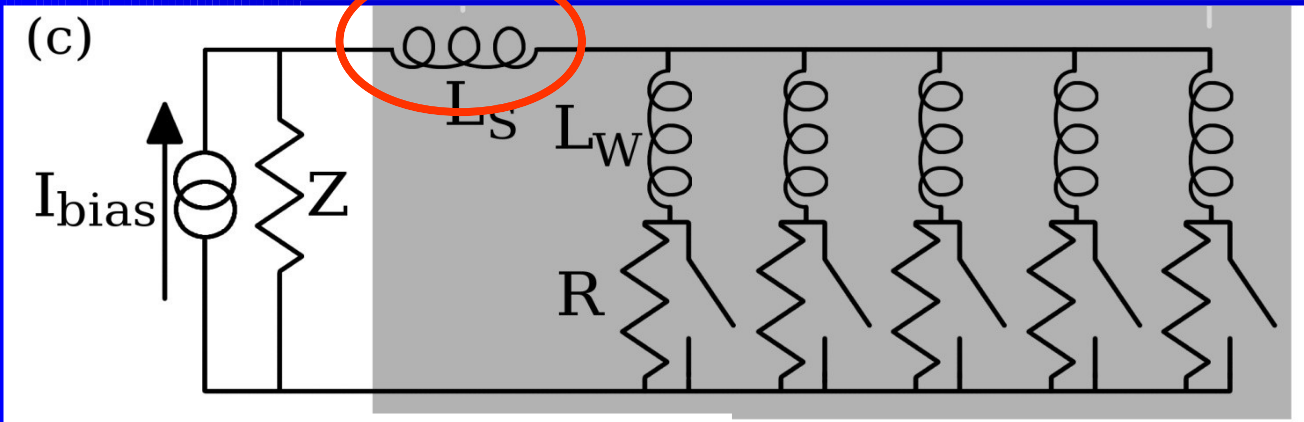

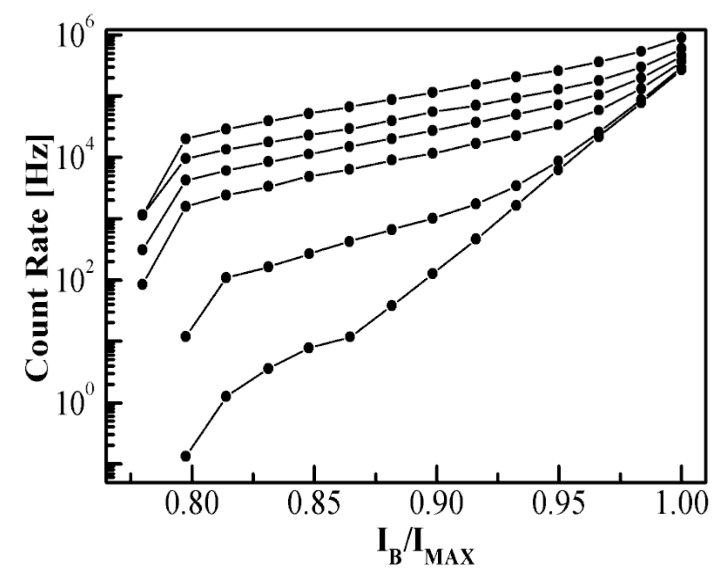

count rate vs bias current
5 wires parallel SSPD

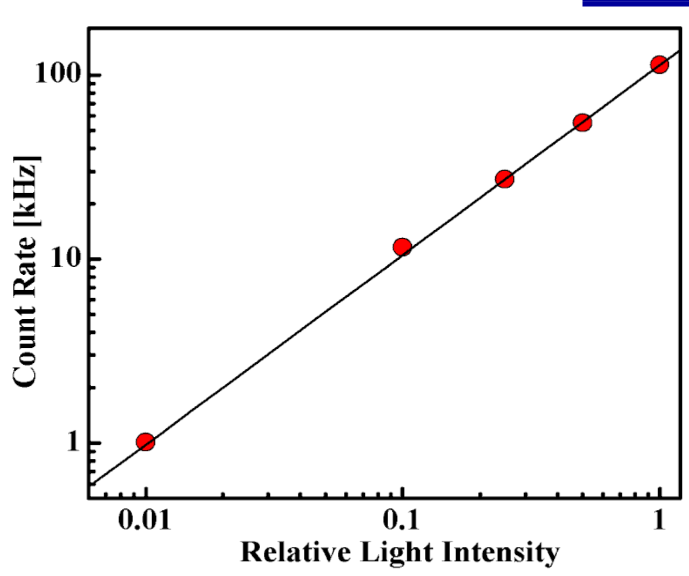

count rate vs ligth intensity
single photon detection

Fast response of 5 wires parallel SSPD

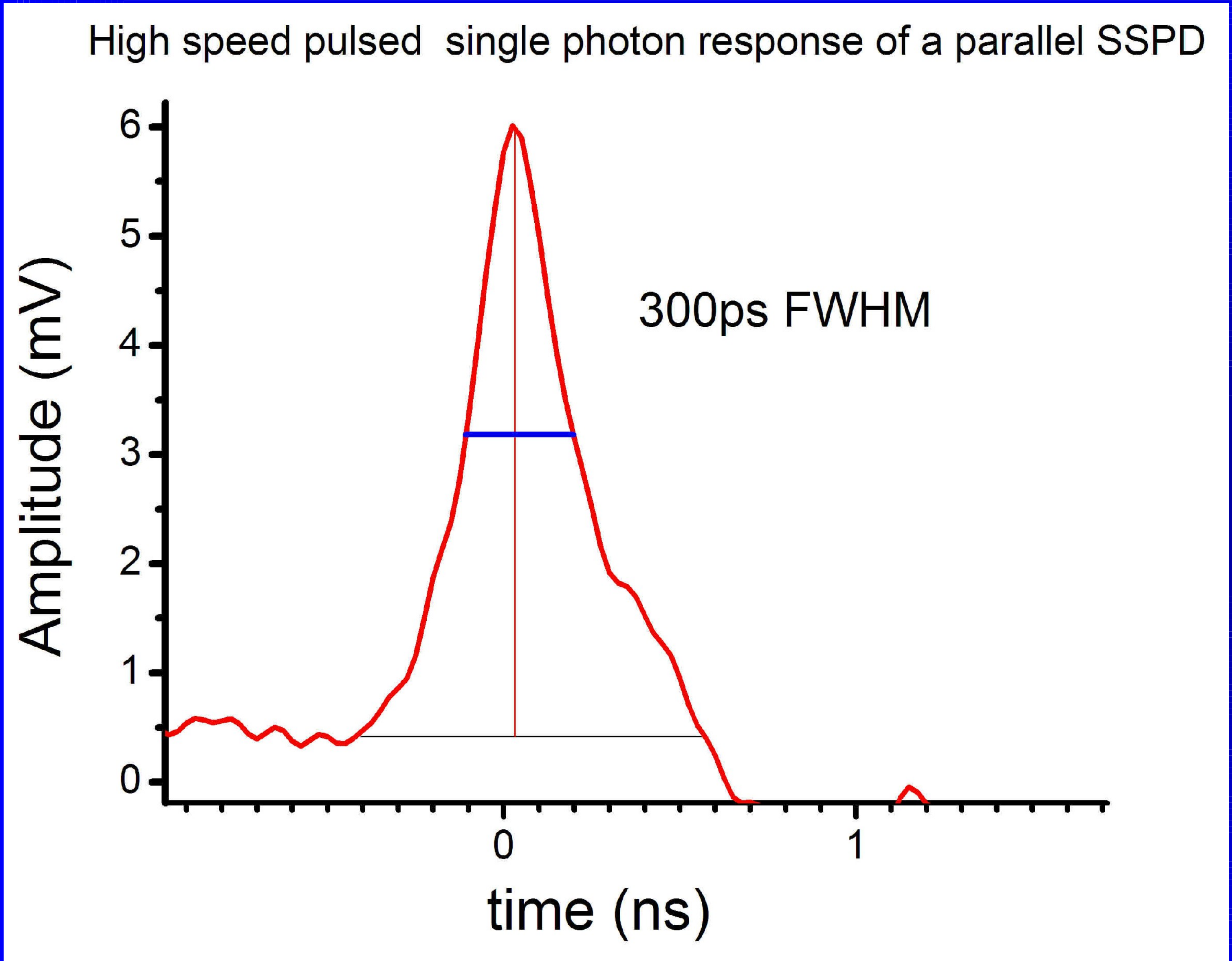

Results recorded with high speed oscilloscope (40GS/s) and medium speed (2GHz) interconnection.

More recent measurement with high speed interconnection (10GHz) have given 90 ps risetime

Different Parallel Wire configurations

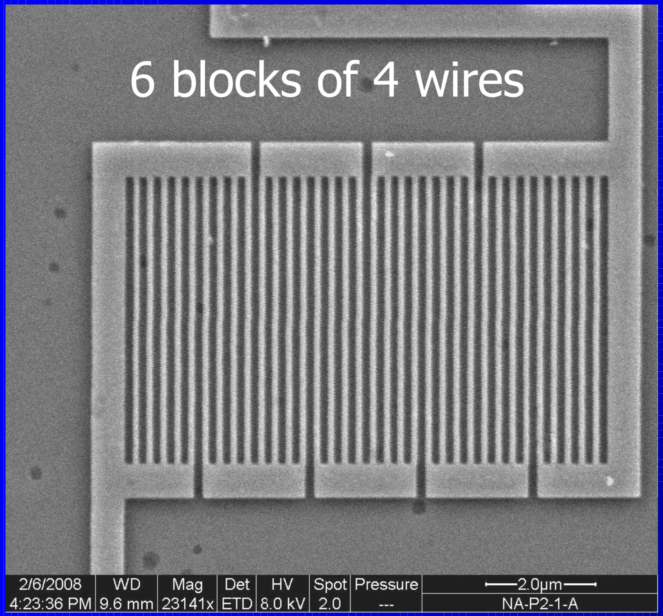

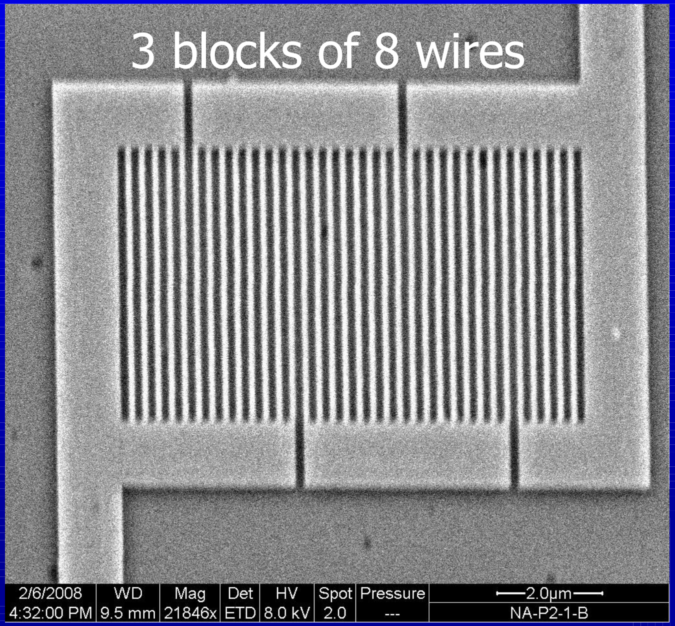

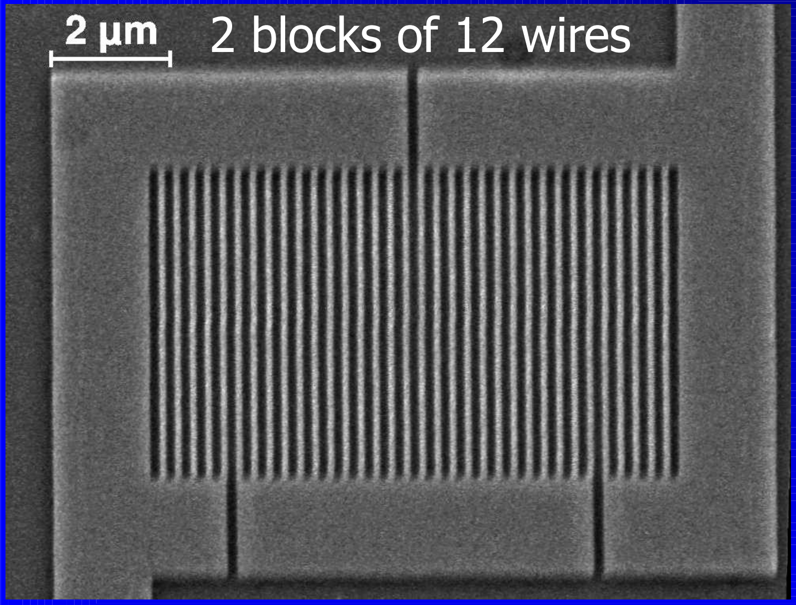

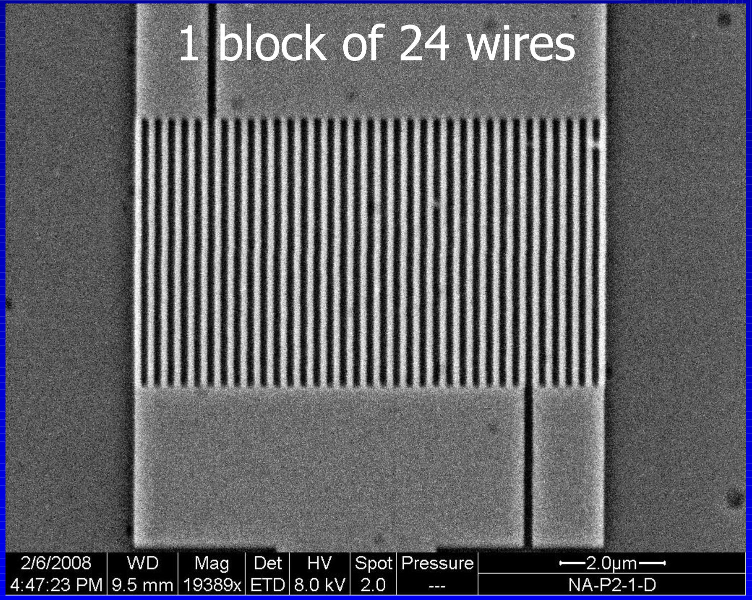

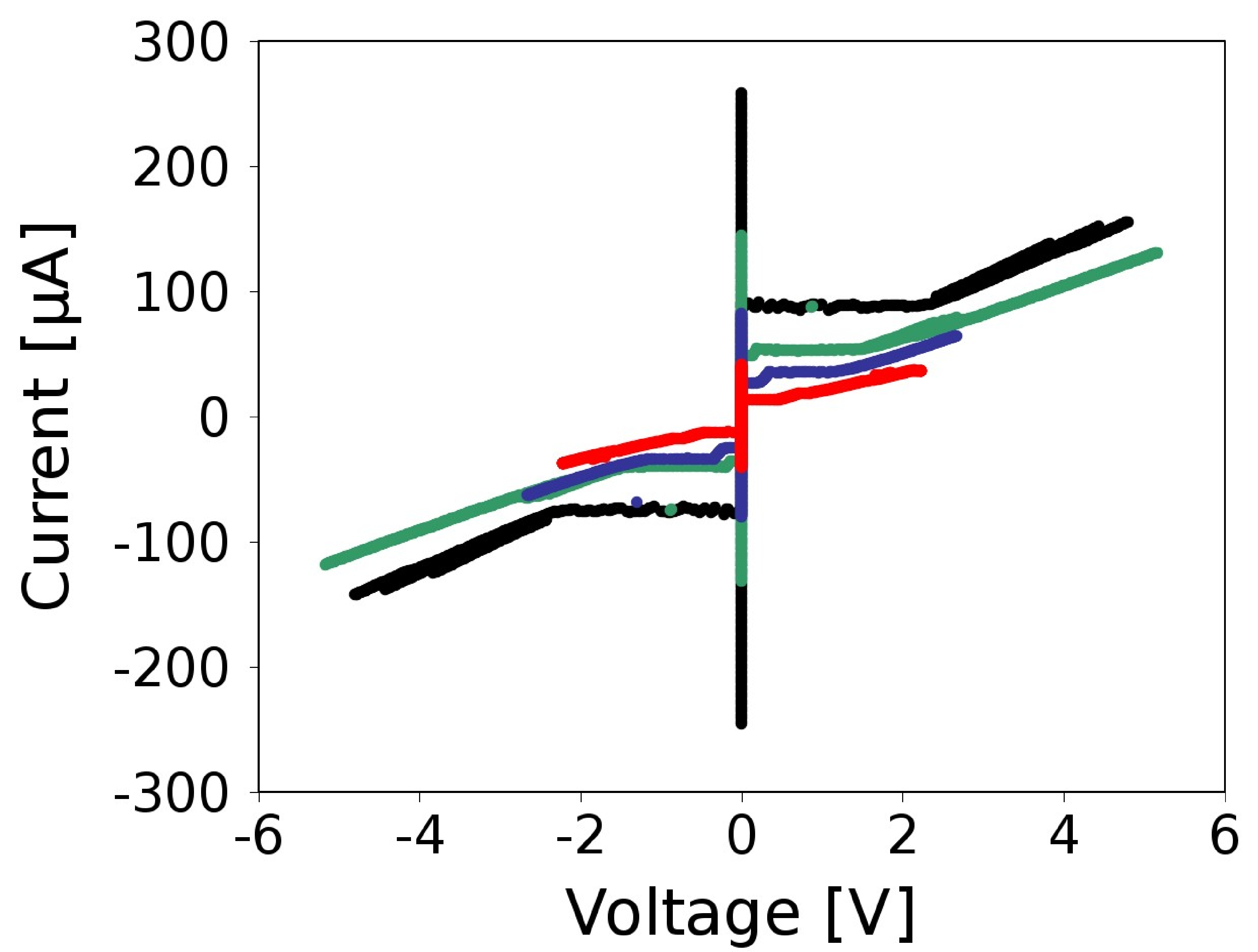
300
200
100
0
-100
-200
-300
Current [µA]
-6
-4
-2
0
2
4
6
Voltage [V]

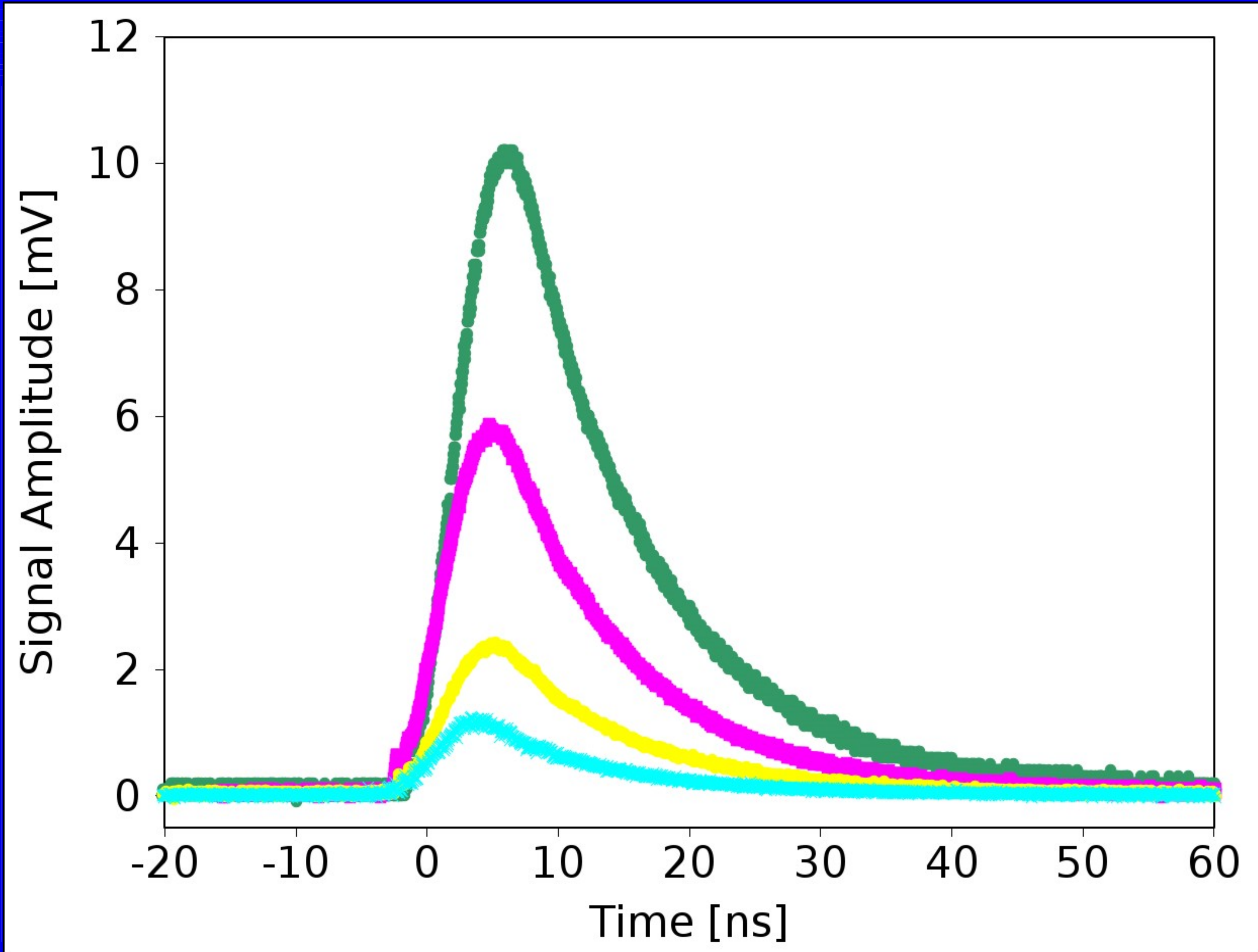

Signal Amplitude [mV]
12
10
8
6
4
2
0
-20
-10
0
10
20
30
40
50
60
Time [ns]

Meander SSPD integrated with pulse amplifier

The parallel configuration can act as pulse discriminator/amplifier:

A small current pulse is injected on the first nanowire and the overall structure switches generating a large voltage pulse

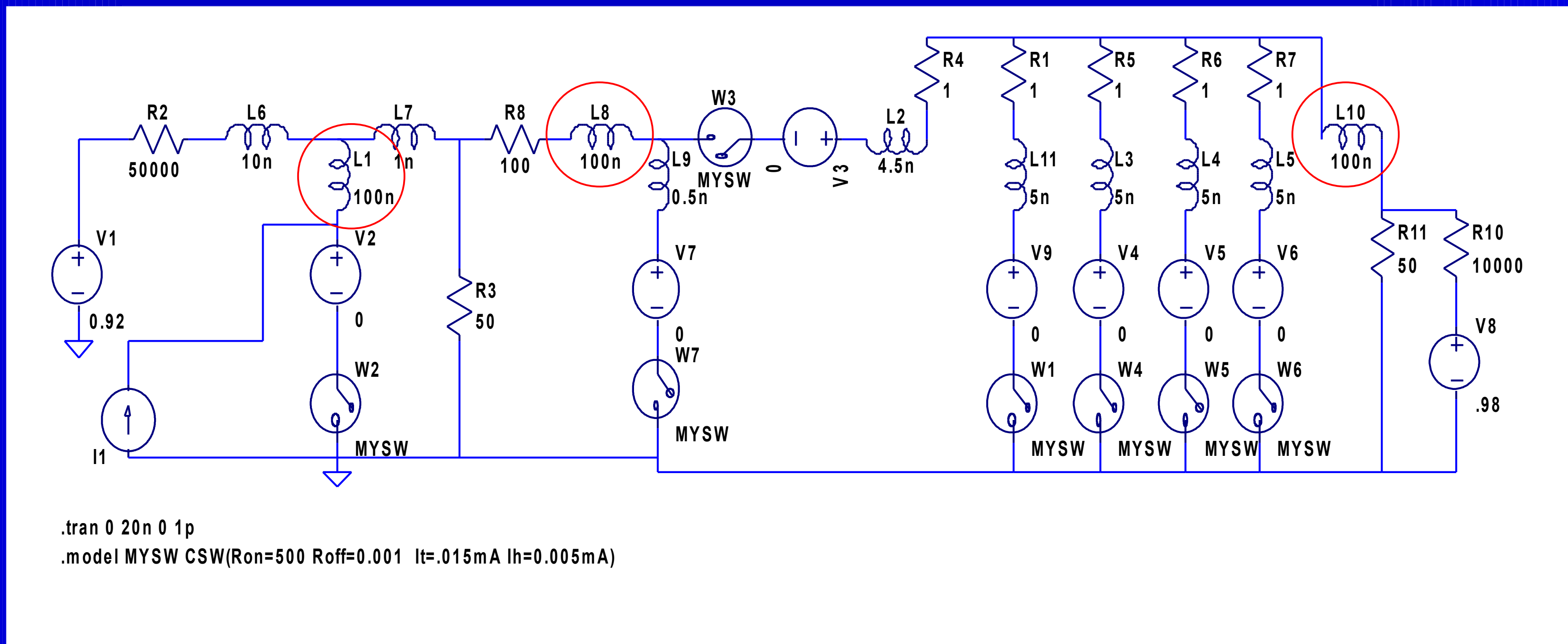

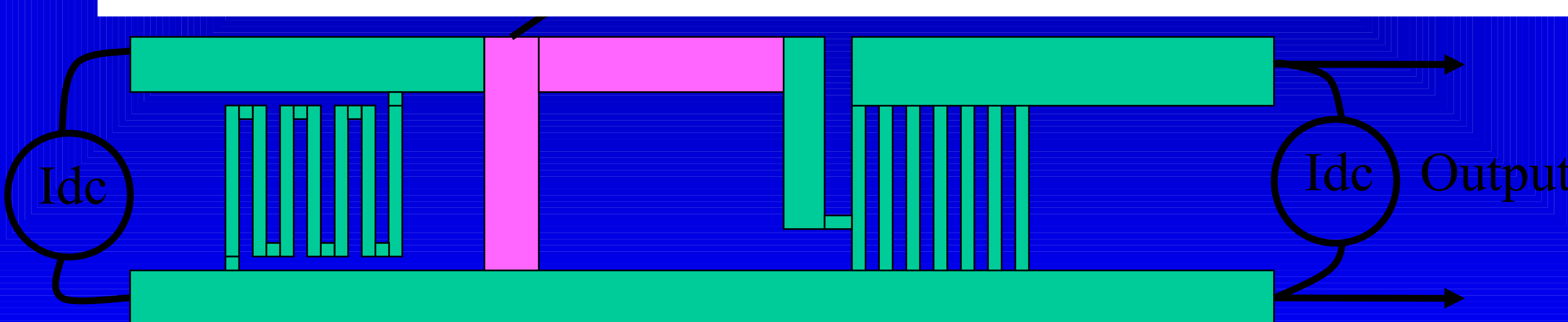

Simulation of the pulse amplifier driven by a standard SSPD with different coupling inductances

Prototype of pulse amplifier

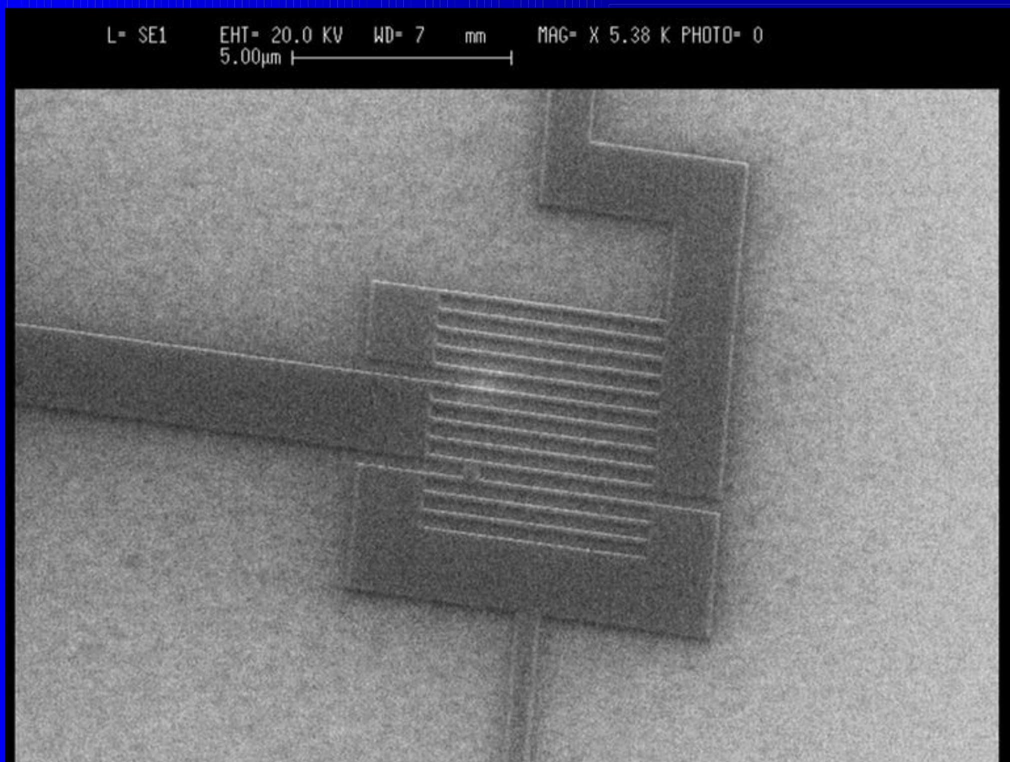

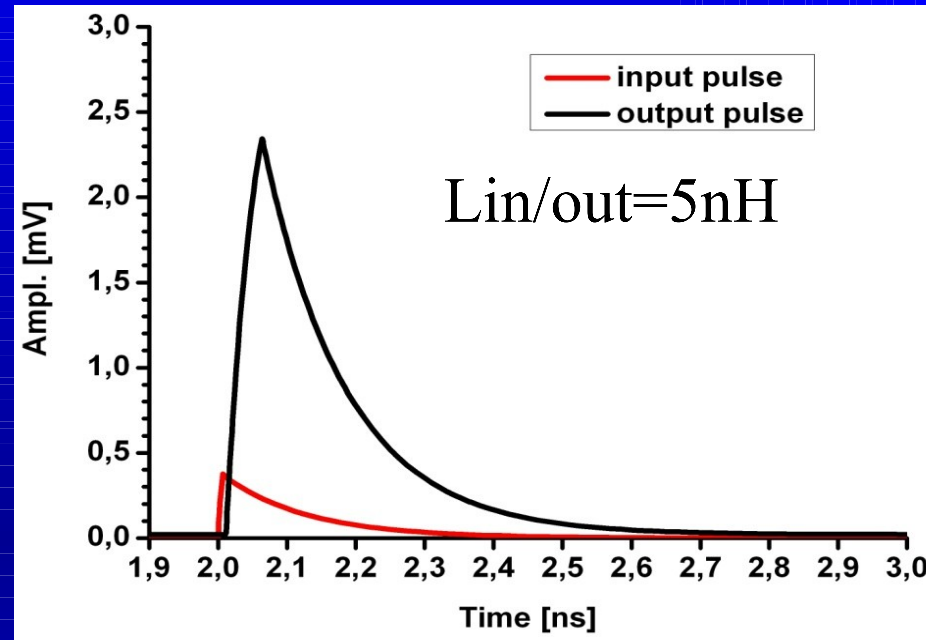

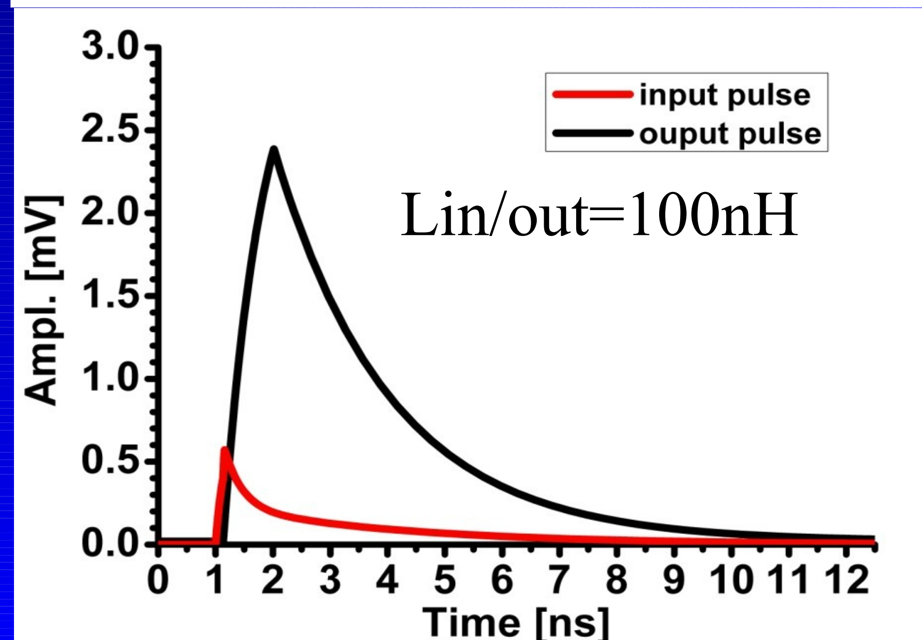

Conclusions (SSPD)

Superconductive Single Photon Detectors are very promising devices for a number of applications

A new parallel array configuration for SSPD has been developed

The parallel configuration exploits a cascade switching mechanism that preserves the sensitivity of “standard” meander SSPD, while providing a **substantial increase** of the signal amplitude and a **strong reduction** of the response time, and makes operation up to 10 GHz possible

Superconductive nanowires can make a new class of devices

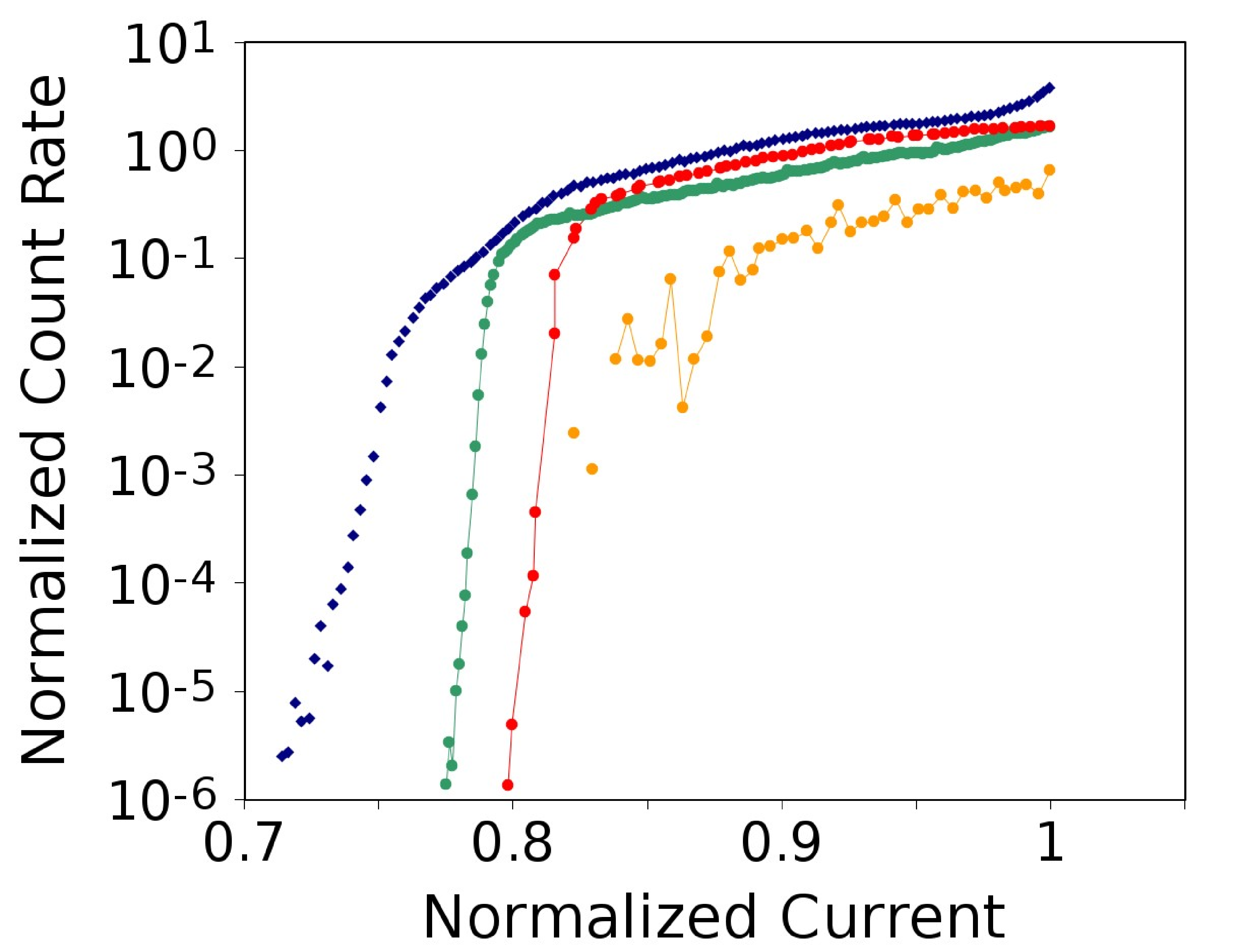

Normalized Count Rate
10^1
10^0
10^-1
10^-2
10^-3
10^-4
10^-5
10^-6
0.7
0.8
0.9
1
Normalized Current

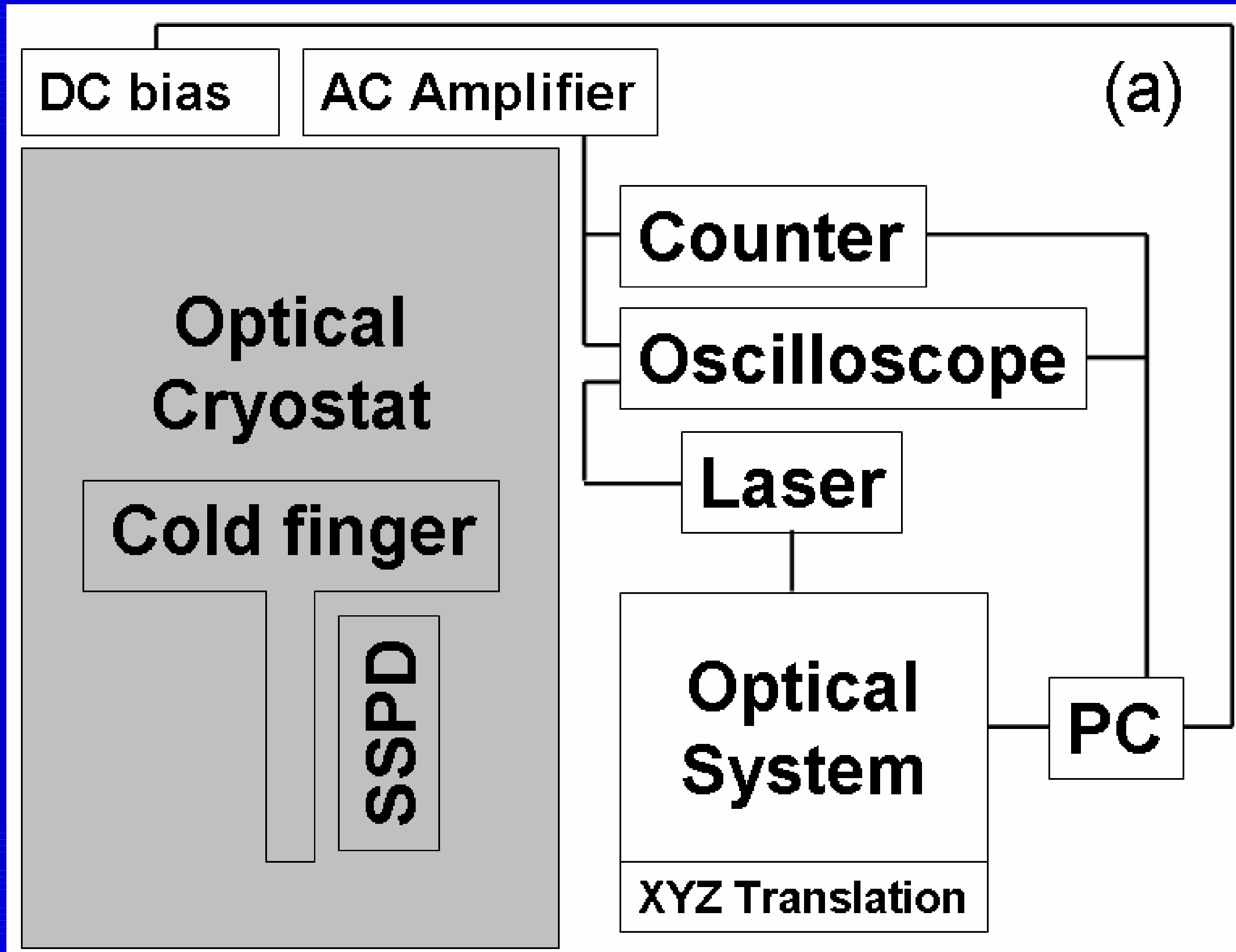
DC bias
AC Amplifier
(a)
Optical Cryostat
Cold finger
SSPD
Counter
Oscilloscope
Laser
Optical System
XYZ Translation
PC

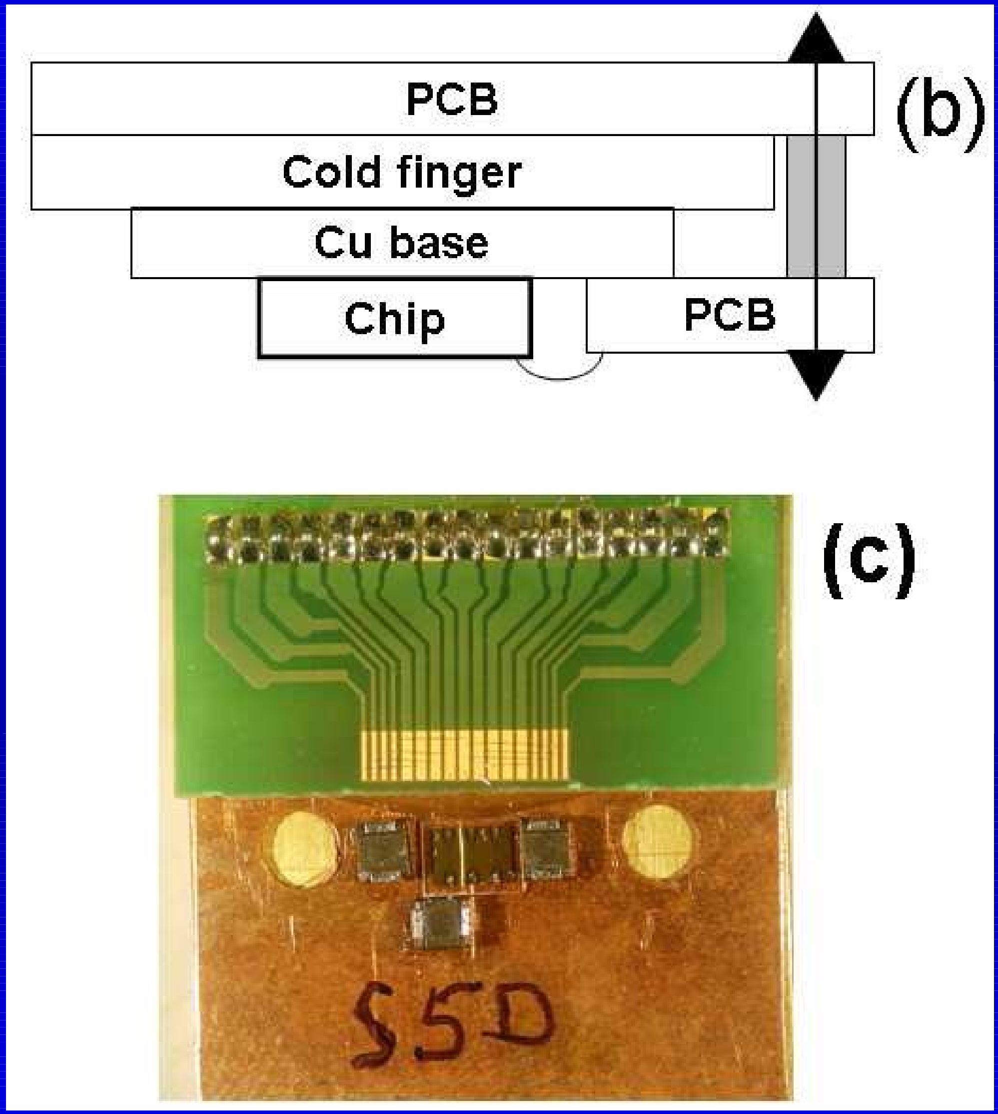
PCB
Cold finger
Cu base
Chip
PCB
(b)
(c)
S5D

Superconductive Detector Applications

Dark Matter detection,
X-ray to mm wave astronomy,
Material analysys,
Mass spectrometry,
Telecommunication,
Quantum cryptography,
CMOS testing,
CT,
Ionizing particles detection
…

In Search of the Dark Matter of the Universe

WIMPs

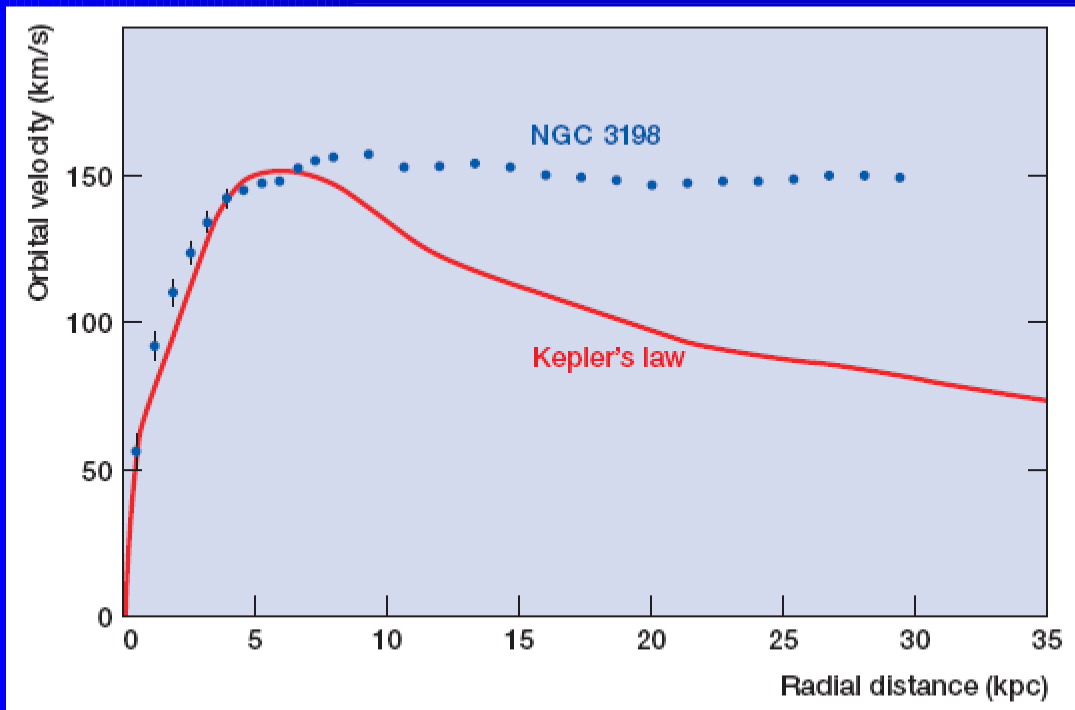

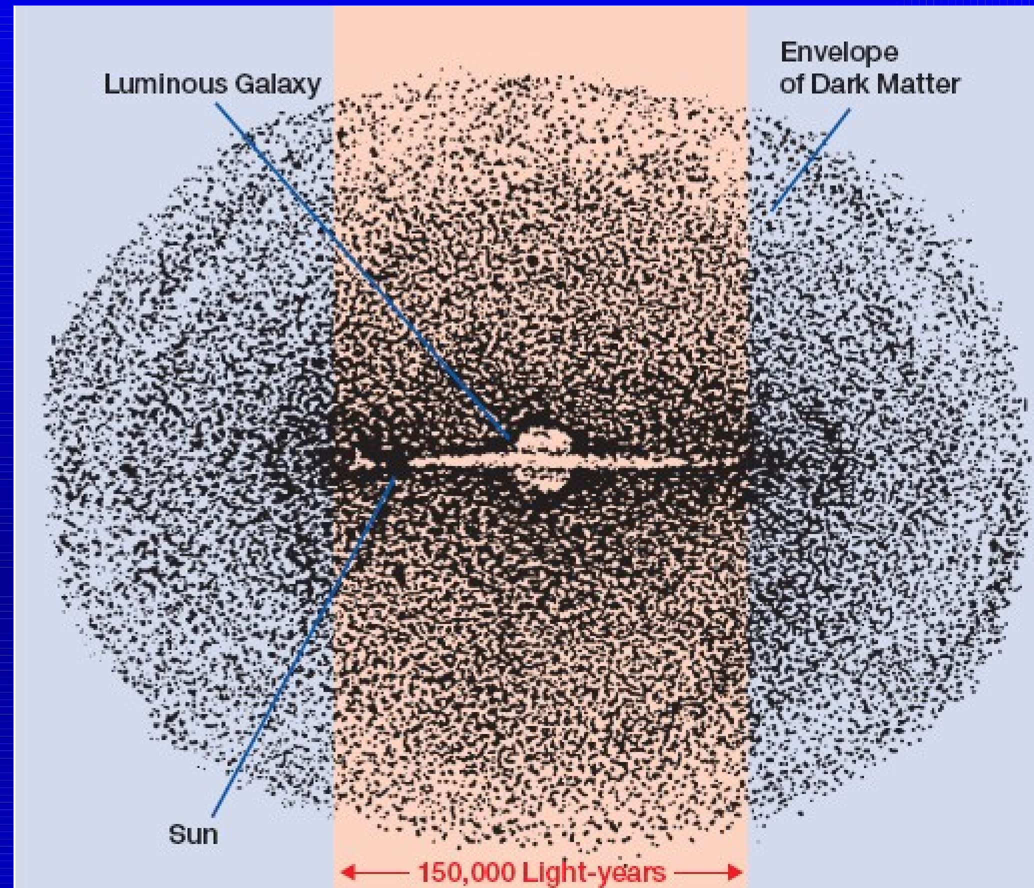

The observation of constant orbital velocities *of stars around the galactic center (here the spiral galaxy NGC 3198) as a function of the radial distance provides convincing evidence for the presence of an extended halo of dark matter surrounding the galaxy. The expected curve from Kepler's law if there would be no dark matter is also shown.*

K. Pretzl, Spatium , N.7 May 2001

There are currently a number of experiments searching for Dark Matter some use superconductive detectors

Present and future experiments on WIMPS

CDMS II	5 kg Ge + 2 kg Si	Soudan
CRESST II	2–10 kg $CaWO_4$	G.Sasso
EDELWEISS 2	120 kg Ge	Frejus
CUORICINO	40 kg TeO_2	G.Sasso
CUORE	790 kg TeO_2	G. Sasso
ORPHEUS	R&D	
ROSEBUD	100–300 g BGO/$CaWO_4$	Canfranc
HERON	Liquid helium	?
TOKIO	NaF + LiF	Japan

E. Fiorini / Nuclear Instruments and Methods in Physics Research A 520 (2004) 1–3

The ORPHEUS Experiment (University of Bern – Prof. K. Pretzl)

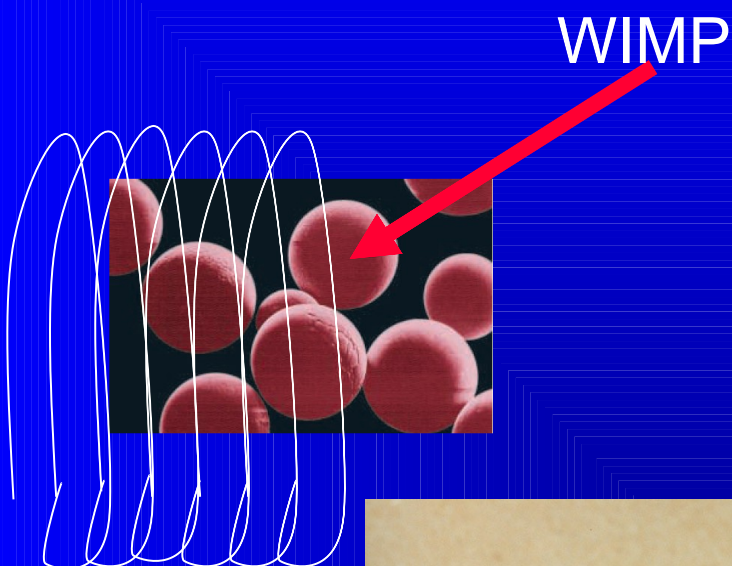

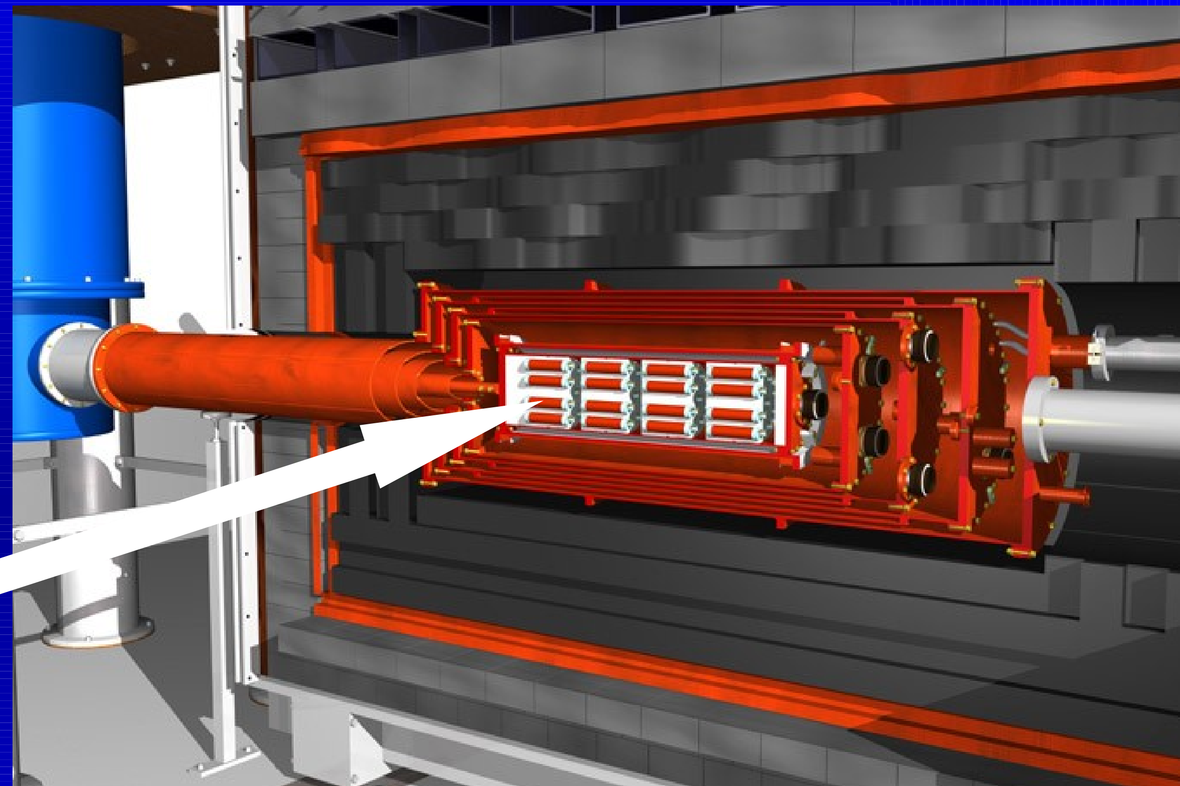

The ORPHEUS detector contains billions of small tin granules with a diameter of 30 micrometers. They are cooled down to 100 mK, where they are in a superconducting state. An interacting WIMP may generate enough heat in a granule to cause a phase transition from the superconducting to the normal conducting state. This phase transition of the granule can be measured with a sensitive read-out system (SQUID).

Dark Matter Search with Crystal absorber and STJ Detectors

a) Dark matter particle scatters off a nucleus. The recoiling nucleus loses energy with neighboring atoms of the crystal.

b) Atoms of the crystal vibrate about some mean position.
Thus phonons generation ⇒ phonon propagation

a) The vast majority of these "primaeval phonons" propagating away from the recoil region are unstable against anharmonic decay (lifetimes of ~ 10 – 100 psec) ⇒ (mean free path ~ 10^2-10^3 nm). However after each decay the anharmonic lifetime increases significantly because the decay rate various as ~ E^5 ⇒
After a number of decays the mean free path becomes greater than the size of the crystal ⇒ phonons propagate ballistically.

d) Phonons reach the surface of the crystal "giving" a signal due to the interaction with the STJ sensor (array).

e) Phonons escape from the target crystal via heat links to the outside world.

To determine recoil direction we should look at phonon flux anisotropy after stage c.

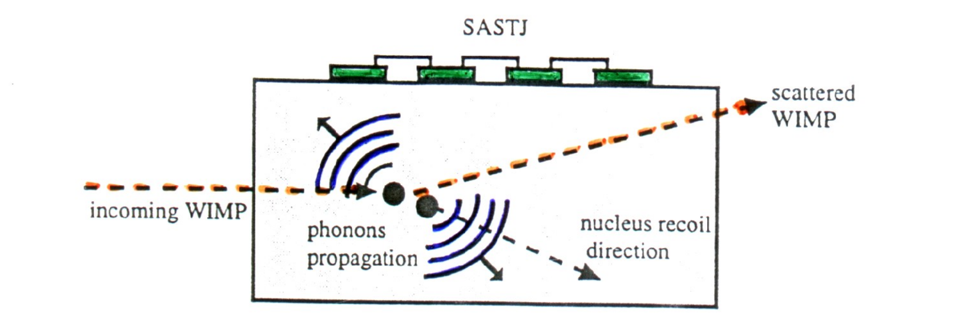

Fig. 3. Scattering of a WIMP on a nucleus in a prototype detector.

APPLICATIONS: EDS-Microanalysis

Typical problem: sub-micron particle

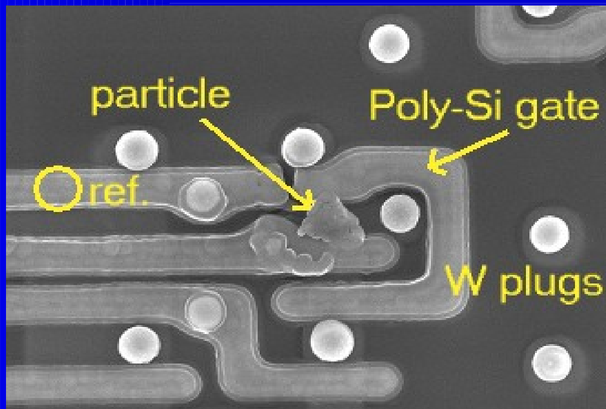

the lower the excitation energy
the better the spatial resolution

Solution:

Low energy excitation

- low excitation energy
  - not enough energy to excite K-lines of heavy elements (Fe, Cu, Ta, ...)
- only excitation of L- and M-lines
  - closely spaced
  - energy resolution of conventional EDS is not good enough (120 eV)
- **use of superconduting detectors**
  - energy resolution < 20eV

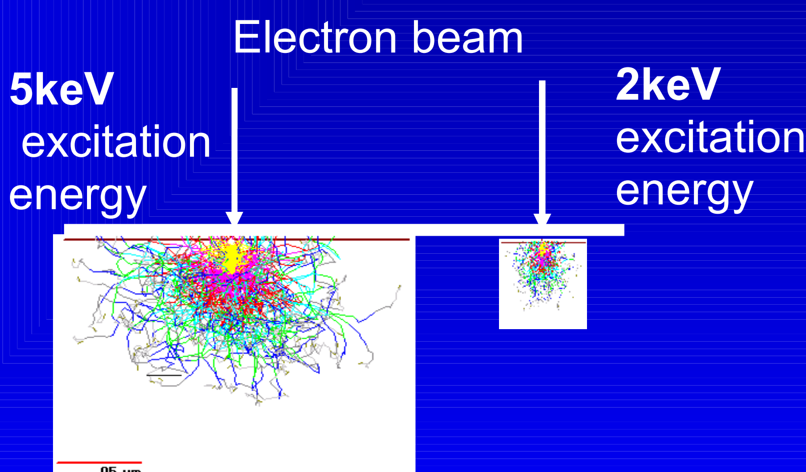

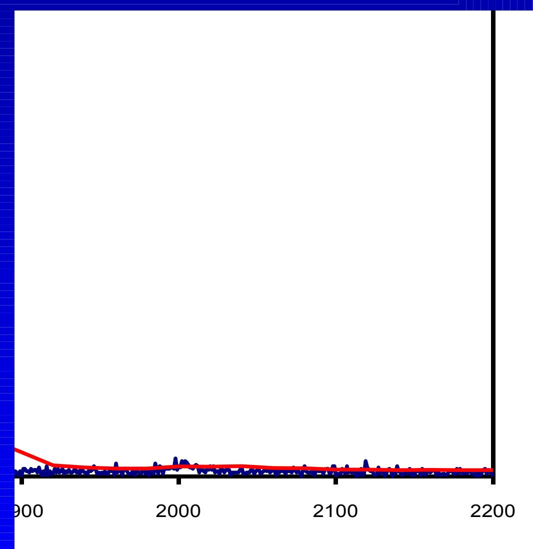

EDS-Polaris system with TES
is commercialized by Vericold Gmbh and by Edax Inc.

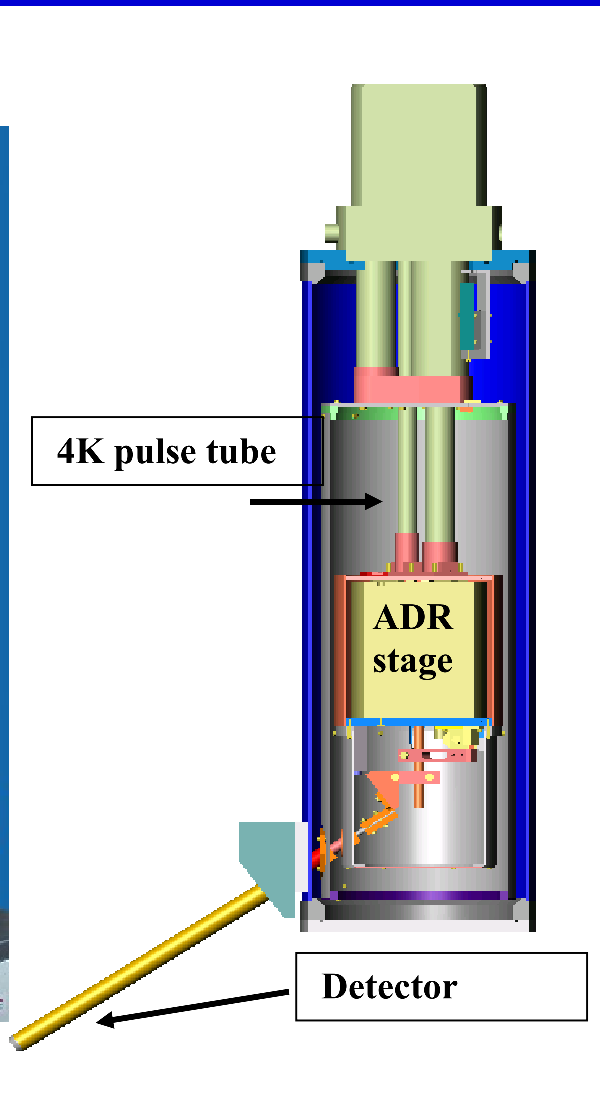

Cryogen-free cryostat for T = 60mK
TES-Detector

- **No harm from spilled liquid coolants**
- **Automation and user-friendliness**
- **Low operational costs**
- **Clean room compatibility**

Installed at CNR-ICIB

Example of typical spectra obtained with POLARIS at CNR-ICIB

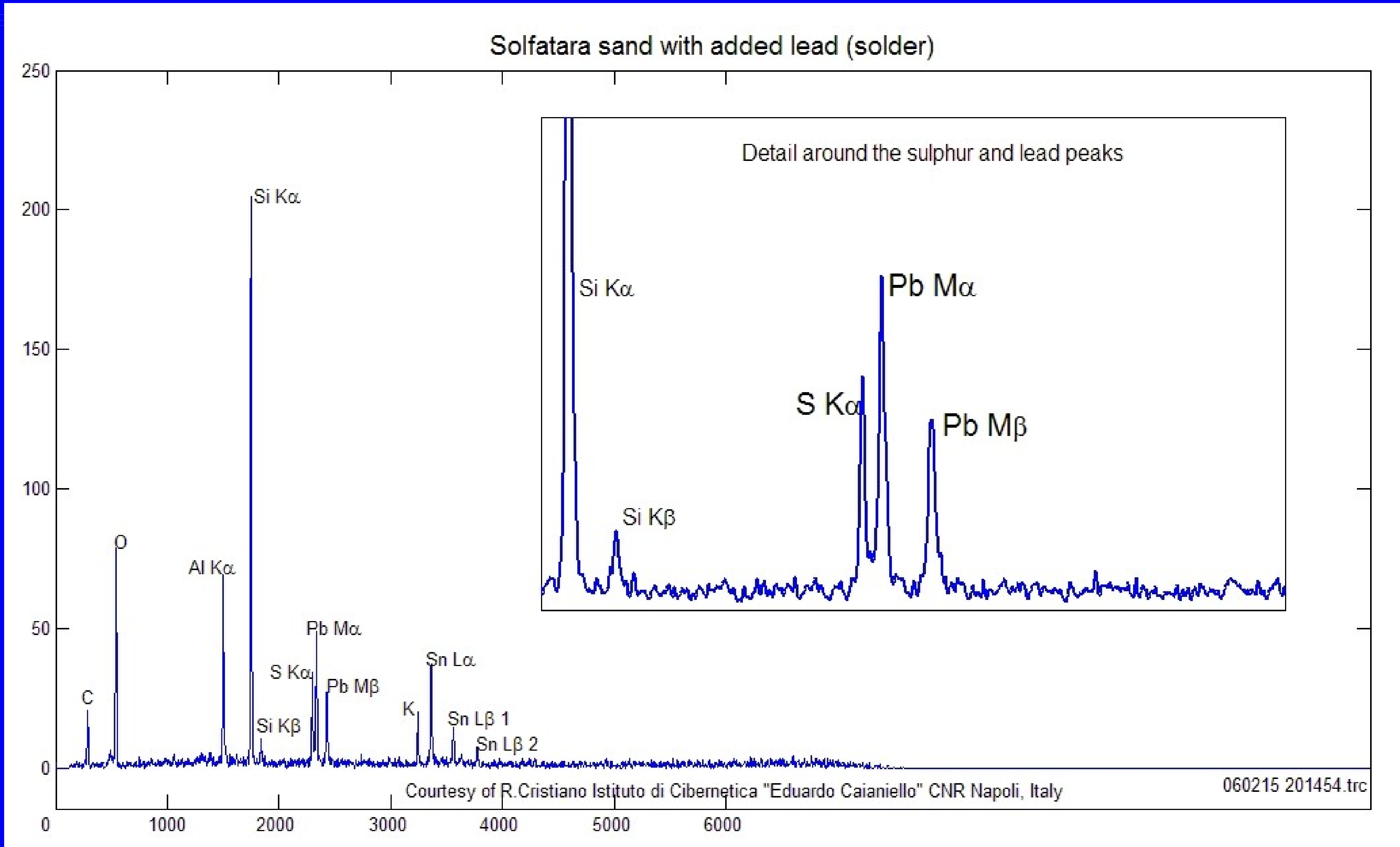

The energy difference between Pb Mα and S Kα is 36 eV.
The low background allows quantitative analysis.
The resolution on the Al Kα (E=1.486 keV) is 15 eV.

APPLICATIONS: X-Ray Astronomy

cosmological aspects of hot matter in the Universe

Next generation (2008-2015) X-ray astrophysics missions relies entirely on the successful development of **efficient imaging spectrometers**.

Requirements

X-Ray Band	0.1-40 keV
Resolving Power E/ΔE	300-3000
Equivalent Coverage Area	32x32 pixels
Pixel size	0.2x0.2 mm^2
Counting Rate	> 4000 c/s

the Constellation-X mission

Constellation-X (Con-X) is a NASA mission now under formulation to provide a 100-fold increase in collecting area with 15″ imaging and a <4 eV energy resolution microcalorimeter arrays with 1000 pixels [2]. The mission will consist of 4 identical observatories located at the Sun–Earth L2 point. Con-X is currently planned for a launch of the first two satellites in 2013 and the remaining two a year later.

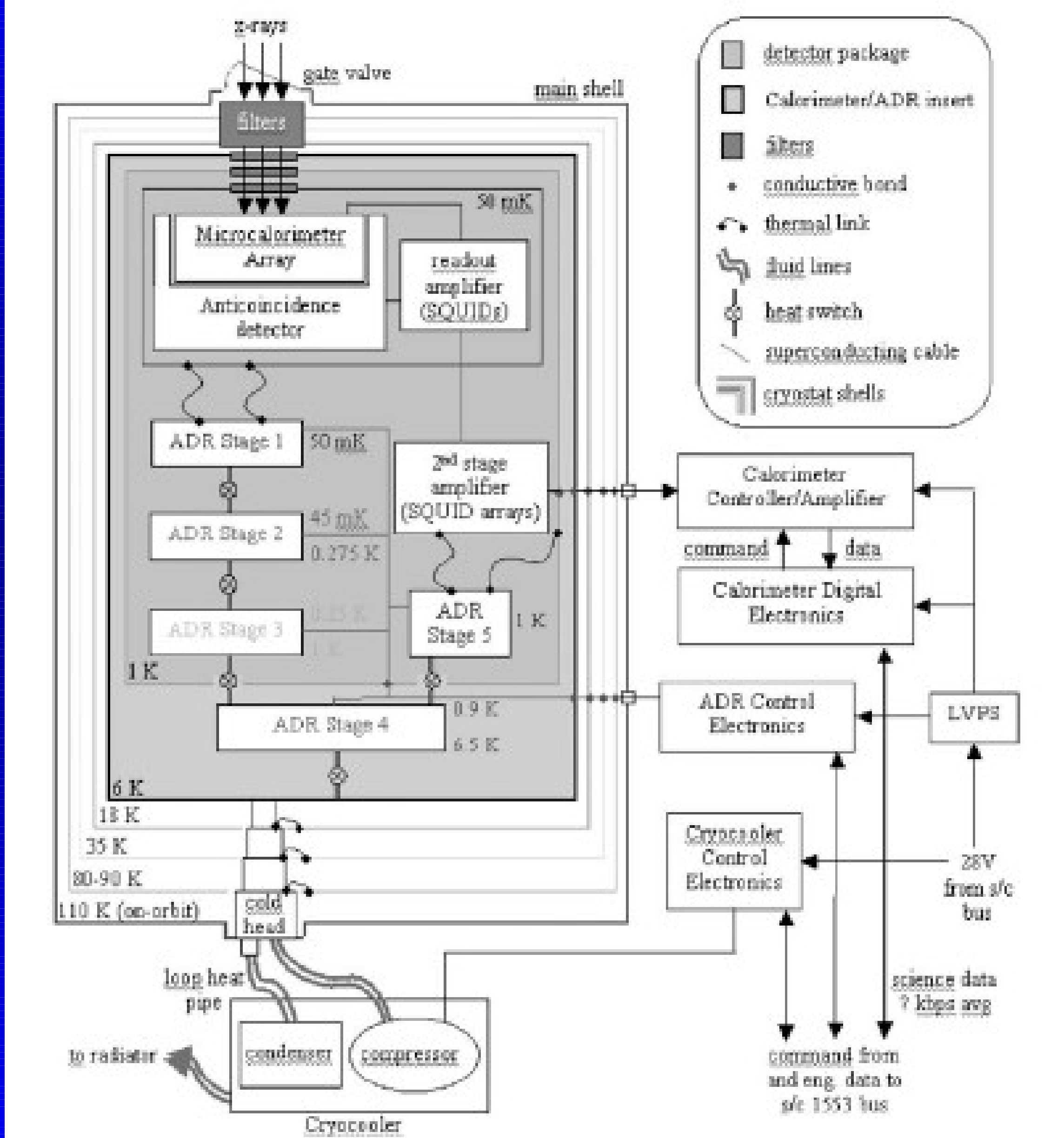

Fig. 1. Block diagram of the Constellation-X X-ray microcalorimeter spectrometer.

R.L. Kelley / Nuclear Instruments and Methods in Physics Research A 520 (2004) 364–367

APPLICATIONS: UV-Visible-NIR astronomy

$\lambda \sim 100 - 1000$ nm

Dispersive spectroscopy is wastful of light

Particular problem when studying faint objects

- **CCDs** combine large sensitive area (several cm^2), high resolution imaging and excellent quantum efficiency (QE), but no photon-counting capability and marginal QE for $\lambda<300$nm
- In UV, **MCPs** are most widely used because of the better QE of 10-40% and photon counting capability with time resolution $\Delta t<1\mu s$

- Unlike optical CCD's **STJ** and **TES** record not just the **position** of the incoming photons, but also their **wavelength** (**$\lambda/\Delta\lambda$=18 towards 60 at 500nm**).
  →**Never before possible in the UV/visible/NIR band**.

STJ and **TES** offer quantum efficiency of 50-70%, **single photon counting** in **NIR**

One space-based STJ (or TES) instrument could cover the entire spectral region from **far –UV** (115nm) through to the **NIR** (>few μm's)

Large sensitive area can be covered either with **Arrays** or with **Diffusive Read Out Imaging Devices** (DROID)

Application: UV-Visible astronomy

ESA S-Cam Instrument   N.Rando *et al* RSI <u>71</u> (2000) 4582

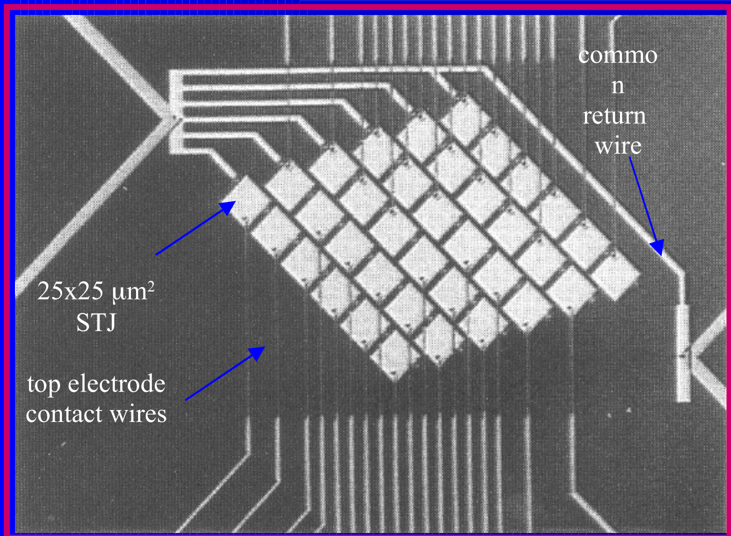

- Operating temperature: 320mK
- S-Cam2   6x6   Ta-STJ $\lambda/\Delta\lambda$=8 at 500nm
  (S-Cam3 10x12 Ta-STJ $\lambda/\Delta\lambda$=13)
- Responsivity 10^4 e^-/eV
- detection efficiency >50%
- Response time   10 μs

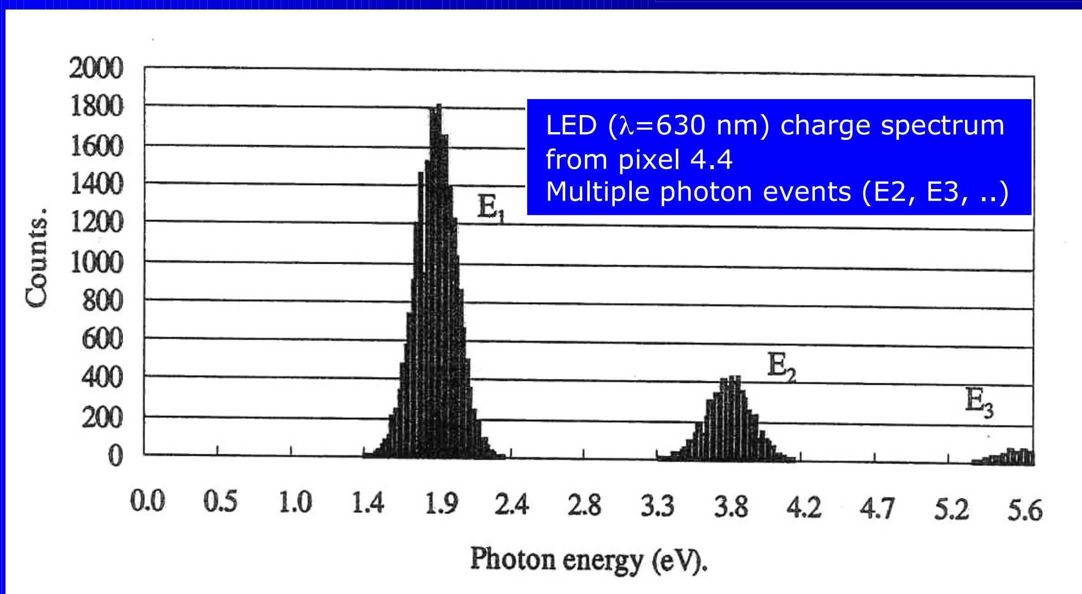

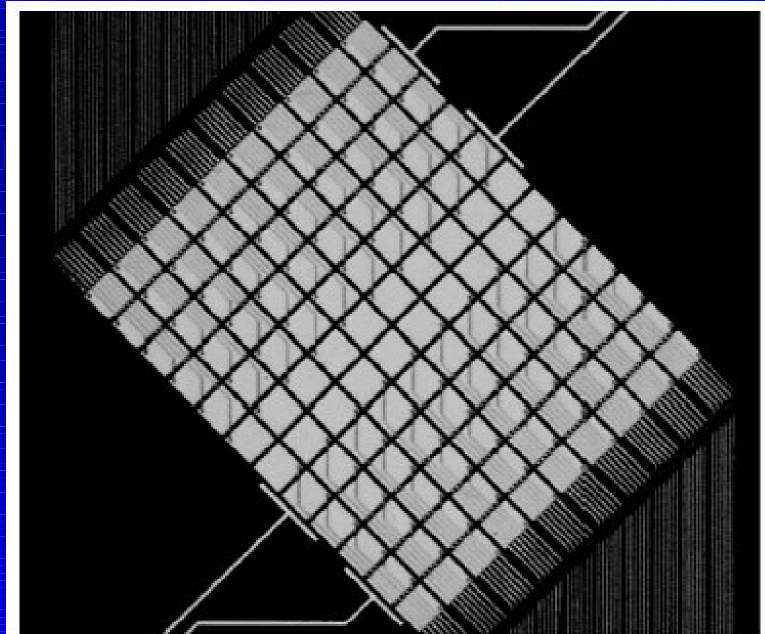

Fig. 2. S-CAM3 array micrograph.

Astronomical Observations:

ESA   **W. Herschel Telescope on La Palma**

RIKEN **SUBARU National Astronomical Obs.**

D.D.E. Martin et al. / Nuclear Instruments and Methods in Physics Research A 520 (2004) 512–515

8 x 8 TES array operating at 90 GHz on the 100 m Green Bank telescope

multiplexed SQUID readout
cryogen free 300 mK cooler

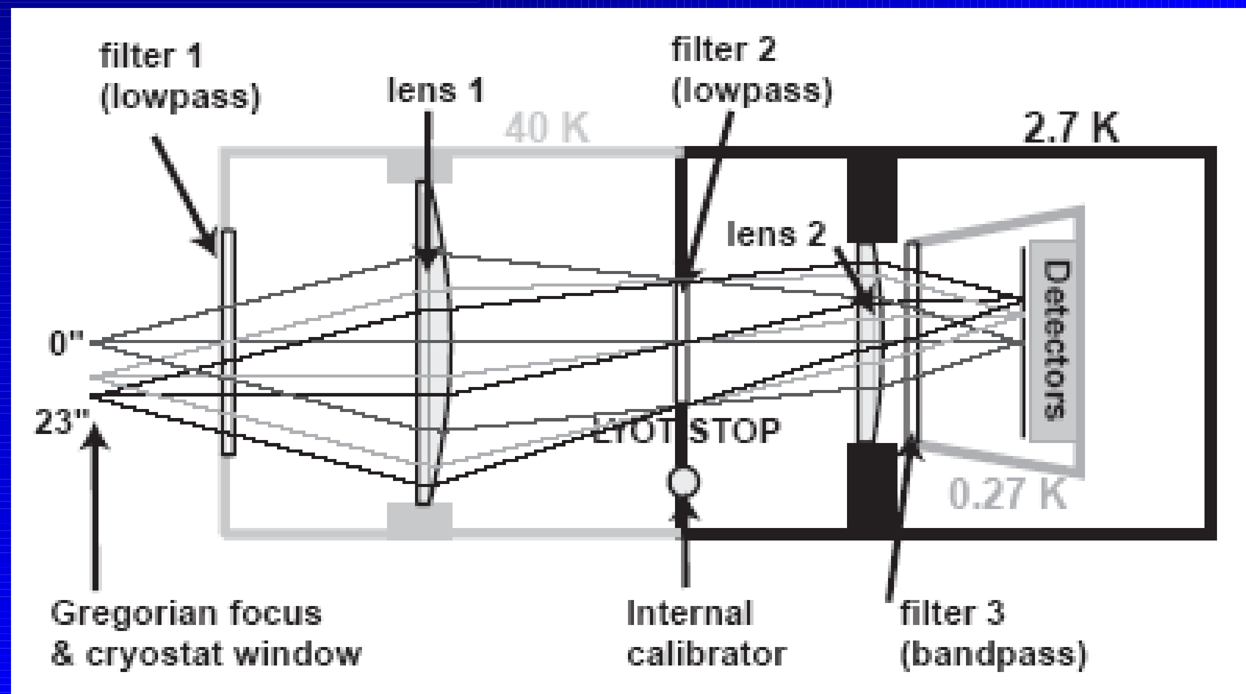

D.J. Benford et al. / Nuclear Instruments and Methods in Physics Research A 520 (2004) 387–389

multiplexed SQUID readout of TES arrays

time division

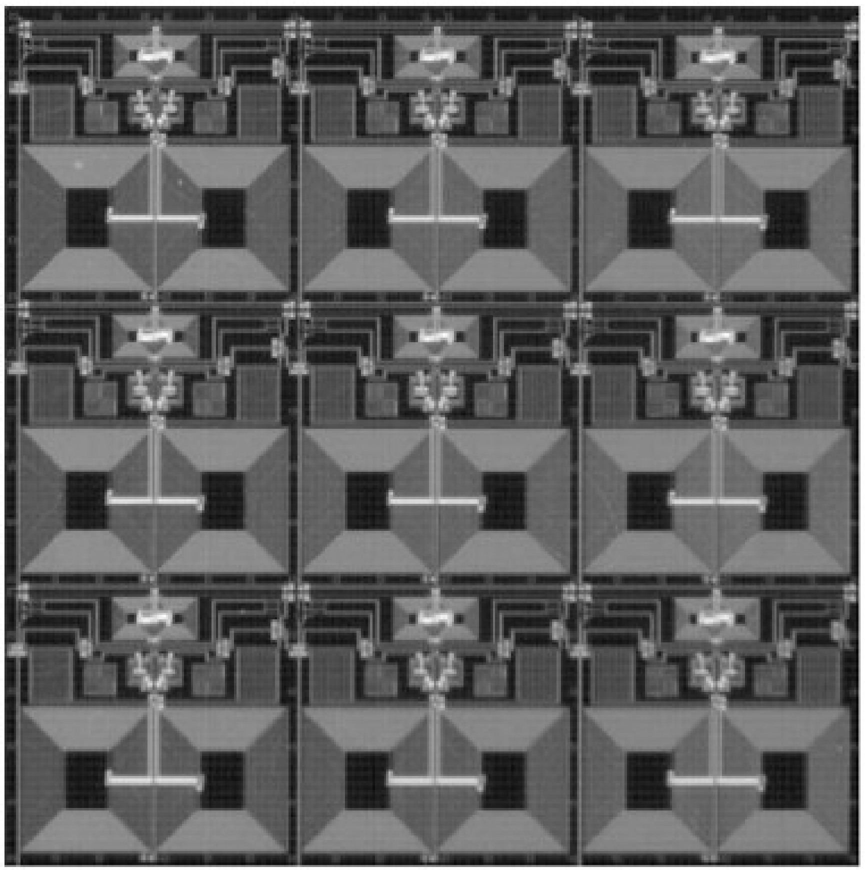

Fig. 4. Photograph of a 3 × 3 array of MUX pixels. Each pixel is 1.135 mm square.

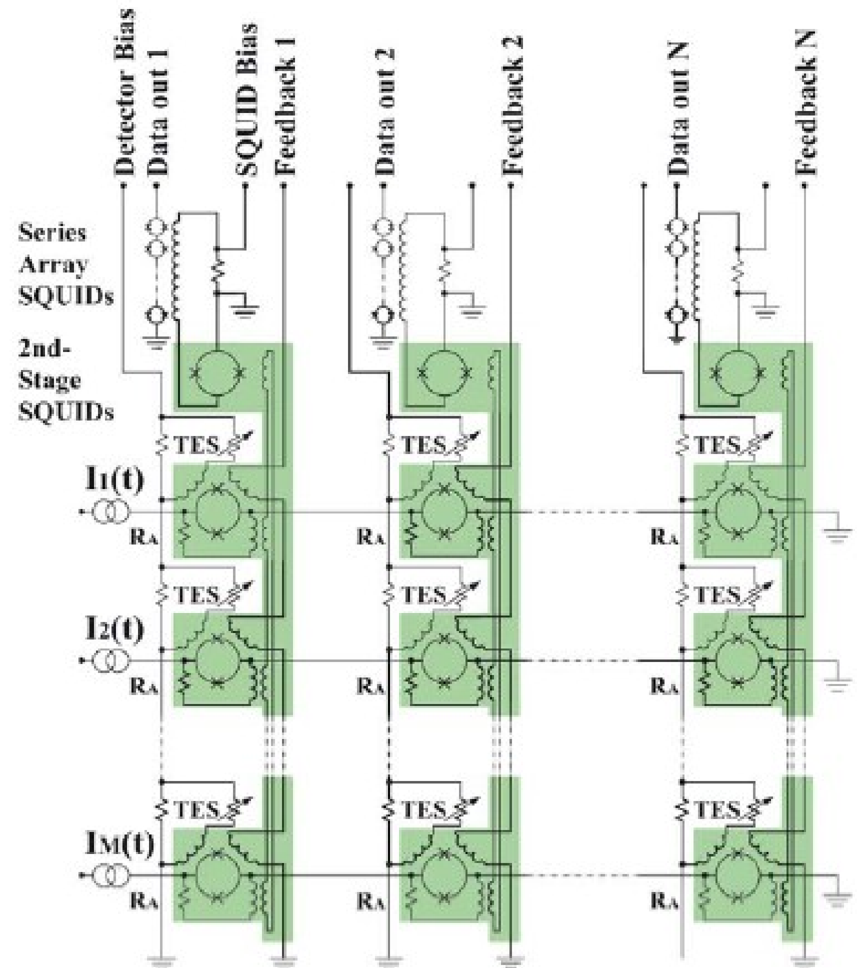

Fig. 1. The SQUID MUX circuit architecture used in the in-focal-plane multiplexer.

K.D. Irwin et al. / Nuclear Instruments and Methods in Physics Research A 520 (2004) 544–547

multiplexed SQUID readout of TES arrays

frequency division

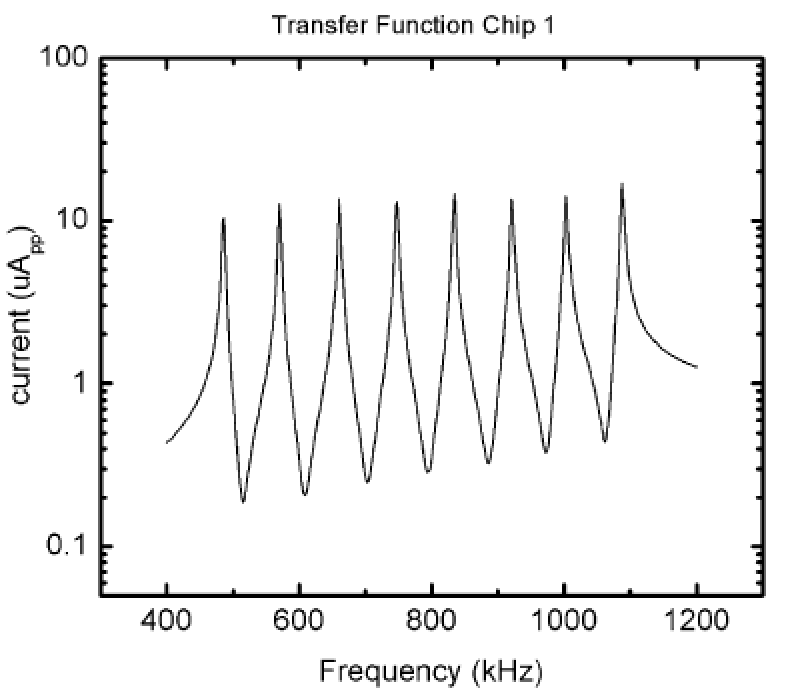

Fig. 2. Transfer function of LC filter chip connected to 0.5 Ω resistors.

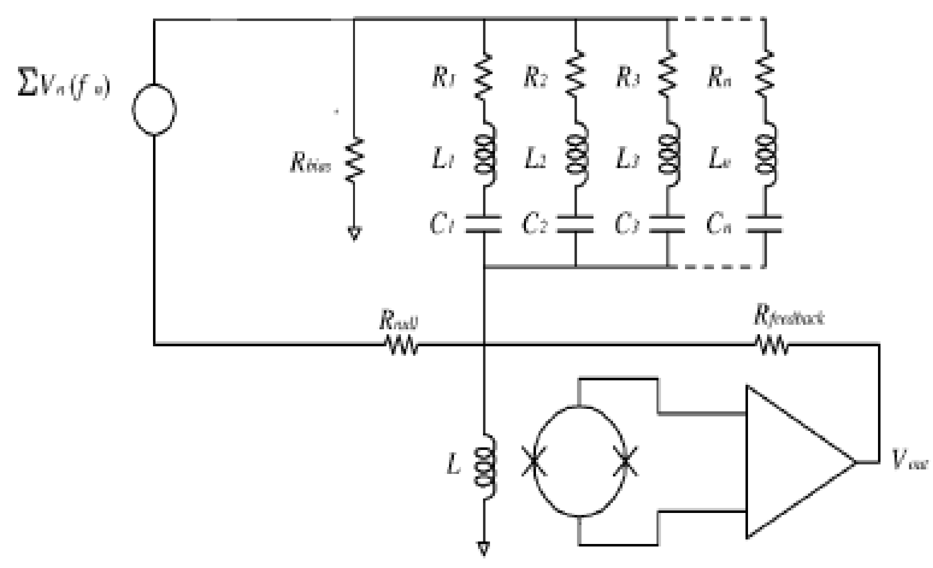

Fig. 1. Diagram of multiplexed readout circuit.

T.M. Lanting et al. / Nuclear Instruments and Methods in Physics Research A 520 (2004) 548–550

APPLICATION: CMOS device debug

Single-photon emission from CMOS transistors collected using NbN SSPD

Normally operating CMOS transistor emits near IR photons (1.25-1.75 μm) when current pulse passes through the channel.

When V_{out} is switching from 1 to 0, *n*MOS emits photons.

When V_{out} is switching from 0 to 1, *p*MOS emits photons.

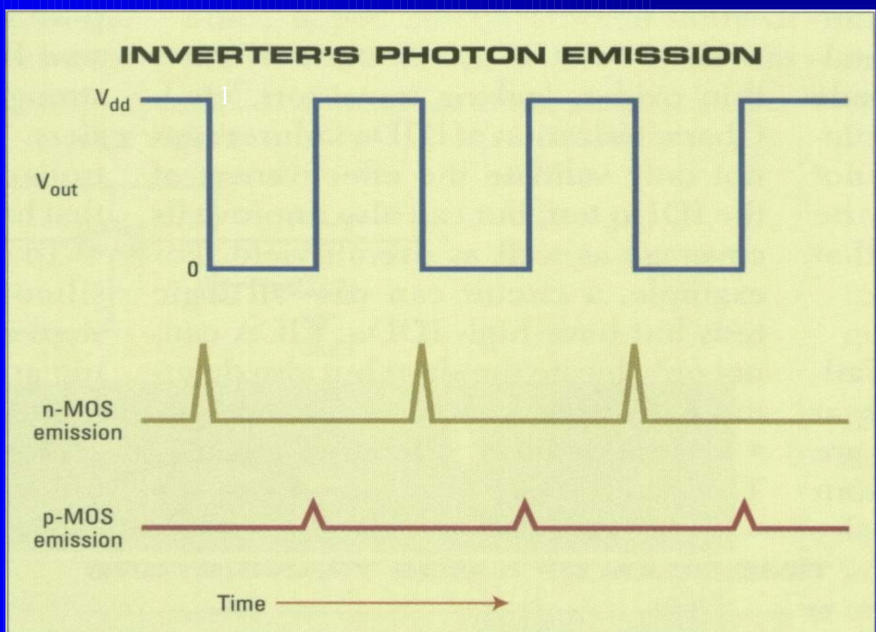

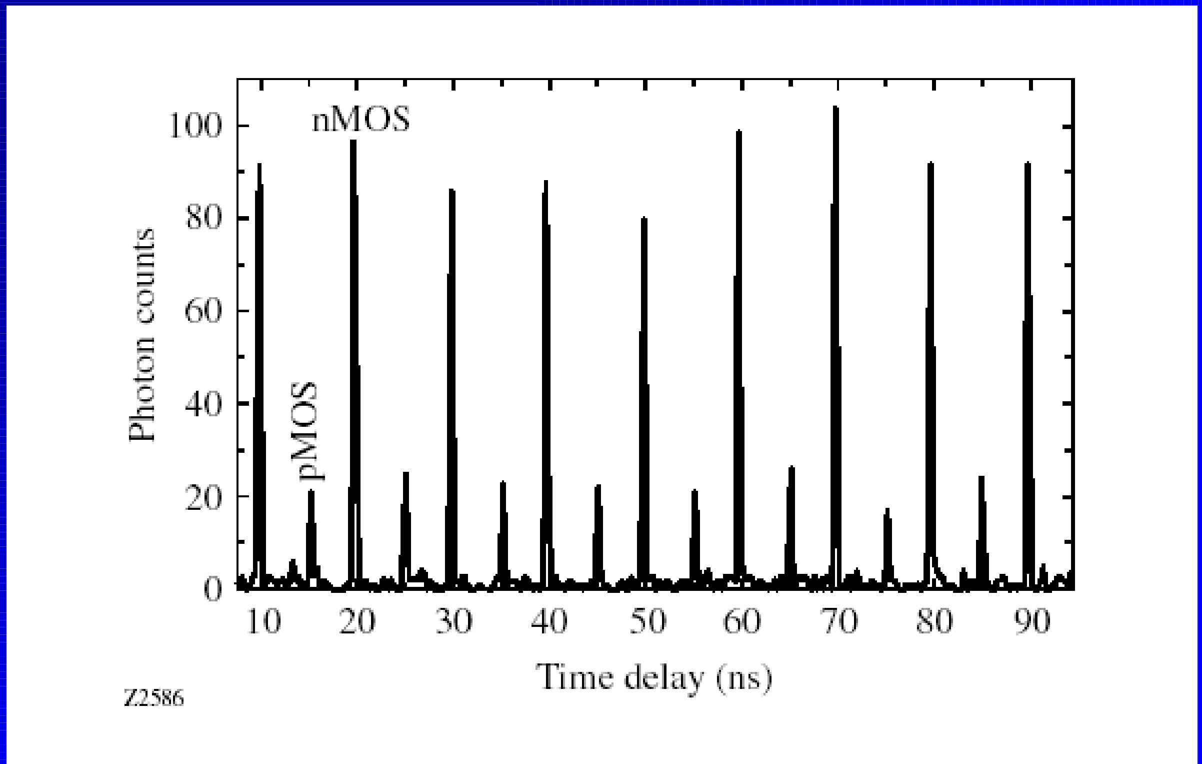

CMOS-Microanalysis

OptiCA® system with **NbN SSPD**
is commercialized by NPTest, Inc.

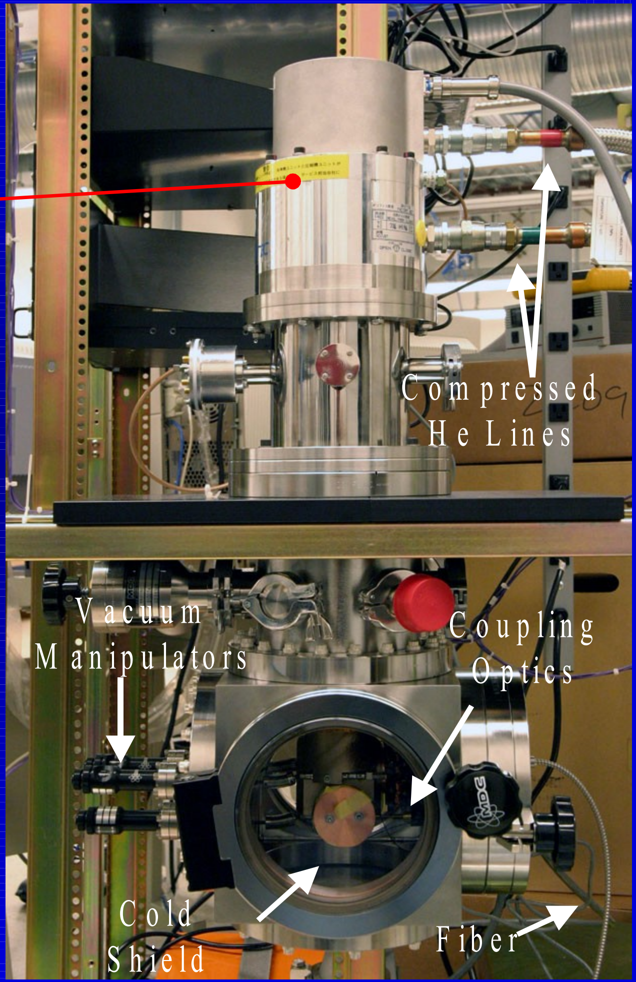

For more information:
http://www.nptest.com/products/probe/idsOptica.htm

Application: fiber optic telecommunication

Data transmission rates:
- **10 GBPS (current)**
- **40 GBPS (expected)**
- **160 GBPS (future)**

Problems:
- **Fast processing electronics**
- **Power dissipation**
- **Sensitivity**

Electric Optic Electric

$\lambda = 1550$ nm

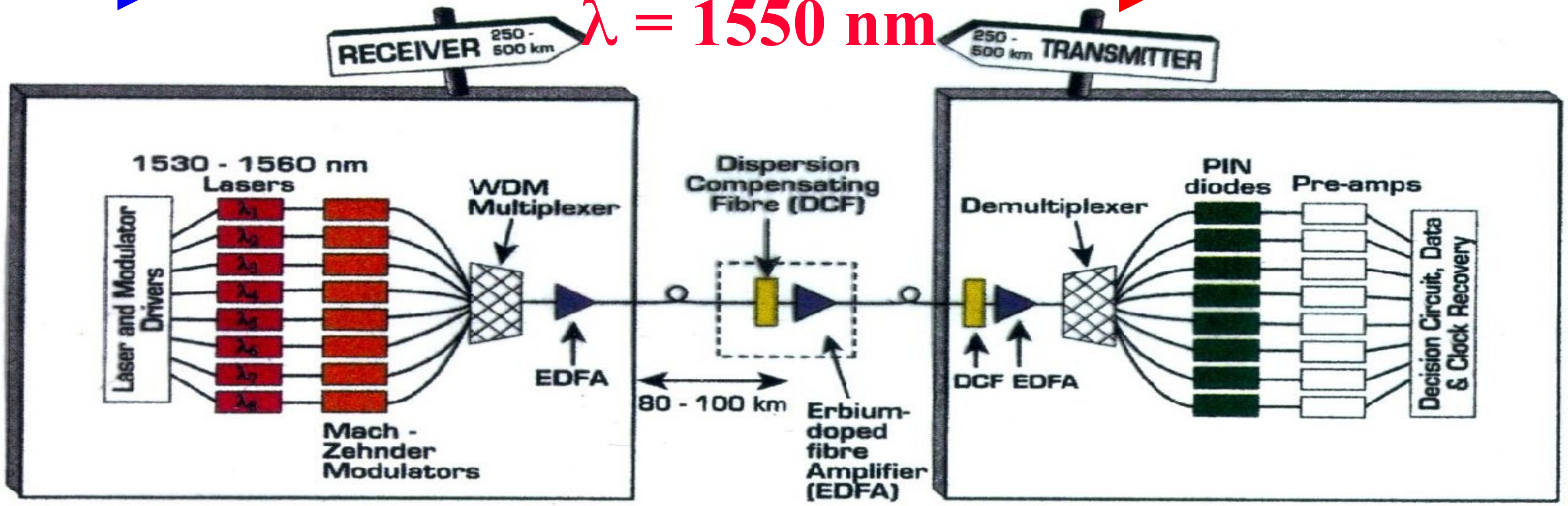

Unidirectional WDM communication link with key transmitter, optical fiber and receiver components.

Solution: Superconductive digital processing logic (RSFQ)

fast (f>40GHz)

low power

Rapid Single Flux Quantum Logic

Rapid Single Flux Quantum electronics is based on the Josephson effect and magnetic flux quantization in loops of superconductor material.

The logic state is represented by a Single magnetic Flux Quantum Φ_0 in a small superconductor loop with a natural fixed value. If the small superconductor loop is broken, a Φ_0 can be transported into or out of the loop. The breaks of the loop realized by Josephson junctions can be controlled by an additional Φ_0. So the contribution of a Φ_0 can be controlled by another Φ_0. Based on this behaviour it is possible to build an equivalent to all basic logic gates used in the semiconductor technology.
The switching time of some pico seconds is very short, because the circuit don't leave the superconducting state, opposite to further superconductor logic devices.

This results in a Rapid logic technology called RSFQ.

In comparison to the semiconductor CMOS electronics, RSFQ electronics has the potential of clock frequencies of some 100 GHz combined with very low power consumption.

Today, the state of development and use of RSFQ is similar to that of CMOS 30 years ago. RSFQ will not replace the large zoo of CMOS applications, however the focus of application is on some critical devices where RSFQ can overcome the limits of CMOS technology.

$$\int_{F_0}^{F_0+2\pi} V(t)\,dt = \frac{h}{2e} = \Phi_0$$

Example of an RSFQ circuit: Output Interface

IEEE TRANSACTIONS ON APPLIED SUPERCONDUCTIVITY, VOL. 11, NO. 1, MARCH 2001

Interface Circuit Using JTLs as Control Lines of SQUID Array

Yoshinobu Tarutani, Kazuo Saitoh, and Kazumasa Takagi

Abstract— **Interface circuits for the RSFQ circuit system were designed, fabricated and their frequency characteristics were investigated. Key elements of the interface circuit were the series array of SQUIDs and a JTL as a control line of the SQUID. The interface circuit was designed to cover the operating frequencies much greater than 10 GHz. A high-frequency**

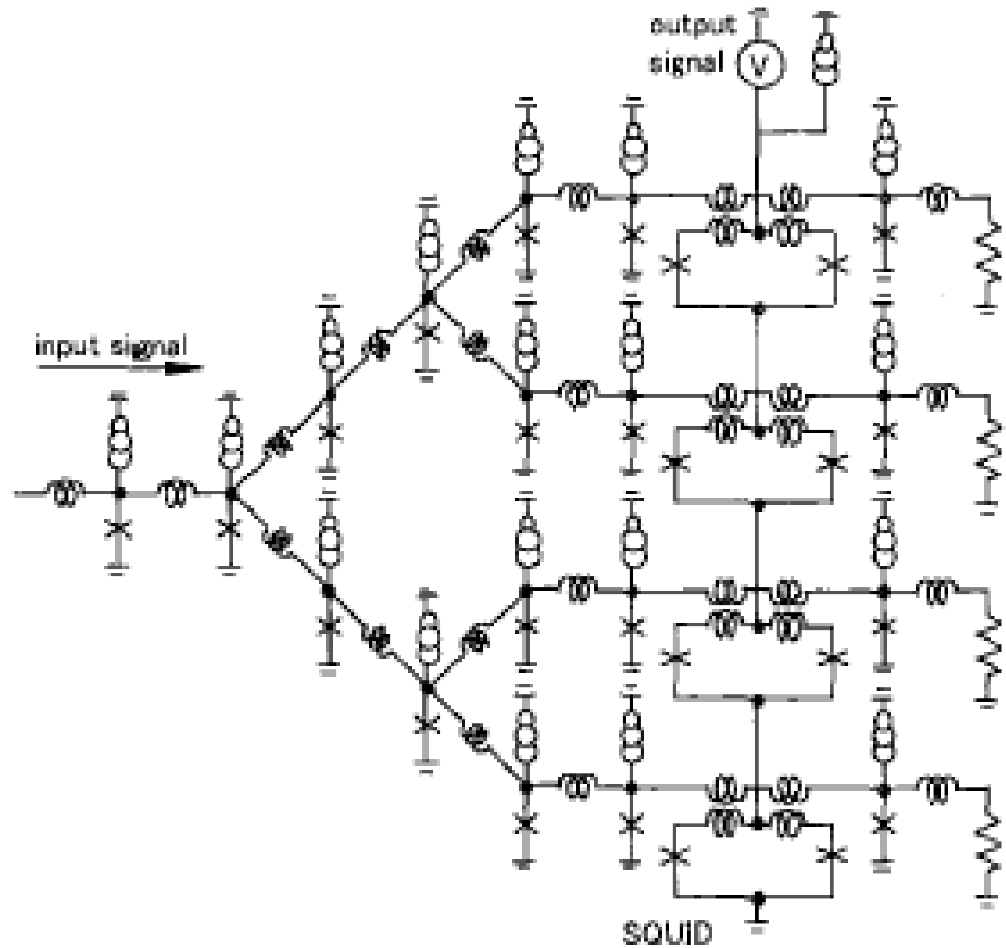

Fig.1 Block diagram of the interface circuit. An example of 4-series SQUID array is shown.

Example of an RSFQ circuit

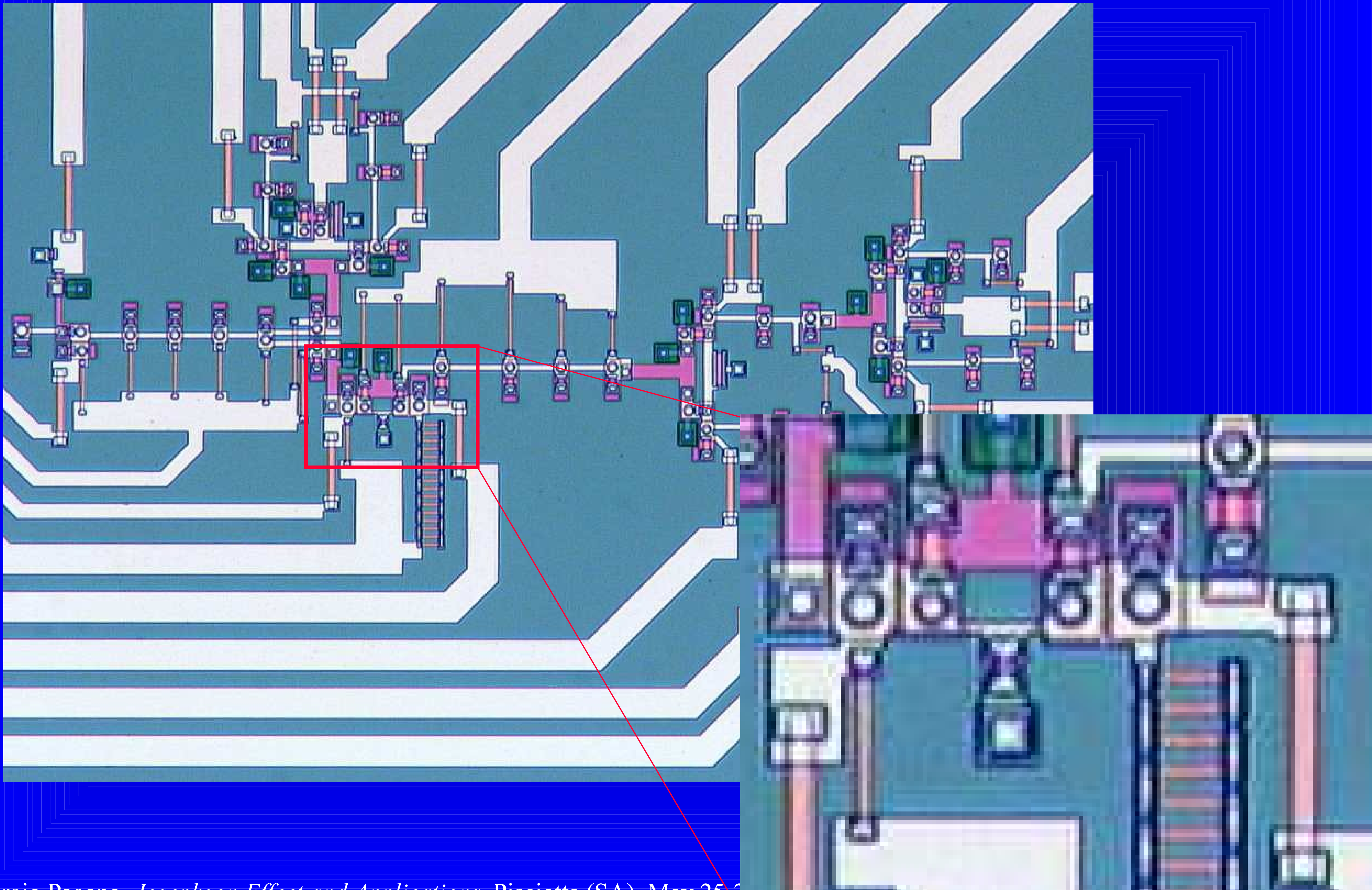

Modulation schemes

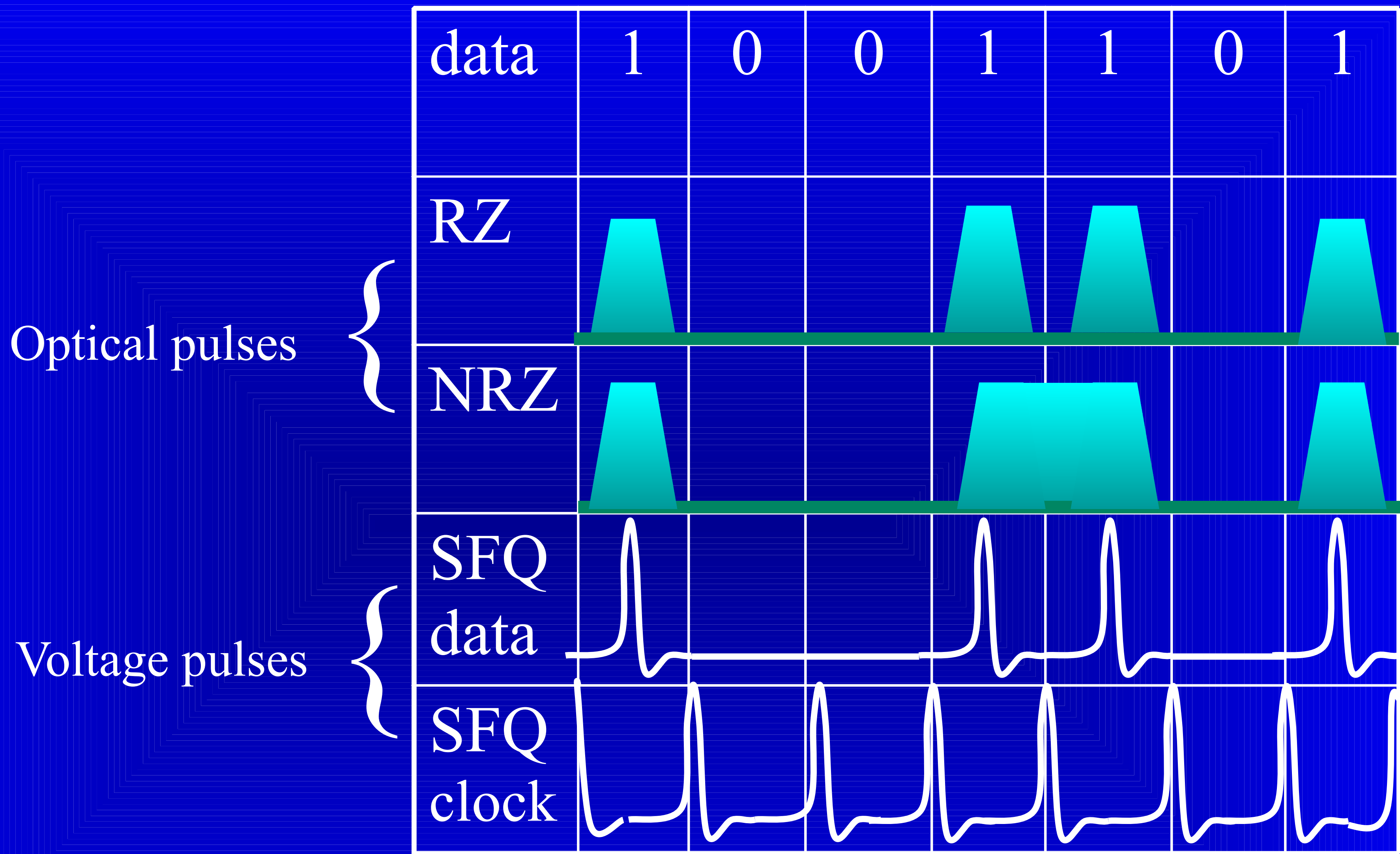

NRZ requires half bandwidth for data transmission
Both RZ and NRZ require clock recovery if a long sequence of zeros is transmitted

Optical to RSFQ interfacing

the optical signal is a sequence of light pulses
at λ=1550 nm each photon has 0.8 eV
at 40Gbps each pulse is 20 ps wide
then 1 μW pulse corresponds to 156 photons

High sensitivity is an important feature

Metal-Semiconductor-Metal (MSM) detector are sensitive and fast.
It is possible to use the Si chip for the detector fabrication
However the cutoff wavelength is too short: they don't work at 1550 nm

Superconductive detectors are very sensitive (Δ<<0.8eV) and can be very fast (depending on the material)

Processing circuit for optical switch

optical switches lack processing capability
CMOS circuits do not guarantee fast enough throughput
GaAs circuits are faster but very power consuming
SFQ circuits exploit the full capability of the optical switch
fast O/SFQ and SFQ/O interfacing is required

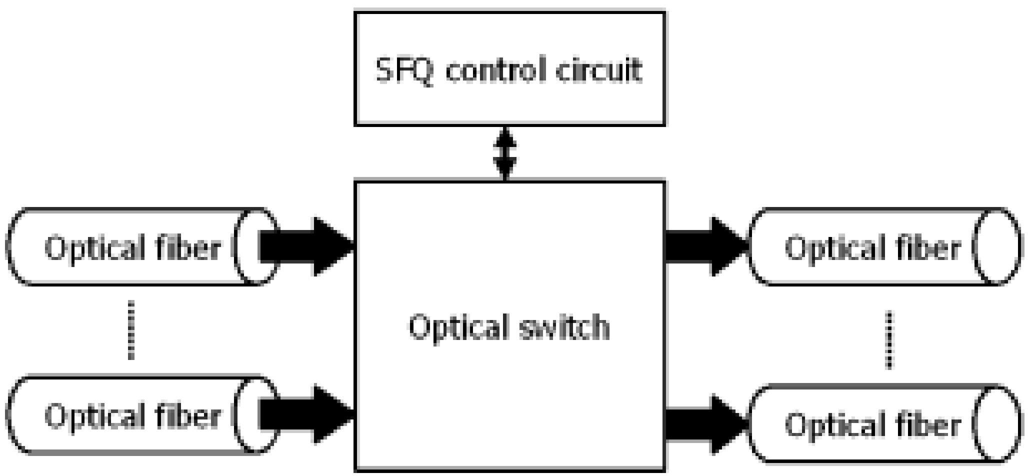

Fig. 1. Basic conceptual diagram of SFQ controlled optical switch.

Application of single flux quantum technology to a next-generation photonic packet switch core

S. Yorozu [a,*], H. Harai [b], Y. Kameda [a], H. Terai [c], Y. Hashimoto [a]

Superconductivity Research Laboratory, NEC Tsukuba Research Laboratories, ISTEC, 34 Miyukigaoka, Tsukuba, Ibaraki 305-8501, Japan
[b] *Communications Research Laboratory, 4-2-1 Nukui-Kitamachi, Koganei, Tokyo 184-8795, Japan*
[c] *Communications Research Laboratory, Kansai Advanced Research Center, Kobe, Hyogo 651-2492, Japan*

Received 29 October 2003; accepted 23 December 2003
Available online 1 June 2004

Physica C 412–414 (2004) 1555–1559

10Gbps→40Gbps→160Gbps

Application: quantum optics telecommunication

quantum cryptography needs single photon detectors featuring:
1. low dark count rate
2. high speed (> 1 Gbps)
3. polarization sensitivity

superconducting single photon detectors meet these needs

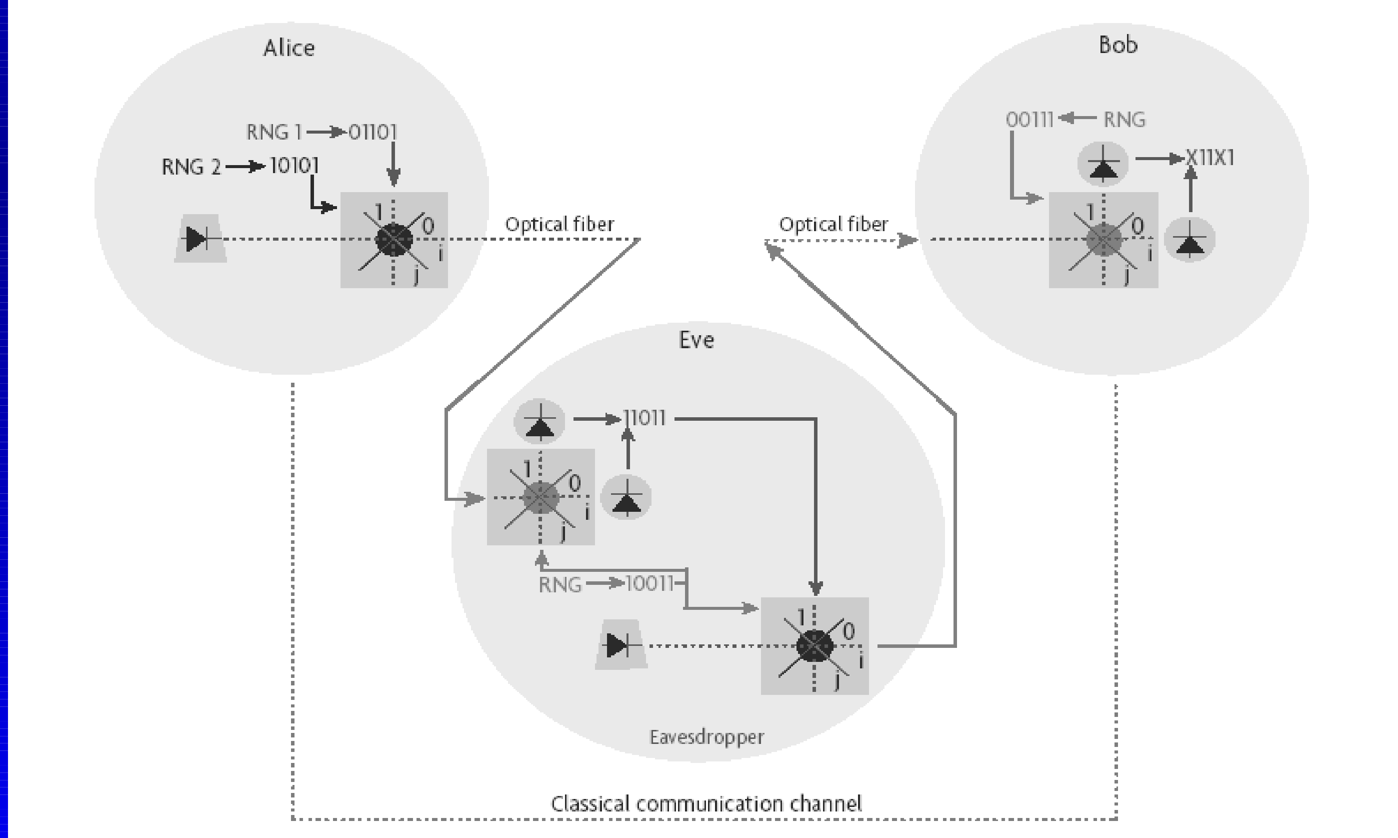

FIGURE 4: SCHEMATIC OF QKD SYSTEM WITH ATTEMPTED EAVESDROPPER

SINPHONIA

Single-photon nanostructured detectors for advanced optical applications

Materials & nanotechnology

New materials
Improved nanofabrication
Improved optical structures
Arrays
Integrated amplification/functionality

Optical characterisation

Efficiency,
Noise
High frequency Modeling

SSPD

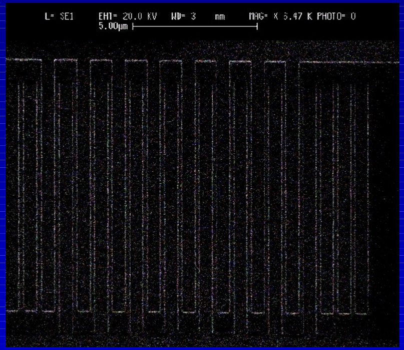

SEM image of SSPD meander (CNR, EPFL)

Applications

Long-distance quantum cryptography
High-speed quantum cryptography
Optical communications

SINPHONIA numbers

IST-NMP joint call FP6-2004-IST-NMP-2
Contact number 16433 Start date: January 2006 Duration: 3 years

Participants:

Role	No.	Name	Short name	Country	Date enter	Date exit
CO	1	Ecole Polytechnique Fédérale de Lausanne	EPFL	Switzerland	Mo. 1	Mo. 36
CR	2	Commissariat à l'Energie Atomique	CEA	France	Mo. 1	Mo. 36
CR	3	Consiglio Nazionale delle Ricerche	CNR	Italy	Mo. 1	Mo. 36
CR	4	Moscow State Pedagogical University	MSPU	Russia	Mo. 1	Mo. 36
CR	5	University of Geneva	GEN	Switzerland	Mo. 1	Mo. 36
CR	6	VeriCold Technologies GmbH	VER	Germany	Mo. 1	Mo. 36
CR	7	id Quantique SA	idQ	Switzerland	Mo. 1	Mo. 36
CR	8	Pirelli Labs	PIR	Italy	Mo. 1	Mo. 36
CR	9	Thales TRT	THA	France	Mo. 1	Mo. 36
CR	10	Scientific Project Management	SciProM	Switzerland	Mo. 1	Mo. 36

Materials, technology: MSPU, CEA, CNR, EPFL
Characterisation: EPFL, CEA, CNR, MSPU, GEN
Applications: VER, idQ, PIR, THA
Coordination: EPFL
Management: SciProM

APPLICATION: Mass Spectrometry

Mass spectrometers are an analytical tool used for measuring the **molecular weight** of a sample.

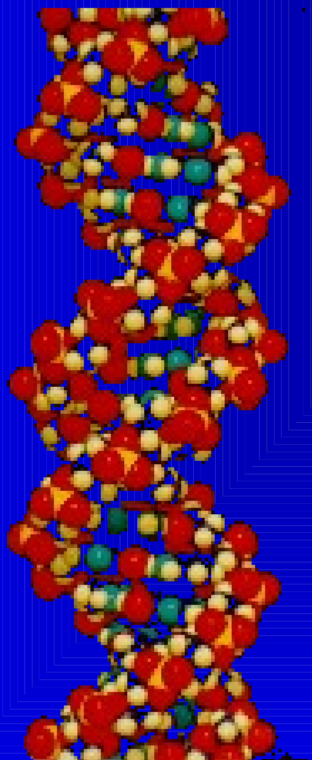

For large samples such as **biomolecules,** molecular weights can be measured to within an accuracy of **0.01%** of the total molecular weight of the sample *i.e.* within a 4 Daltons (Da) or atomic mass units (amu) error for a sample of 40,000 Da. This is sufficient to allow minor mass changes to be detected, *e.g.* the substitution of one amino acid for another, or a post-translational modification.

Mass spectrometry with MALDI TOF

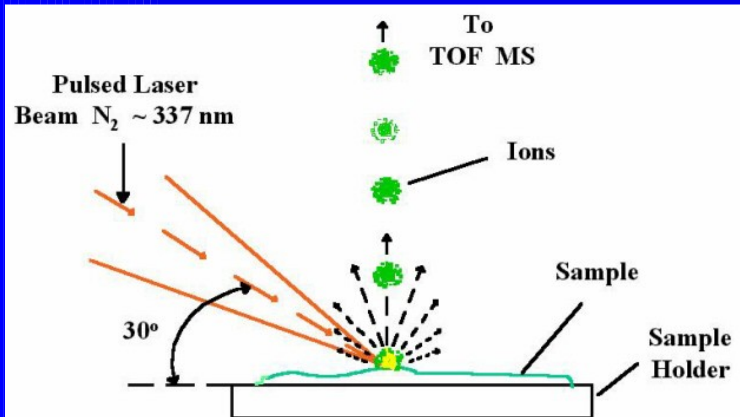

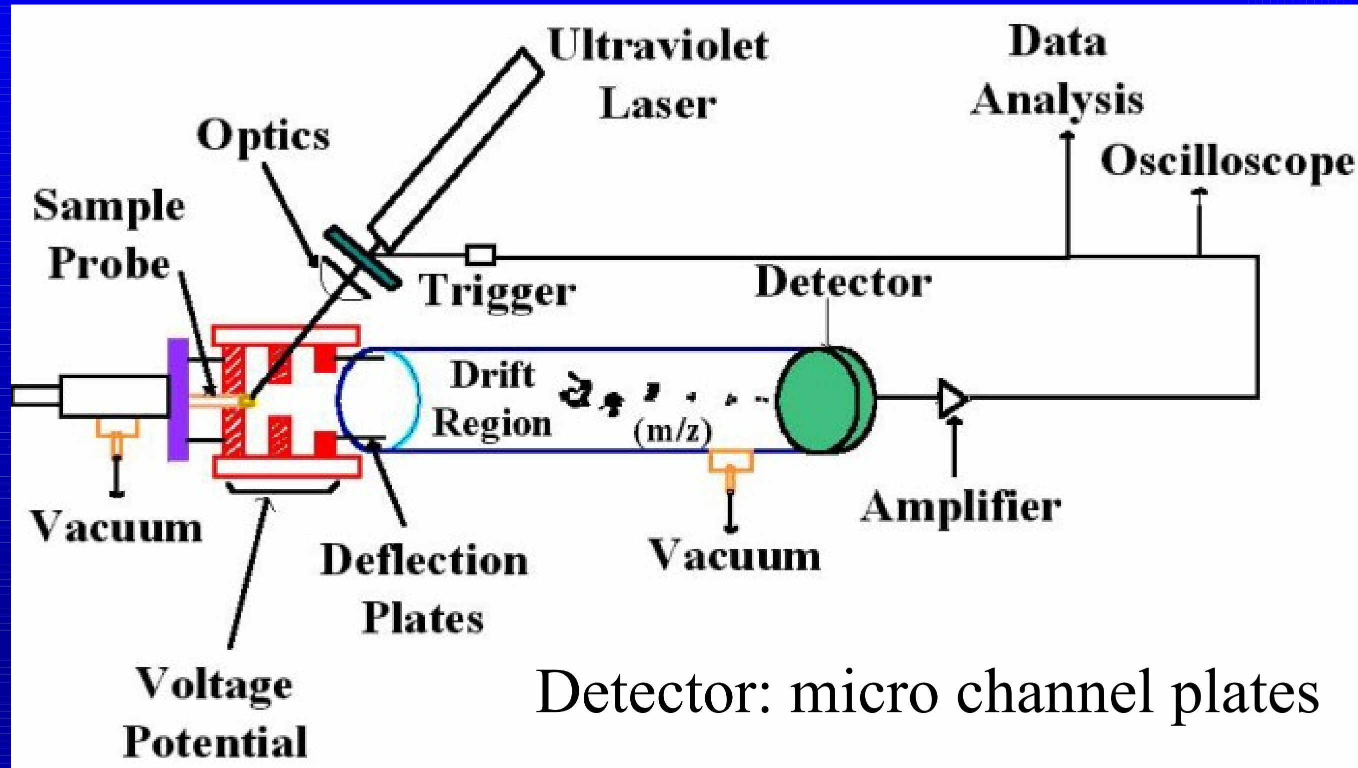

Detector: micro channel plates

$v=(2zU/M)^{½}$

$$Tof = L\sqrt{\frac{M}{2zU}}$$

$$\frac{\Delta Tof}{Tof} = \frac{1}{2}\frac{\Delta M}{M}$$

v = fragment velocity
z = fragment charge
M = fragment mass
U = accelerating potential
Tof = time of fligth

Typical values: L = 1 m, M = 10-100 kDa, U = 2-10 kV
Results: v ~ 10^4 m/s, Tof ~ 100 μs, **ΔM/M ~ 10^{-4} → ΔTof ~ 10 ns**

Mass specrometry with superconductive detectors

In superconductive detectors the macro molecule fragment kinetic energy ($E_{kin} = zU$) is converted into phonons and quasiparticles.
A current pulse is then generated and sets the arrival time.

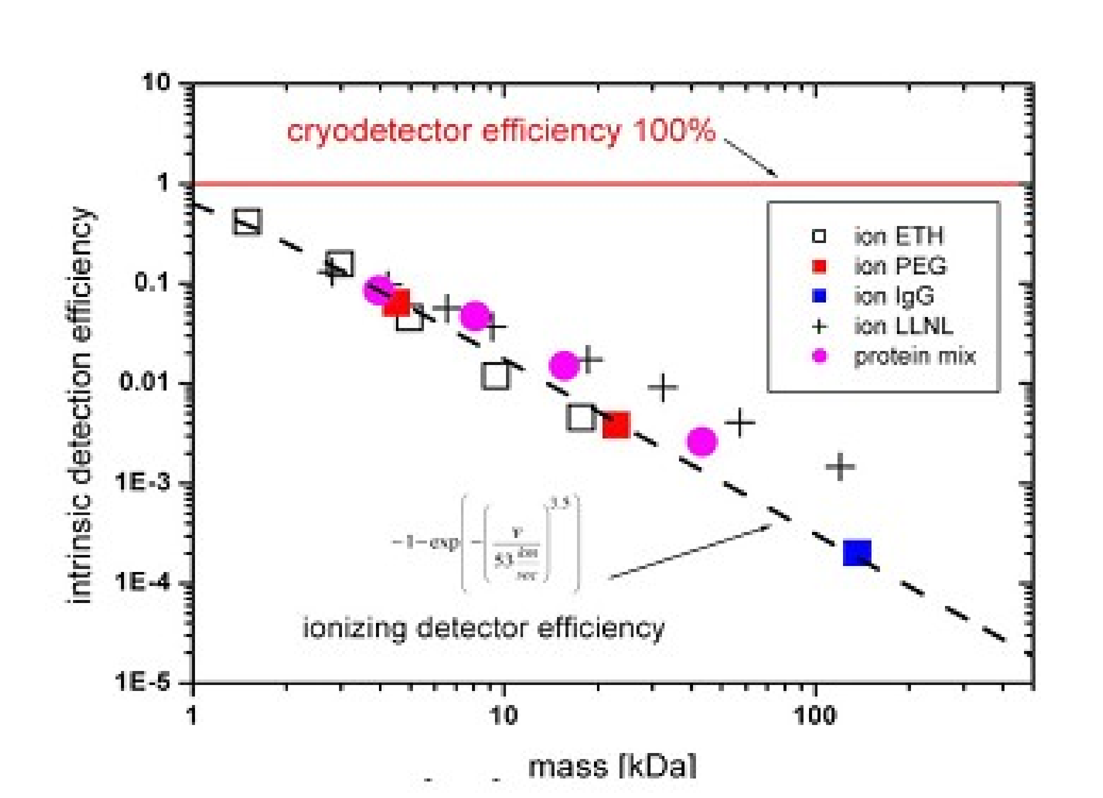

Conventional microchannel plate detectors lose efficiency for large masses.

Mass specrometry with superconductive detectors

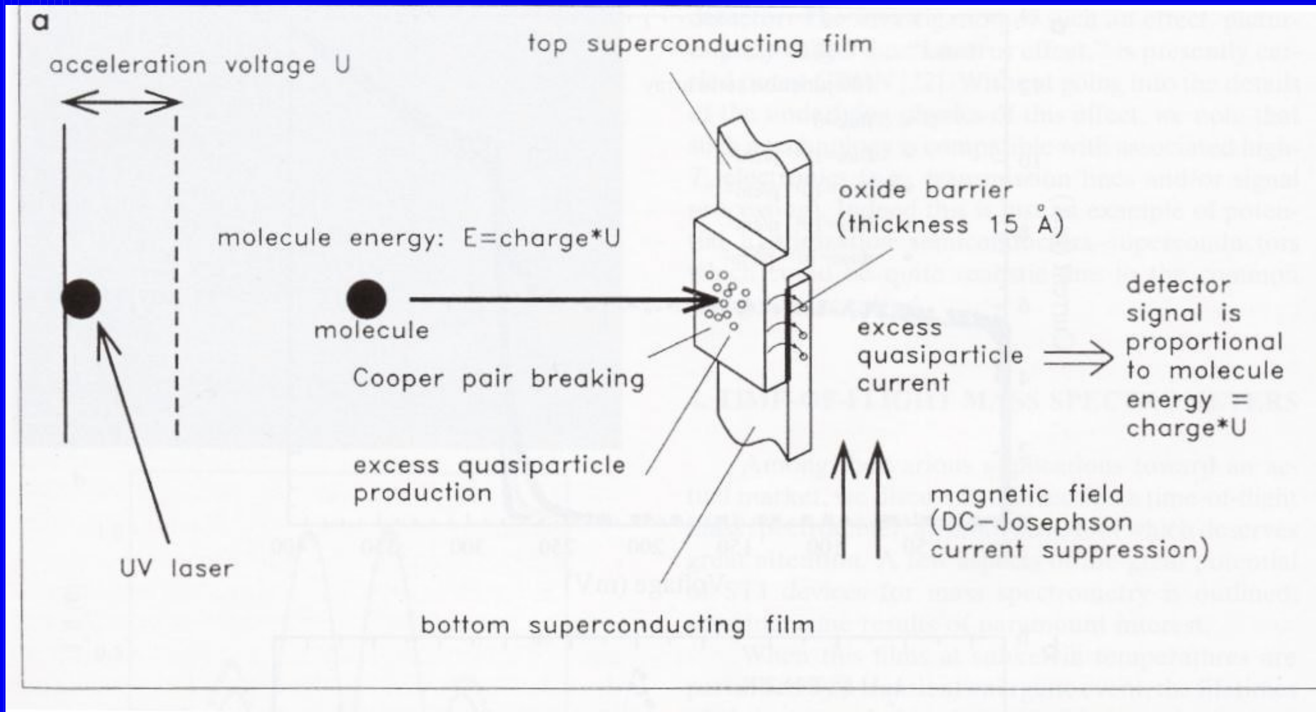

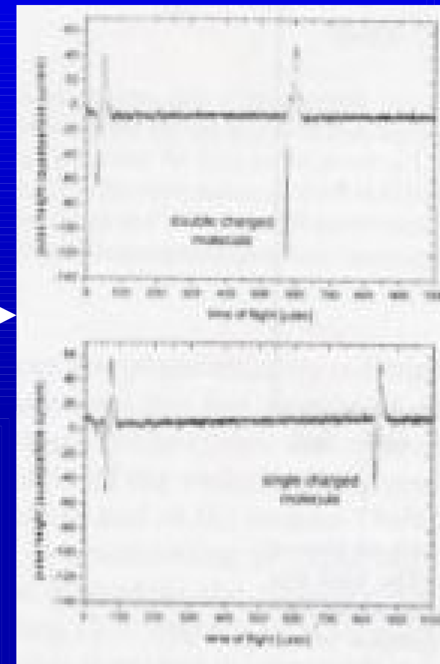

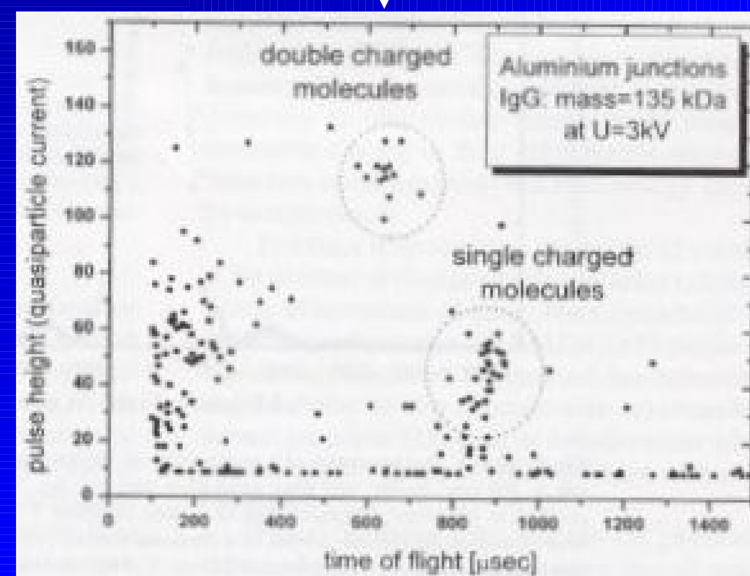

Courtesy of D. Twerenbold

Advantages of superconductive detectors:

1) constant detection efficiency for large masses
2) can discriminate between different ion charge states

Disadvantages:

1) low operating temperature (100-300 mK)
2) low speed (μs)

Cryogenic Mass Spectrometer

Micromizer with STJ-detectors
Comet AG, Flamatt, Switzerland; www.comet.ch

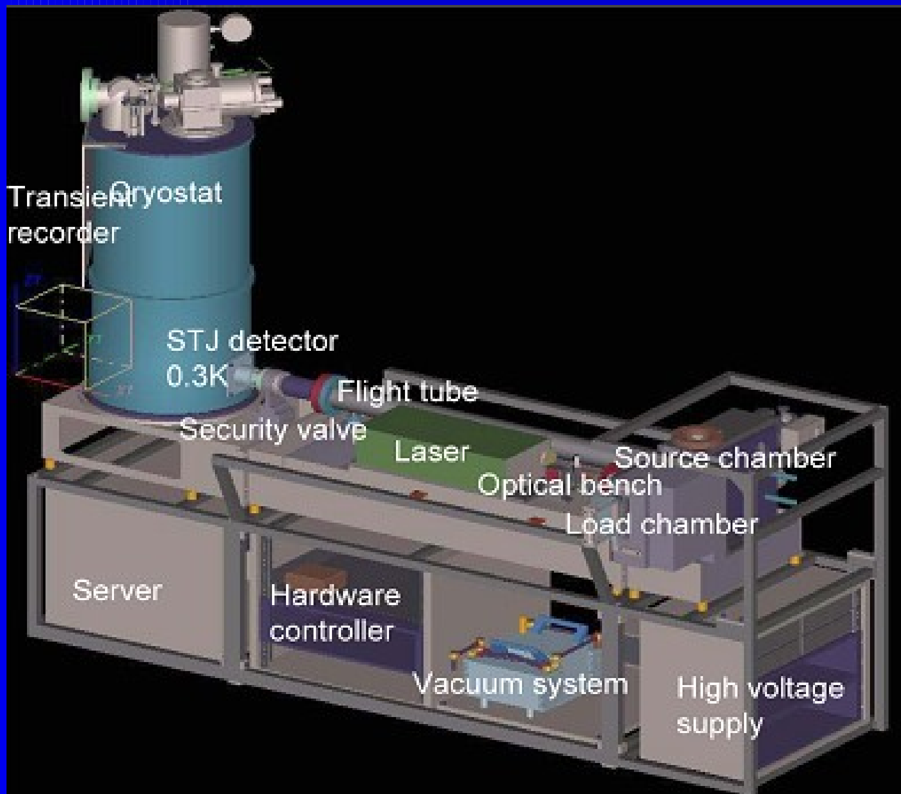

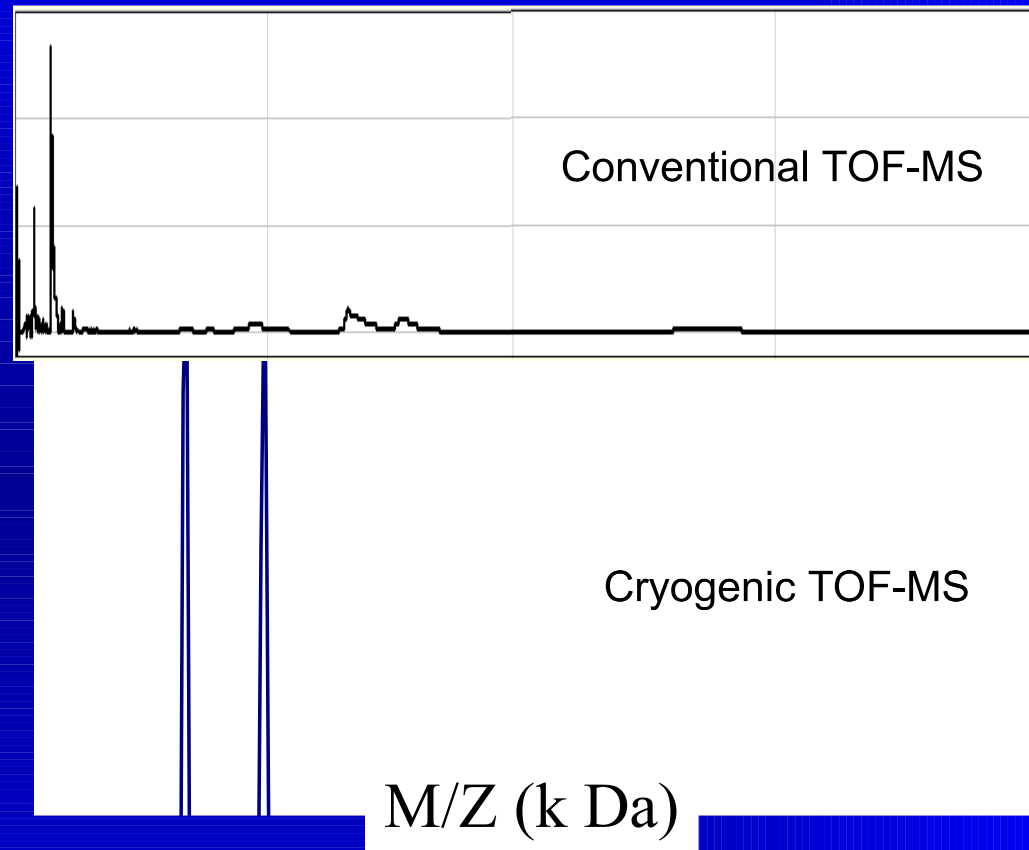

Applications:
Protein complex research: Identification of large proteins and fragments
Virus detection: Medical diagnostics, national security (LLNL)
Genetics: DNA/ RNA genotyping, recognition of mutations

Simultaneous Energy and Time Measurement

Superconductive detectors improve sensitivity, but have limited mass resolution

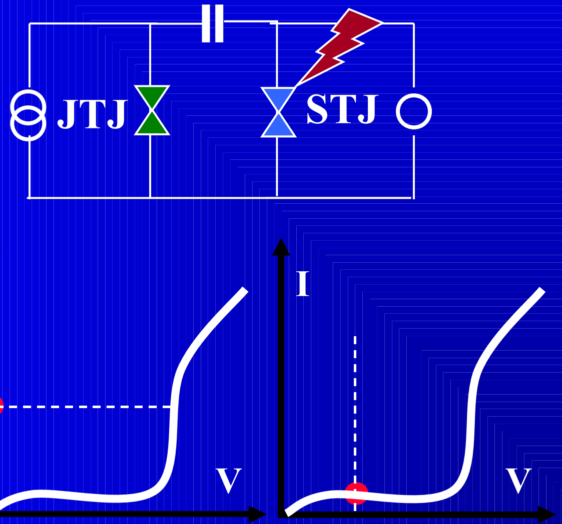

$$\frac{\Delta m}{m} = 2\frac{\Delta t}{t}$$

Δt >100 ns with a $\Delta t/t > 10^{-3}$ (far away from the 10^{-6} value of ionizing detectors !)

Dual Detector:

- The STJ measures the energy
- The JTJ measures the arrival time

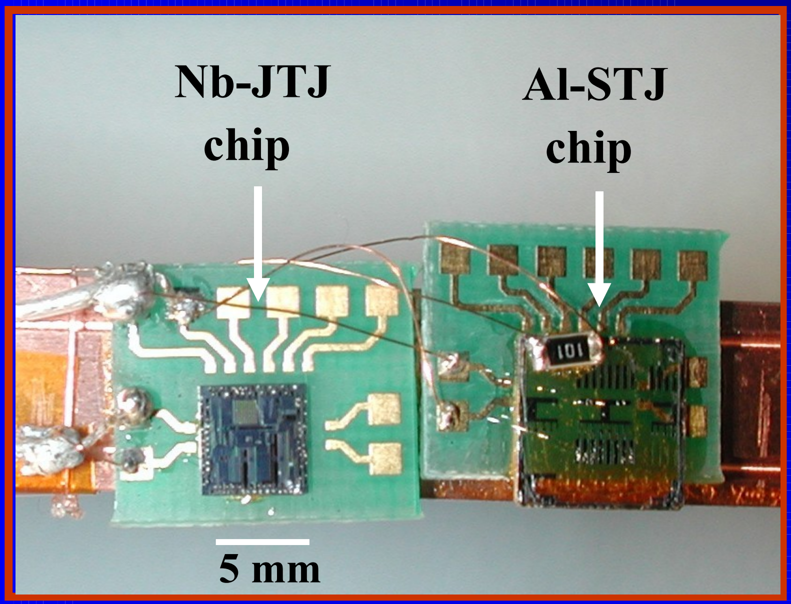

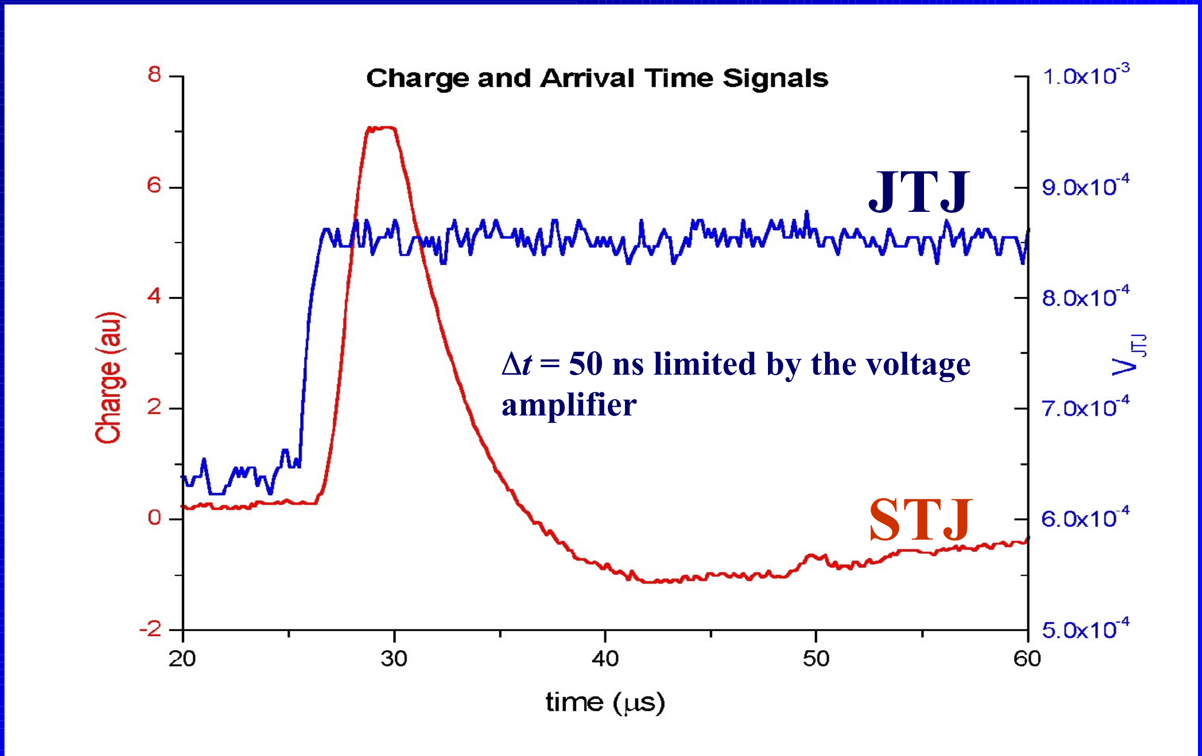

CNR-ICIB group: E.Esposito *et al.*, APL 82 (2003) 2109

Mass spectrometry with superconductive detectors 2

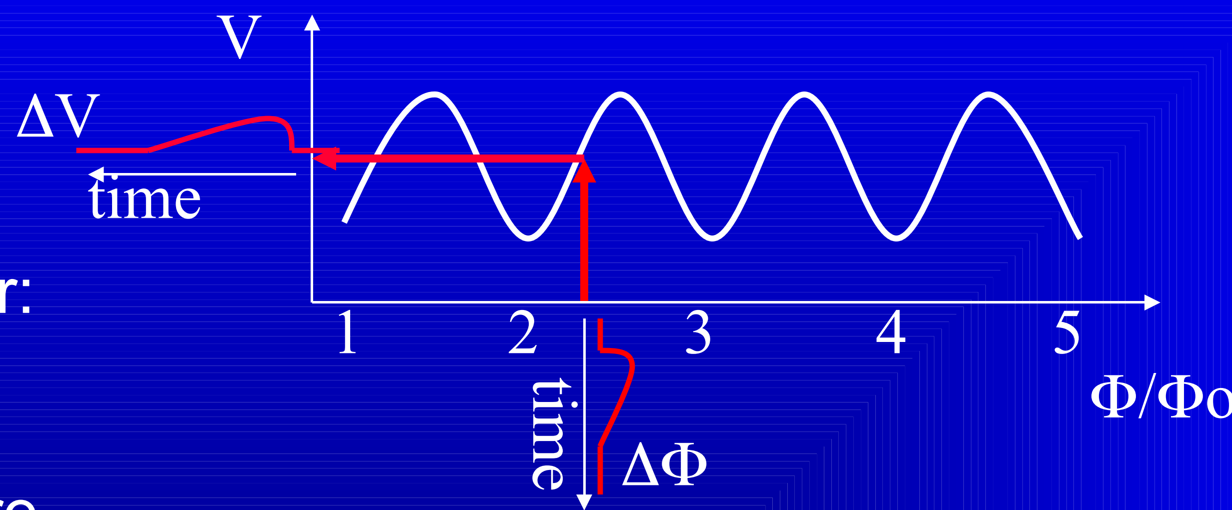

use a NbN meander as kinetic inductance detector:

Fast

Energy resolution

High operating temperature

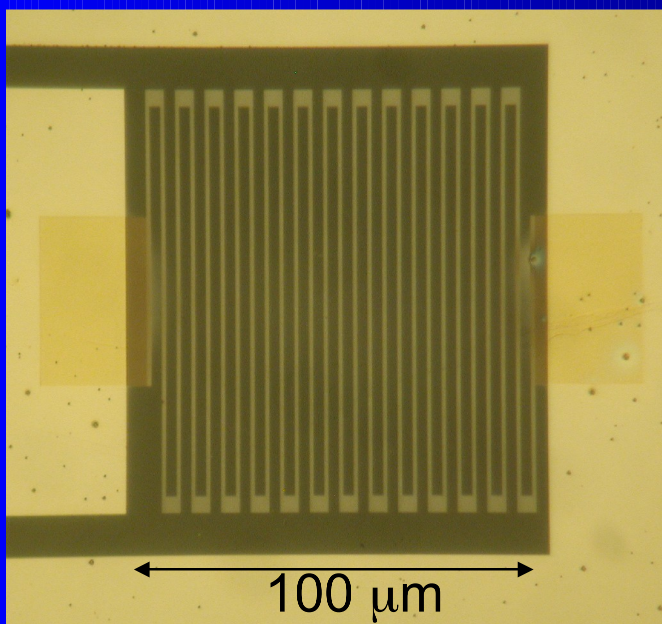

CNR ICIB&IFN 2005

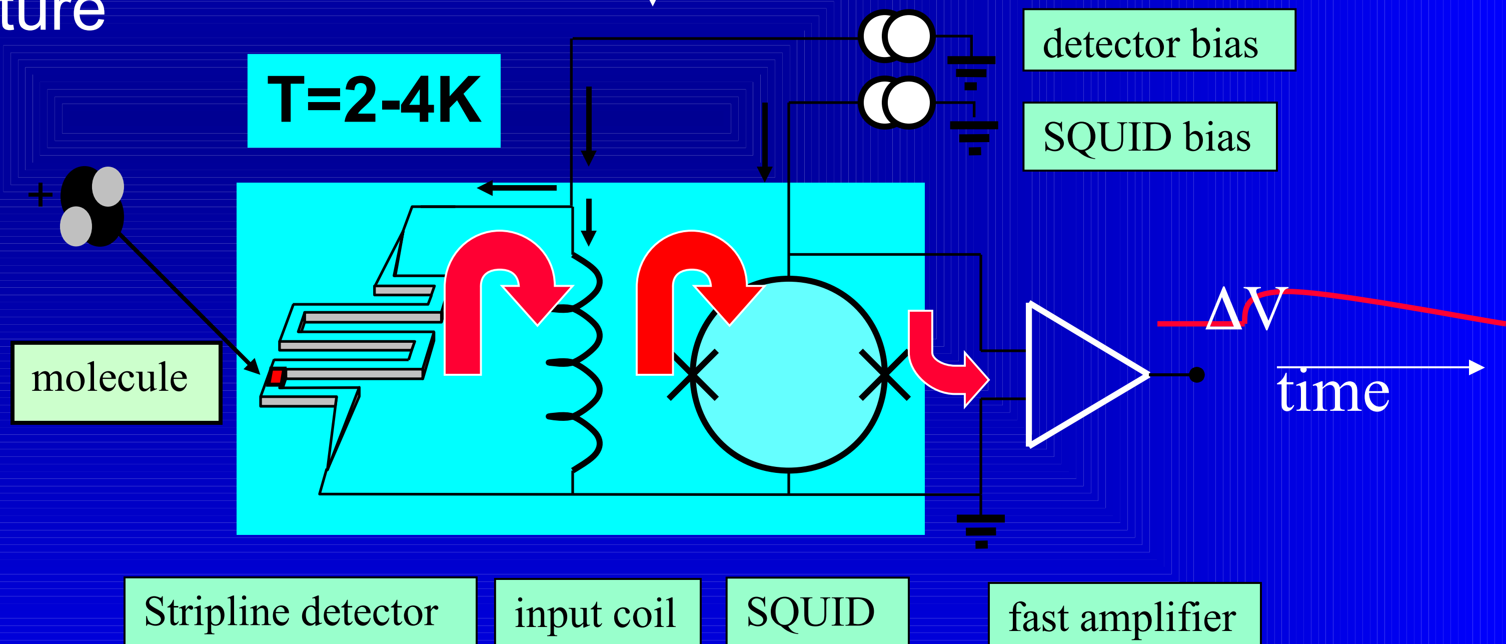

S. Pagano, E. Esposito, M. Ejrnaes, C. Nappi, R. Cristiano, *Kinetic Inductance Detectors for Mass Spectroscopy,* IEEE Trans Appl. Sup. (2005)

Multispectral/fluorescence CT using superconducting tunnel junction detector for 3-D material analysis

Y. Takizawa[a,*], H. Sato[a], S. Shiki[a], C. Otani[b], M. Kurakado[a], T. Taino[c], H.M. Shimizu[a]

[a] *Image Information Division, RIKEN, 2-1 Hirosawa, Wako, Saitama 351-0198, Japan*
[b] *Kawase Initiative Research Unit, RIKEN, 2-1 Hirosawa, Wako, Saitama 351-0198, Japan*
[c] *Department of Electrical and Electronic Systems, Saitama University, 255 Shimo-Ohkubo, Saitama-shi, Saitama 338-8570, Japan*

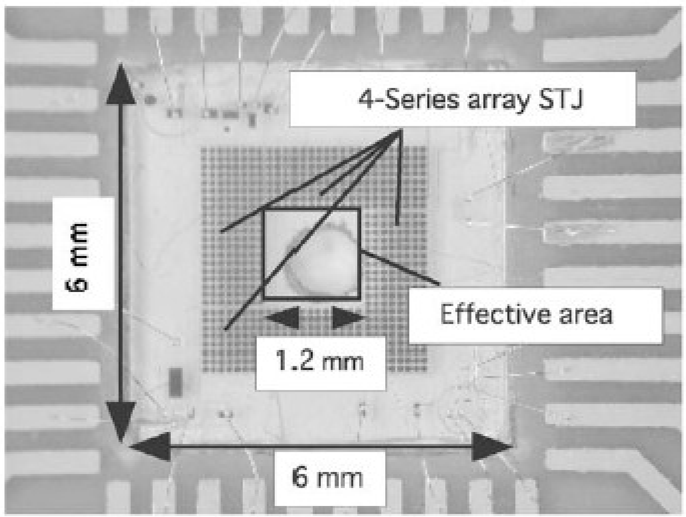

Fig. 1. Substrate-absorption-type cryogenic detectors using series array STJs.

Y. Takizawa et al. / Nuclear Instruments and Methods in Physics Research A 520 (2004) 617–620

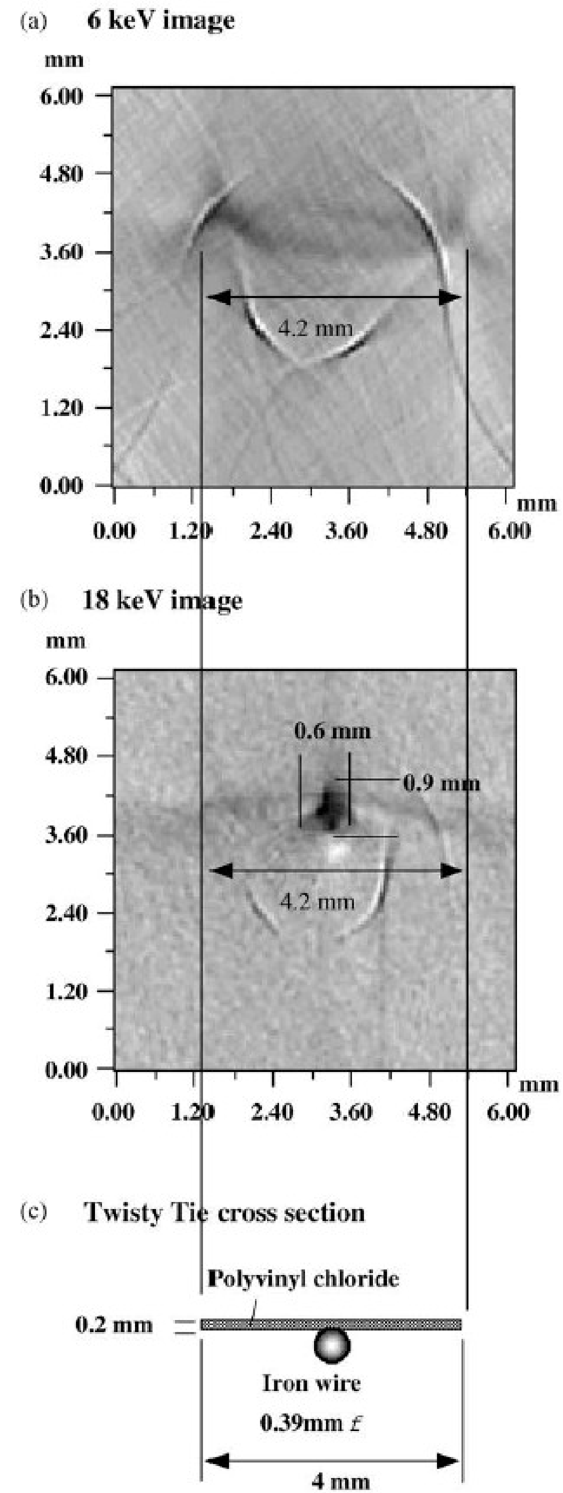

Fig. 4. Cross section images of twisty tie. (a) 6 keV image; (b 18 keV image; (c) size of twisty tie.

More biological applications

synchrotron based x-ray absorption spectroscopy

Cryogenic X-ray spectrometers [3] offer an advantage whenever conventional semiconducting detectors cannot resolve the fluorescence line of interest, and grating spectrometers lack the efficiency to collect data within an acceptable period of time. A short measurement time is crucial for biological samples that suffer from radiation damage.

FRET

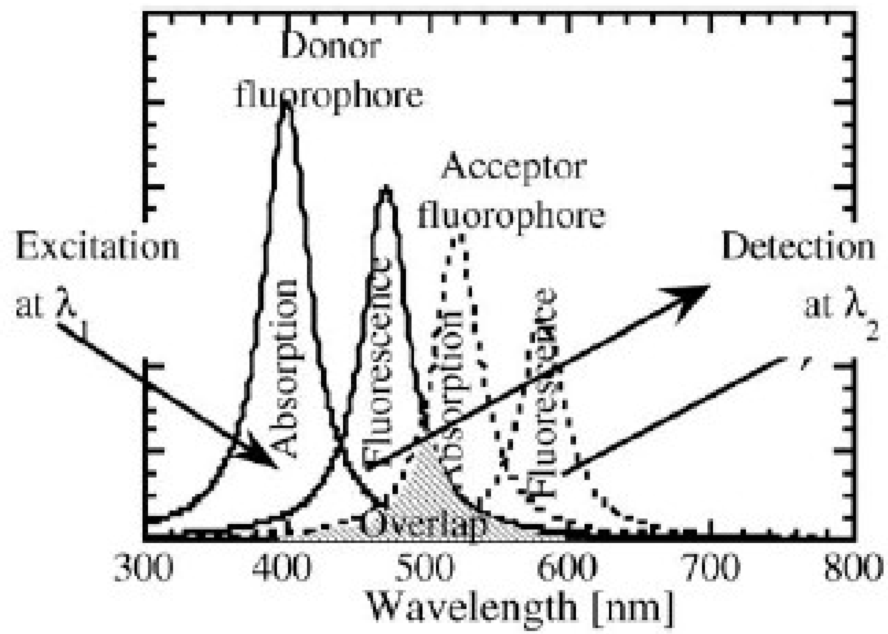

Fig. 2. Schematic of fluorescence resonance energy transfer. Fluorophores can be designed that change their emission wavelength with environmental conditions.

Cryogenic detectors can enable single molecule FRET studies on systems whose fluorescence wavelength changes with the environmental conditions. Several markers, for instance, change their fluorescence wavelength as a function of local pH or ion concentration and can be used to monitor environmentally driven conformational changes.

 S. Friedrich / Nuclear Instruments and Methods in Physics Research A 520 (2004) 621–624

Concluding remarks

- Superconducting detectors have unique performances over a wide range of applications
- Superconducting detecting systems are the core of advanced instrumentation

useful references

A. Rothwarf and B.N. Taylor, Phys Rev Letters 19 (1967) 27-30

S.B. Kaplan, et al., Phys. Rev. B 14 (1976) 4854-4873

A.G. Kozorezov, et al., Phys. Rev. B 61 (2000) 11807-11819 and NIM A 520,p. 3-7 (2004)

A.D. Semenov, G.N. Gol'tsman and R. Sobolewski Supercond. Sci. Technol. 15 (2002)R1-R16

Proceedings of LTD10, Nuclear Instruments and Methods A 520, 2004